CRIMP, MICROSTRUCTURE, AND BIOMECHANICS: ANALYZING THE EYE USING POLARIZED LIGHT MICROSCOPY

by

Ning-Jiun Jan

Bachelor of Science in Bioengineering, California Institute of Technology, 2011

Submitted to the Graduate Faculty of

Swanson School of Engineering in partial fulfillment

of the requirements for the degree of

Doctor of Philosophy in Bioengineering

University of Pittsburgh

2018

UNIVERSITY OF PITTSBURGH

SWANSON SCHOOL OF ENGINEERING

This dissertation was presented

by

Ning-Jiun Jan

It was defended on

June 15, 2018

and approved by

Kira L. Lathrop, MAMS, Assistant Professor, Department of Ophthalmology and Bioengineering

Rouzbeh Amini, PhD, Assistant Professor, Department of Biomedical Engineering, University of Akron

Nils Loewen, MD, PhD, Associate Professor, Department of Ophthalmology

Jonathan Vande Geest, PhD, Professor, Department of Bioengineering

Dissertation Director: Ian A. Sigal, PhD, Assistant Professor, Department of Ophthalmology and Bioengineering

CRIMP, MICROSTRUCTURE, AND BIOMECHANICS:

ANALYZING THE EYE USING POLARIZED LIGHT MICROSCOPY

Ning-Jiun Jan, PhD

University of Pittsburgh, 2018

Glaucoma is the second leading cause of irreversible blindness worldwide. Elevated intraocular pressure (IOP) is the main risk factor for glaucoma, though sensitivity to IOP varies widely. A leading theory states that the breadth of sensitivity is due to the biomechanical variability between eyes. According to this theory, biomechanically weak eyes suffer glaucoma at lower IOPs whereas robust eyes withstand higher IOPs without glaucomatous neural tissue damage. Therefore, in order to prevent, diagnose, and treat glaucoma, we need to have a better understanding of ocular biomechanics.

Ocular biomechanics are intimately tied to the anisotropy and nonlinearity of eye tissue. Both of these macroscale properties are largely determined by the organization of collagen, the main load-bearing component of the eye. The anisotropy is related to the mesoscale collagen structure, whereas the nonlinearity is related to the microstructural collagen fiber waviness or crimp. Although many have studied the collagen anisotropy, few studies of ocular crimp exist. Hence, the microstructural basis for eye biomechanics remains unclear, precluding a mechanistic assessment and understanding of individual sensitivity to IOP. The main goal of this project was to characterize the collagen crimp in the eye.

The lack of information on ocular crimp stems largely from the absence of a suitable imaging technique that can quantify ocular crimp with high resolution over a wide field-of-view. We established a method using polarized light microscopy (PLM) to quantify collagen fiber orientation in the eye and characterized the accuracy, repeatability, and robustness of our method. We then used PLM to characterize the crimp distribution in the eye. We also characterized how the crimp differed in eyes fixed at different IOPs and tracked how ocular crimp changed with stretch. Our studies revealed many complex aspects of collagen architecture in the eye, including the existence of fibers that are arranged radially around the optic nerve head and highly uniform crimp in the lamina cribrosa and cornea. Our findings helped elucidate the role of crimp in determining eye biomechanics and provided insight into collagen patterns that play a central role in the pathophysiology of glaucoma.

TABLE OF CONTENTS

LIST OF TABLES

LIST OF FIGURES

PREFACE

Acknowledgements

This dissertation is the culmination of the guidance from many people in my life. First and foremost I want to thank Professor Ian Sigal who has been my mentor throughout my time in the Ocular Biomechanics Laboratory. The lessons you have taught me will stay with me long after I leave the lab. There have been many obstacles along the way and you helped me face them and overcome them. I could not have asked for a more supportive or patient advisor to teach me and help me accomplish all that I have done for my PhD. Thank you.

I would like to thank the rest of my dissertation committee, Professors Kira L. Lathop, Dr. Rouzbeh Amini, Dr. Nils Loewen, and Dr. Jonathan Vande Geest. Thank you for your contributions to this dissertation.

I would also like to thank all the current and past members of the Ocular Biomechanics Laboratory, including all the undergraduate students who have helped me collect and analyze data during their time in our lab. I would like to especially acknowledge past members Jonathan Grimm and Celeste Gomez, and current member Alex Gogola. Jonathan, for the first half of my PhD I pestered you almost every day with questions about research. You were my best friend in the lab and I was lucky to have such a smart and caring lab member to help me with my research. Celeste, the undergraduate work you started with so many years ago became the beginning of my dissertation. Thank you for all those hours you dedicated to our research, imaging and analyzing

so many sections. Alex, you have helped me with so much of the nitty and gritty parts of my research, thanks for not groaning when I asked for another version of a spreadsheet or with coding a plugin.

There have also been many others who have helped with the research, including the many collaborators at the University of Pittsburgh. I would like to especially thank Professor Kira Lathrop, who was my first mentor in imaging. You have played a large role in establishing many of the PLM imaging protocols we use today. In addition, you are also a role model to me as a woman in science.

Lastly, I want to thank all of my family and friends. I want to thank my parents, Chieh-Chih Jan and Gwo-Ming Jan, who have been so supportive. Many times, you have come to visit me just to put a smile on my face when the going was tough. I would also like to thank my husband, Gaurav Giri, my partner on the tandem bike. Countless times you have done or said just the right thing to help me through the day, including keeping me on track to finish my PhD. Another thank you to all my friends, especially all the members of FRESA. Dancing, singing, and just hanging out with you guys has been a wonderful time, and I know I will continue to be friends with many of you after I move away.

Abbreviations

IOP – intraocular pressure

LC – lamina cribrosa

LME – linear mixed effect

ONH – optic nerve head

PLM – polarized light microscopy

PPS – peripapillary sclera

SD – standard deviation

1.0 INTRODUCTION

1.1 GLAUCOMA

Glaucoma is a group of eye diseases that results in gradual vision loss. Vision loss is slow and progresses from the periphery towards the center of the visual field (Figure 1) (Quigley, 2005). Estimates suggest that by 2040, more than 100 million people will suffer from glaucomatous vision loss. (Tham et al., 2014) There is currently no cure for glaucoma. Treatments can delay or stop the progression of glaucoma, but vision loss is irreversible (Weinreb, Aung, & Medeiros, 2014). Because of this, early detection and diagnosis of glaucoma are of the utmost importance.

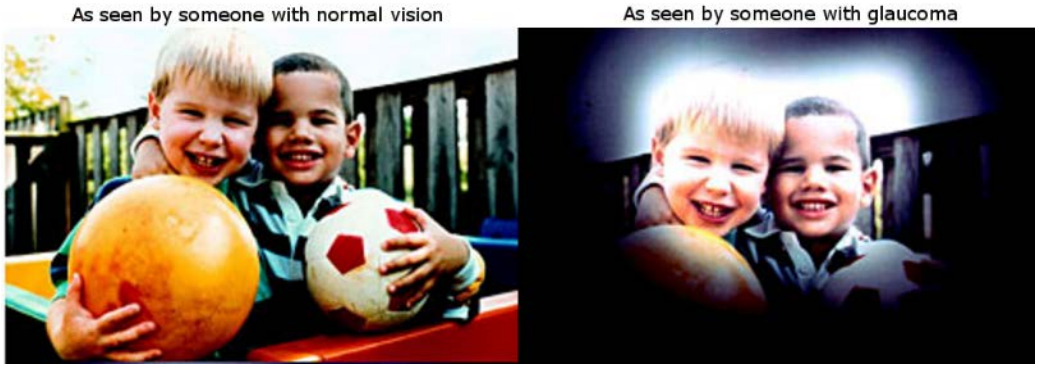

Figure 1. Glaucomatous vision loss starts at the periphery.

To the left is a picture of what a person with normal vision may see while the right depicts the same scene simulated as viewed by a person with glaucoma. People with glaucoma first lose peripheral vision and over time, central vision decreases until they completely lose vision. Figure adapted from nei.nih.gov.

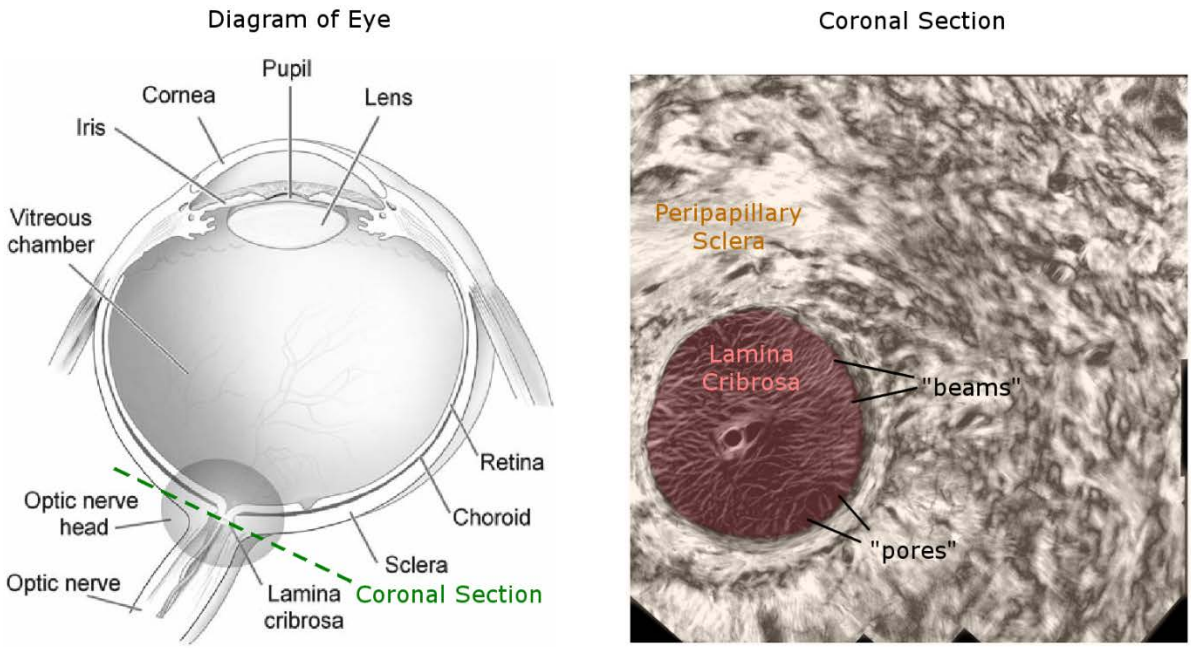

Figure 2. Glaucomatous neural tissue degeneration initiates in the LC.

On the left is a diagram of a human eye (adapted from nei.nih.gov), with a dotted line indicating a coronal cross-section through the LC. On the right is a coronal section through a human ONH. Light enters the eye from the cornea and this visual information is collected by the retina. The RGC axons of the retina converge on the posterior pole at the ONH. The axons then exit the eye through the LC to carry this visual information to the brain. These axons traverse the LC (red) of the ONH through “pores”, the dark openings in the LC between collagenous trabeculae “beams”. Surrounding the ONH and LC is the PPS (orange).

Glaucomatous vision loss is caused by a characteristic death of retinal ganglion cell (RGC) axons at their point of exit from the eye in an area called the optic nerve head (ONH) (Quigley, 2005). Specifically, neurodegeneration initiates within the lamina cribrosa (LC), which is surrounded by the peripapillary sclera (PPS) (Burgoyne, Crawford Downs, Bellezza, Francis Suh, & Hart, 2005).

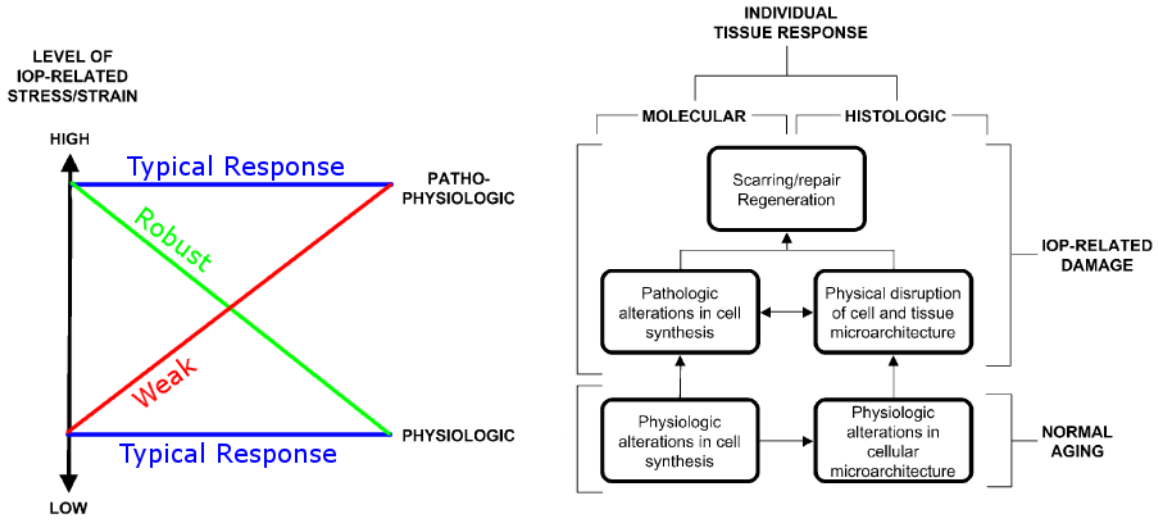

Figure 3. Diagram of physiologic and pathophysiologic responses from different levels of IOP-related stresses and strains.

Typically, high levels of IOP-related stresses and strains would induce a pathophysiological response in the tissue and result in glaucomatous IOP-related damage. On the other hand, low levels would result in the tissue following a physiologic response with normal aging. However, eyes that are weak or robust to changes in IOP-related stresses and strains would have different responses. Robust eyes would sustain a physiologic response even with high levels of IOP-related stresses and strains and weak eyes would have a pathophysiologic response despite experiencing low levels of IOP-related stresses and strains. Figure adapted from (Burgoyne et al., 2005).

The main risk factor for glaucoma is elevated intraocular pressure (IOP), and IOP remains the only modifiable risk factor. (Guedes, C Tsai, & A Loewen, 2011; Nemesure B, 2003) However, IOP alone is a poor predictor of glaucomatous neural loss (Vogel et al., 1990). It is well-established that the higher the IOP, the more likely someone is to develop glaucoma and for their glaucoma to worsen, however there does not exist a universal cutoff at which a patient will be safe from vision loss (Burgoyne et al., 2005). Among those with elevated IOP, or ocular hypertension, there is a wide variability of risk for developing glaucoma, where some individuals are only a third as likely to develop glaucoma compared to others with ocular hypertension (Bengtsson & Heijl, 2005; Gordon et al., 2002). In addition, some people develop glaucoma despite having normal or low

IOP in a form of glaucoma often called normal-tension glaucoma (Casson, Chidlow, Wood, Crowston, & Goldberg, 2012; Malik, Swanson, & Garway-Heath, 2012). The relationship between glaucoma and IOP is complex, with the etiology of glaucoma still not well understood. A better comprehension of the pathophysiology of glaucoma, including the origin of patient-specific sensitivity to IOP, is necessary to improve diagnosis and treatment.

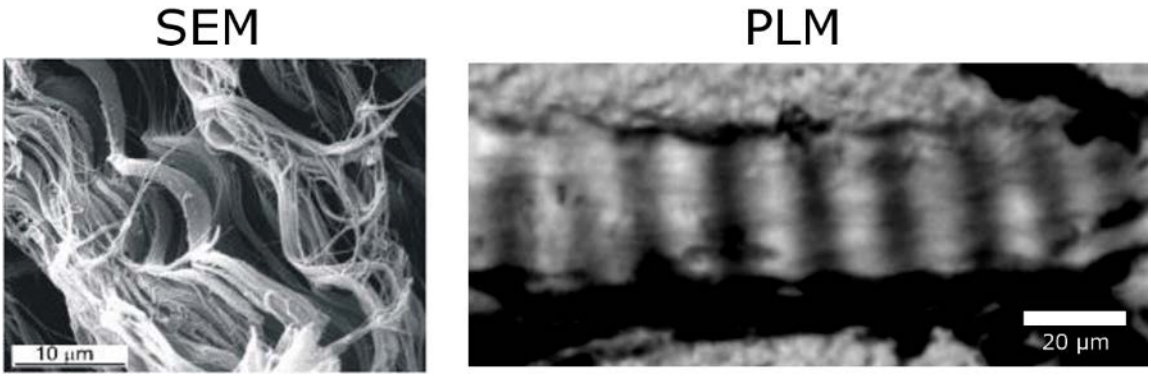

Figure 4. Collagen fibers are naturally wavy, and this waviness is known as crimp.
The left panel shows a scanning electron microscopy (SEM) image of crimped collagen fibers in tendon. This panel was adapted from (Freed & Doehring, 2005). On the right is a polarized light microscopy (PLM) image of crimped collagen in a LC trabecular beam.

A leading hypothesis postulates that the wide range in sensitivity to IOP and glaucoma susceptibility is due to the naturally occurring biomechanical variability between eyes (Figure 3) (Burgoyne, 2011; Sigal, Flanagan, Tertinegg, & Ethier, 2004). Within this theory, individuals with biomechanically strong eyes are less likely to incur glaucomatous changes even at high levels of IOP. Conversely, individuals with normal-tension glaucoma have biomechanically weak eyes, where even at low levels of IOP, they can suffer from glaucomatous nerve damage. Following this paradigm, there exist biomechanical markers that can be used to determine sensitivity to IOP and susceptibility to glaucoma (Sigal & Ethier, 2009). Once identified, preventative measures can be

taken to prevent vision loss. Furthermore, it may even be possible to develop techniques to correct the biomechanical aspects that increase the sensitivity to IOP in the first place. The long-term goal of this project is to identify biomechanical markers of individual-specific sensitivity to IOP, and therefore glaucoma.

1.2 BIOMECHANICS AND COLLAGEN CRIMP

Detection of biomechanical markers of individual-specific sensitivity to IOP has been difficult, in part because there is still an incomplete understanding of normal eye biomechanics. Though it is known that the collagen structure largely determines the biomechanics of the eye, there are still many aspects of normal eye collagen structure that have not been characterized. Exactly how the collagen structure of an eye determines its IOP-induced response is an area of much interest in ocular biomechanics.(Campbell, Coudrillier, & Ethier, 2014; C Ross Ethier, Mark Johnson, & Jeff Ruberti, 2004; Sigal & Ethier, 2009) On the meso-scale level, the collagen tissue anisotropy affects the directional stiffness in the eye, while on the microstructural level, the waviness of the collagen fibers, or crimp (Figure 4), affects the strain-dependent stiffness. (Fratzl, 2008; Holzapfel, 2001) The meso-scale tissue anisotropy of the posterior pole has been the focus of multiple studies, (Coudrillier, Boote, Quigley, & Nguyen, 2013; M. J. Girard, A. Dahlmann-Noor, S. Rayapureddi, J. A. Bechara, B. M. E. Bertin, et al., 2011; Ischreyt, 1898; K. M. Meek & Fullwood, 2001; Jacek Klaudiusz Pijanka, Abass, Sorensen, Elsheikh, & Boote, 2013; Jacek Klaudiusz Pijanka et al., 2012) however, there is a distinct lack of data of the microstructural crimp.

The importance of crimp has been noted in the biomechanics community. (Fratzl, 2008; Holzapfel, 2001; Pierlot, Lee, Amini, Sacks, & Wells, 2014) The morphology of the crimp is

directly related to the amount of “slack” in collagen bundles in a process known as recruitment (Figure 5). A crimped collagen bundle is easy to stretch until taut in that only a small amount of force is needed to straighten a wavy collagen bundle. After straightening, the collagen bundle becomes much stiffer, requiring much more force to elongate the bundle. In a group of crimped collagen bundles with different amounts of slack, more and more bundles will become uncrimped, or recruited, with increasing stretch, making the overall macro-scale tissue appear stiffer. In this manner, the original configuration of the crimped collagen bundles and the rate at which they uncrimp when stretched largely determine the nonlinear stiffening response of the tissue. Note that crimp is not the only factor that can affect the nonlinear biomechanics of tissue. Other factors include the strain-dependent rotation and realignment of the collagen fibers, fiber slip, and other components of the ground matrix including elastin and proteoglycan content (Birch, Thorpe, & Rumian, 2013; C Ross Ethier et al., 2004; Fazio et al., 2014; Fratzl, 2008; Holzapfel, 2001). Despite the importance of characterizing the crimp microstructure in the eye and how the crimp gets recruited to understand eye mechanics, to the best of our knowledge there are no experimental studies of crimp in the ONH nor the rest of the posterior sclera and few that even mention this characteristic for the eye. Possibly due to the difficulty in characterizing the collagen fiber orientation on a micron-scale across large areas of the posterior pole, of the few studies addressing crimp in the sclera, most have resorted to predicting the crimp structure using inverse models rather than experimentally.(Grytz & Meschke, 2010; Grytz, Meschke, & Jonas, 2011)

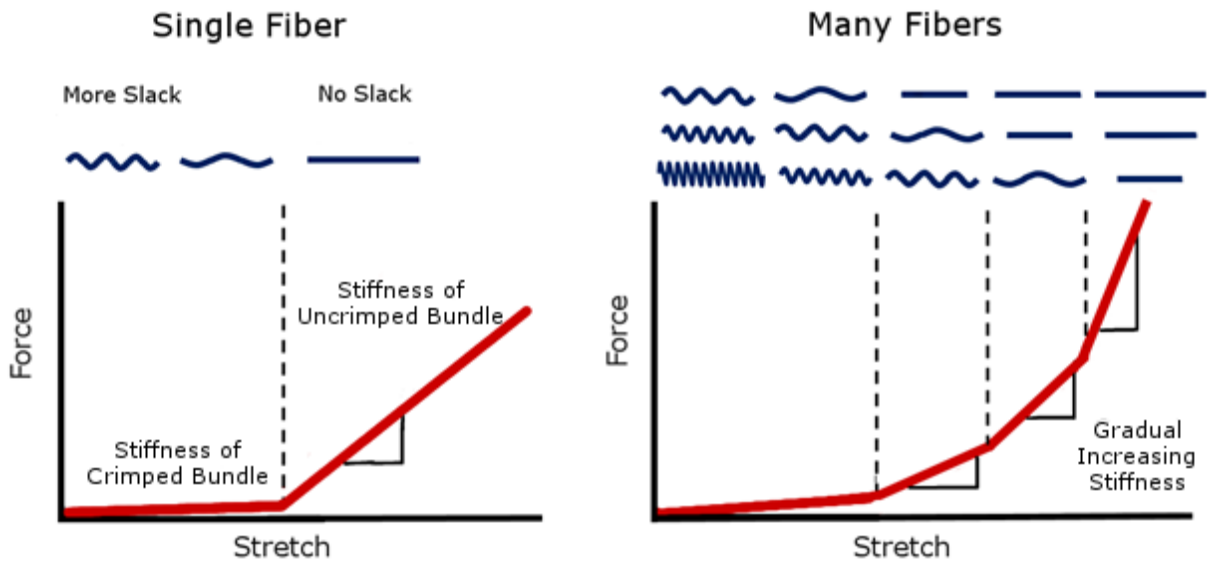

Figure 5. Uncrimping is related to tissue stiffening.

Straight fibers are stiffer than crimped fibers (left). As more fibers uncrimp, the overall tissue stiffness increases (right). This process is called recruitment.

In this project, we aim to characterize the ocular collagen crimp and how the crimp recruits with IOP and stretch. By understanding the complex biomechanical relationship between crimp and recruitment in eye tissue, we can achieve a greater understanding of the biomechanical basis of IOP sensitivity in glaucoma. This, in turn, can be used to help prevent, diagnose, and treat glaucoma.

1.3 THE NEED FOR POLARIZED LIGHT MICROSCOPY

One reason for the significant lack of information on collagen crimp in the eye is that there has not been an established imaging technique that allows measuring crimp. Measuring crimp requires an accurate and robust quantification of collagen fiber orientation with micron-scale resolution over cm-scale regions over a wide range of tissue densities. At the start of this project, we hypothesized

that polarized light microscopy (PLM) would be able to satisfy these requirements. PLM is an imaging modality that can be used to quantify the orientation of collagen fibers (Figure 6) (Bromage et al., 2003; J. Diamant, A. Keller, E. Baer, M. Litt, & R. Arridge, 1972; Keikhosravi et al., 2017). Using PLM to quantify the collagen fiber crimp in the posterior pole is innovative and has important advantages over other methods traditionally used by the ocular biomechanics community. PLM has been used for visualizing and quantifying crimp in other tissues like tendon and ligament (J Diamant et al., 1972; Hansen, Weiss, & Barton, 2001; Komatsu, Mosekilde, Viidik, & Chiba, 2002), however, to the best of our knowledge, none have applied PLM to the eye in order to systematically quantify the collagen fiber orientation and crimp. Though tendon and ligaments are similar to collagenous ocular tissues, there are differences in their structural hierarchies (Keith M. Meek & Boote, 2009) and overall organization (Girard et al., 2014; Keith M. Meek & Boote, 2004; Jacek K. Pijanka et al., 2015; Ruberti & Zieske, 2008). It cannot be taken for granted that PLM will apply to ocular tissues as it does to other tissues, and the performance of the technique must be assessed. Therefore, there is an unmet need for the characterization of the performance of PLM in quantifying the fiber orientation and crimp in the eye.

Crimp in the cornea was visualized more than 20 years ago (Andreo & Farrell, 1982; Gallagher & Maurice, 1977). Some experimental measures of corneal crimp have been reported (Liu et al., 2014; R. H. Newton, J. Y. Brown, & K. Meek, 1996). The only quantifications of crimp for the sclera and ONH have been predicted using inverse models, which have yet to be validated with experimental measures. (Grytz & Meschke, 2010; Grytz et al., 2011) Of the few studies that quantify the collagen crimp in the cornea, manual tracings were used. (Liu et al., 2014; Richard H Newton et al., 1996) Manual tracings are subject to artifacts, especially in tissue with complex overlapping interweaving fibers and tissues with high collagen density, where it is difficult to

distinguish individual fibers. In addition, manual tracings are labor-intensive and time-consuming (Rezakhaniha et al., 2012). Analyzing cm-scale pieces of tissue for micron-scale collagen fiber crimp becomes impractical.

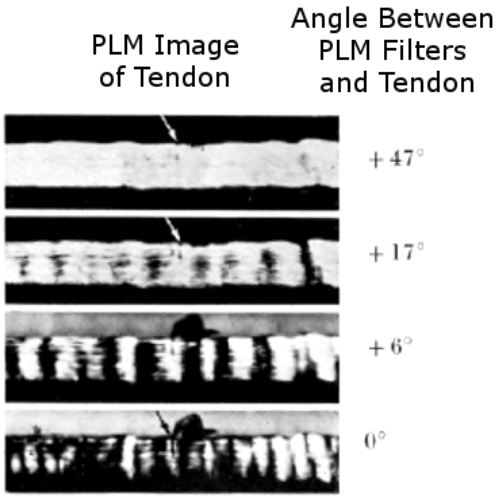

Figure 6. PLM can be used to quantify collagen fiber orientation.

PLM images of tendon taken at different angles between PLM filters and tendon sample. The signal intensity from the PLM is related to the orientation of the collagen fibers relative to the PLM filters. Using multiple images, the intensity changes can be used to determine the collagen fiber orientation. Figure adapted from (J Diamant et al., 1972).

Alternatively, a more time-efficient method that has been used to quantify the micron-scale collagen fiber orientation is the use of intensity-based edge-detection algorithms or Fourier analysis of high resolution images (Neu & Genin, 2014; Jacek Klaudiusz Pijanka et al., 2012; Rezakhaniha et al., 2012; van Zuijlen et al., 2002), of high resolution images, like those from nonlinear (Keyes, Yan, Rader, Utzinger, & Vande Geest, 2011; Winkler et al., 2011), confocal microscopy images (Rezakhaniha et al., 2012) or those constructed from Synchrotron radiation (Aghamohammadzadeh, Newton, & Meek, 2004; Coudrillier et al., 2013; Coudrillier et al., 2016). The accuracy of this method, however, is highly dependent on the image resolution and quality,

and whether the orientation of the edges in the image accurately reflect the collagen fiber orientation within. If the image quality is poor, for example, due to overexposure in dense areas of the tissue, this method will be unable to detect the edges of the fibers. Due to the large difference in collagen density between the LC and PPS (Figure 7), it is often difficult to acquire images that are optimized for both LC and PPS tissues in the ONH. In addition, the accuracy of this method is subject to artifacts when there are many overlapping fibers. The resolution of the method becomes increasingly important in this case, since higher resolution is required to distinguish between individual fibers. Because many areas of the ONH and remaining sclera contain complex collagen fiber structure, with interweaving, overlapping fibers, this method is difficult to apply to the eye. This edge detection method is also subject to artifacts from the presence of pigment, since the edges of the pigment will influence the orientation calculations.

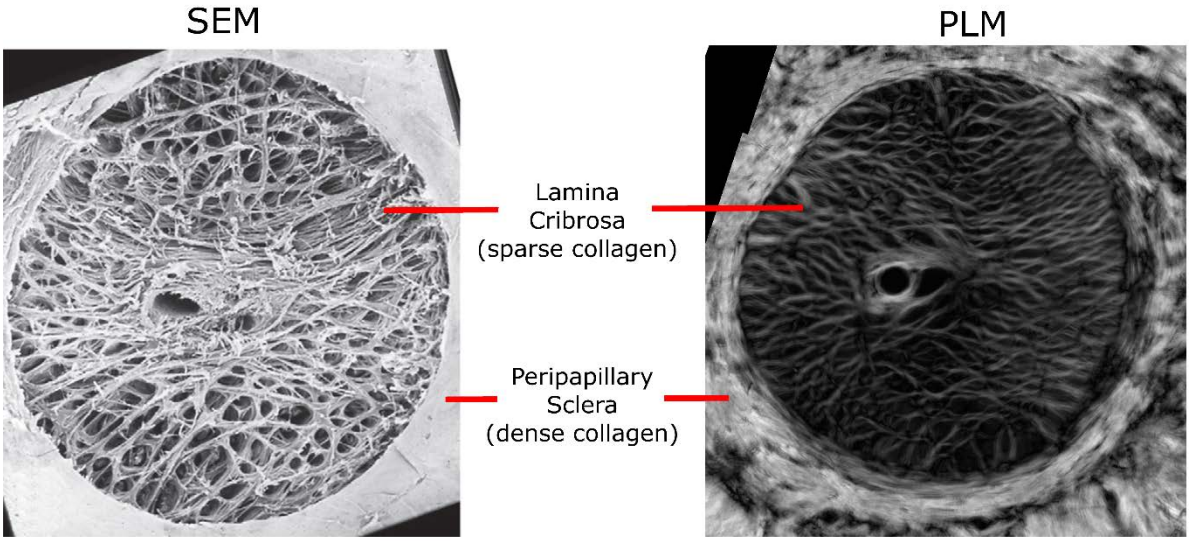

Figure 7. The LC has much sparser collagen than the surrounding PPS.

On the left is a scanning electron microscopy (SEM) image of a human ONH that has gone through tissue digestion to remove all non-collagenous tissues. On the right is a PLM image of a human ONH section. Both images show sparse collagen in the LC and dense collagen in the PPS. Note that in the SEM image it is difficult to discern individual fiber bundles in the PPS while the collagen texture is preserved in the PLM image. Left panel adapted from (Quigley, 2011).

There also exist other methods that quantify collagen fiber orientation without the need to resolve fiber edges. These methods include magnetic resonance imaging (MRI), (Ho et al., 2015; Ho et al., 2014) small-angle light scattering (SALS), (M. J. Girard, A. Dahlmann-Noor, S. Rayapureddi, J. A. Bechara, B. M. E. Bertin, et al., 2011; Yan, McPheeters, Johnson, Utzinger, & Vande Geest, 2011) and wide-angle x-ray scattering (WAXS). (Jacek Klaudiusz Pijanka et al., 2013) However, studies applying these methods to the eye have reported resolutions much worse than that required for quantifying collagen crimp. In order to visualize and quantify the collagen crimp in the eye, micron-scale resolution is required. At lower resolutions, the resulting orientation calculations would combine the contributions from overall collagen anisotropy and the microstructural crimp. Studies applying the three imaging modalities listed above report lateral resolutions >100 μm/pixel, (M. J. Girard, A. Dahlmann-Noor, S. Rayapureddi, J. A. Bechara, B. M. E. Bertin, et al., 2011; Ho et al., 2014; Jacek K. Pijanka et al., 2015) which are too low to detect micron-scale undulations in fiber orientation.

All of this evidence points to the need for a differentmethod for quantifying crimp in eye tissue. We hypothesize that PLM can quantify micron-scale collagen fiber orientation and crimp across large cm-scale areas of eye tissue. The information we derive using PLM can have far reaching applications in understanding both individual-specific IOP sensitivity and glaucoma susceptibility.

1.4 PROJECT AIMS

The long-term aim of this project is to identify biomechanical markers of individual-specific sensitivity to IOP. Specifically, the goal is to characterize the collagen architecture and crimp in

the eye and how the crimp recruits with IOP and stretch. In order to accomplish this goal, we first had to establish the performance of PLM for the study of ocular collagen architecture, and then use it to characterize ocular collagen crimp and its changes under IOP loading and stretch. The project was thus organized into the following three aims:

1.4.1 Specific Aim 1

Characterize the performance of PLM for the study of ocular collagen architecture and crimp.

1A) Test the prediction that PLM provides accurate and repeatable micron-scale collagen fiber orientation and crimp measurements in eye tissue, robust to fixation, the presence of pigment, changes in magnification, and large differences in collagen density and organization between the LC and PPS.

1B) Test the prediction that PLM can quantify the micron-scale collagen fiber orientation and crimp across large cm-scale regions of the eye.

1.4.2 Specific Aim 2

Characterize the baseline crimp in the eye by testing the hypotheses that:

2A) The collagen bundles of LC trabeculae beams are crimped at baseline. Specifically, we test the hypothesis that LC trabeculae beams inserting into the scleral canal have different crimp than those that do not.

2B) PPS collagen bundles are crimped at baseline. Specifically, we test the hypotheses that the crimp of the PPS is different than that of the LC and that regions of the PPS farther away from the LC have larger differences in crimp.

2C) Collagen bundles around the whole globe are crimped at baseline. Specifically, we test the hypotheses that there are significant differences in crimp between regions around the eye globe.

1.4.3 Specific Aim 3

Characterize how ocular collagen crimp changes with mechanical loading by testing the hypotheses that:

3A) ONH crimp changes with increased IOP. Specifically, we test the hypothesis that the rate of recruitment of the PPS collagen bundles is different than that of the LC beams.

3B) Equatorial scleral crimp changes with uniaxial stretch. Specifically, we test the hypothesis that rate of recruitment of equatorial sclera is independent of tissue depth.

1.4.4 Dissertation Outline

The dissertation has been organized into 8 chapters as follows:

Chapter 1: Introduction to glaucoma, biomechanics, and crimp, including evidence that a new imaging modality is needed to analyze collagen crimp in the eye. This chapter also introduces the aims of the project.

Chapter 2: The development of PLM for use in eye tissue, including tests of accuracy, repeatability, and robustness. This chapter addresses Specific Aim 1A.

Chapter 3: PLM is leveraged to quantify the collagen fiber orientation across cm-scale ONH tissue. This chapter addresses Specific Aim 1B.

Chapter 4: The baseline crimp distribution in the ONH and how the crimp in the LC differs from that of the PPS. This chapter addresses Specific Aim 2A and 2B.

Chapter 5: The baseline crimp distribution around the eye globe. This chapter addresses Specific Aim 2C.

Chapter 6: ONH crimp changes with IOP increases, including recruitment of the collagen fibers in the LC beams and PPS. This chapter addresses Specific Aim 3A.

Chapter 7: Effects of uniaxial stretch on the equatorial collagen fibers crimp. This chapter addresses Specific Aim 3B.

Chapter 8: Dissertation Synopsis. This chapter summarizes the findings for each aim, the limitations of the project, and future work.

2.0 DEVELOPING AND TESTING THE USE OF POLARIZED LIGHT MICROSCOPY IN EYE TISSUE

The content of this chapter, other than the "addendum" at the end, was previously published in (Jan et al., 2015).

2.1 INTRODUCTION

Several leading causes of visual impairment such as myopia (Pruett, 1988), glaucoma (Sigal & Ethier, 2009), and keratoconus (Romero-Jiménez, Santodomingo-Rubido, & Wolffsohn, 2010) are associated with abnormal ocular connective tissues (Girard et al., 2014). Hence, to preserve vision, it is important to characterize two elements central to connective tissues, namely the orientation and organization of the collagen fibers that form them (K. M. Meek & Fullwood, 2001; Watson & Young, 2004). Several techniques have been developed for measuring collagen fiber orientation and organization, including small angle light scattering (M. J. A. Girard et al., 2011; Dongmei Yan, Sheridan McPheeters, Gregory Johnson, Urs Utzinger, & Jonathan P. Vande Geest, 2011b), x-ray scattering (Coudrillier, Abel, Albon, Campbell, & Ethier, 2014; Coudrillier et al., 2013; Keith M. Meek & Boote, 2009; Jacek K. Pijanka et al., 2012), non-linear microscopy (Donald J. Brown, Naoyuki Morishige, Aneesh Neekhra, Don S. Minckler, & James V. Jester, 2007; M. J. A. Girard et al., 2011; Morishige et al., 2007) and magnetic resonance imaging (Ho et al., 2014;

Mountain, Bjarnason, Dunn, & Matyas, 2011), or for estimating them using inverse numerical methods (M. J. A. Girard, J. C. Downs, M. Bottlang, C. F. Burgoyne, & J. K. F. Suh, 2009; Grytz et al., 2011). The complexity of the eye calls for a technique that provides data at multiple scales, including high resolution (micron-scale) and broad field-of-view (several mm to cm)(C. Ross Ethier, Mark Johnson, & Jeff Ruberti, 2004). The techniques mentioned above, however, are not fully satisfactory because they lack the resolution or field-of-view, are slow and subjective (e.g. requiring manual fiber tracings), or are susceptible to artifacts (e.g. due to the presence of pigment).

We hypothesized that polarized light microscopy (PLM) would overcome these obstacles and prove a valuable technique for use in ophthalmology. PLM has been proven effective to characterize collagen of tendons (J. Diamant, A. Keller, E. Baer, M. Litt, & R. G. C. Arridge, 1972; Szczesny et al., 2012), ligaments (Komatsu et al., 2002) and other soft tissues (Kalwani et al., 2013). The possibility of using PLM in the cornea was discussed almost two decades ago for ex-vivo tissues (R. H. Newton, J. Y. Brown, & K. M. Meek, 1996), and more recently to study the cornea stroma in vivo (Misson, 2007). However, the accuracy, repeatability and robustness of the technique when applied to ocular tissues remains to be determined.

Tendon and ligaments are generally similar to collagenous ocular tissues in terms of extracellular matrix composition (Nordin & Frankel, 2001), but there are differences in their structural hierarchies (Keith M. Meek & Boote, 2009) and overall organization (Girard et al., 2014; Keith M. Meek & Boote, 2004; Jacek K. Pijanka et al., 2015; Ruberti & Zieske, 2008). Therefore, it cannot be taken for granted that PLM will apply to ocular tissues as it does to other tissues, and the performance of the technique must be assessed. Our goals were to quantify the accuracy, repeatability and robustness of PLM to measure micron-scale collagen fiber orientation of ocular

tissues, demonstrate that this can be achieved with broad, cm-scale, field-of-view, and thus establish PLM as a technique that yields objective information on the microstructure of the eye.

2.2 METHODS

Below, we describe, roughly in order of increasing complexity, the series of tests used to evaluate the accuracy, repeatability and robustness of PLM when used to measure collagen fiber orientation of ocular tissues. Achilles tendon and silk were used as reference materials, as their fiber orientations are well reported. Finally, we demonstrate the power of PLM by imaging a whole-globe section. Image processing and analyses were done using standard and custom code in Fiji (Schindelin et al., 2012).

2.2.1 Sample preparation.

Fresh eyes and Achilles tendons from two years old healthy sheep were obtained from a local slaughterhouse and processed within 8 hours of death. The eyes were cannulated through the anterior chamber and intraocular pressure set using a fluid column to either a low (0 or 5 mmHg) or high (50 mmHg) pressure (normal sheep intraocular pressure is 10-15 mmHg (A Bouhenni, Dunmire, Sewell, & Edward, 2012)). The eyes were then immersion fixed with 10% formalin overnight while maintaining intraocular pressure. The anterior poles were excised with a razor and cryosectioned sagittally into 30 µm thick sections. The posterior poles were excised using an 8 mm trephine and cryosectioned coronally into 30 µm thick sections. One eye was cryosectioned

sagittally whole, into 30 µm thick sections. Note that no labels or stains were applied to the eye tissue sections.

The tendons were loaded longitudinally using clamps affixed to a set stretch within the linear region of the loading profile (i.e. after the toe-region from collagen fibers straightening or uncrimping and before failure) (Hansen et al., 2001). After allowing for equilibration in the loaded condition for one hour in phosphate buffered saline (PBS), the PBS was replaced with 10% formalin and left overnight to fix. The tissue was cryosectioned into 50 µm thick longitudinal sections. One slide was dehydrated using ethanol, stained with hematoxylin and eosin (H&E), and mounted with xylene.

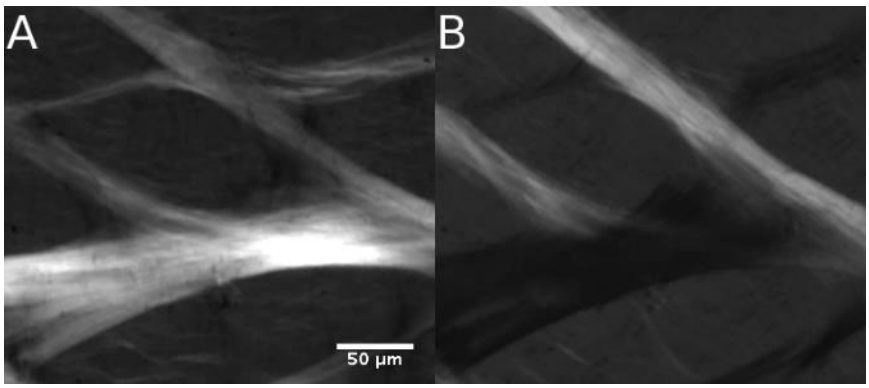

Figure 8. Example polarization microscopy images of sheep lamina cribrosa trabeculae.
The images were acquired with two different filter setups (A and B) differing by a 45° rotation. Although the trabecular structure of the lamina cribrosa is discernible in both images, the intensity varies with the relative orientation of the fibers and the filters.

2.2.2 Imaging and visualization.

Tissue samples were imaged using standard bright-field imaging as well as PLM according to the protocols described by Kalwani and colleagues (Kalwani et al., 2013). Briefly, a white light source and two polarizing filters were used (Hoya, Tokyo, Japan). The light passed through a polarizer,

the sample, and an analyzer. A birefringent material, such as collagen, alters the polarization state of the light, resulting in increases or decreases of the light intensity observed after the analyzer depending on the relative orientation between the sample and the filters (Figure 8). Multiple images were acquired with various filter orientations relative to the sample separated by 45°. The images were registered and the signal intensities from the multiple images were used to compute local orientation at each pixel (Kalwani et al., 2013). For visualization, the fiber orientation at each pixel was also weighted by a parameter we denoted "energy" (Eq. 1):

$$energy^2 = (I_{90} - I_0)^2 - (I_{135} - I_{45})^2 \quad (1)$$

where I_α is the pixel intensity at an angle α to the analyzer direction (Figure 9). Energy is thus large when there is a substantial change in signal with angle, and zero when there is no change, such as outside of the tissue.

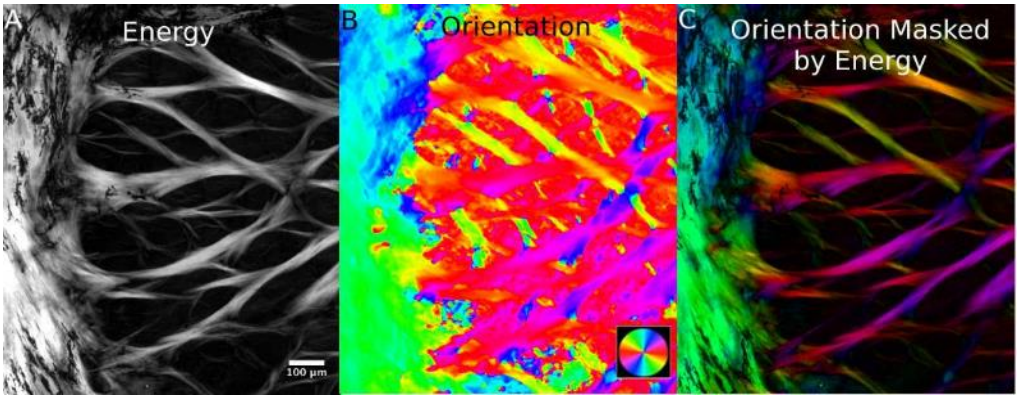

Figure 9. Example results in a region of the peripheral lamina cribrosa and sclera.
The main output from our technique was a local (pixel) measure of orientation (B). In a direct plot of orientation it is difficult to distinguish the structures of interest. To improve visualization, we also computed for each pixel the energy, as defined in the main text (A). The energy was then used to scale the brightness of the orientation maps producing an image of orientation "masked by energy" (C). This image allows easily discerning the trabecular structure of the lamina cribrosa simultaneously with the collagen fiber orientation. For clarity, all other orientation images in this manuscript are shown masked. Analyses were done with unmasked orientations.

To increase generality, we evaluated PLM with two microscope-camera pairs. For an Olympus BX60 microscope (Olympus, Tokyo, Japan) with a SPOT camera (SPOT Imaging Solutions, Sterling Heights, MI), image resolution was 1.48 μm/pixel using the 4x objective (NA 0.13) and 0.73 μm/pixel using the 10x objective (NA 0.3). For an Olympus SZX16 microscope with an Olympus DP80 camera and 0.8x objective (NA 0.12), image resolution was 0.37 μm/pixel with the 11.5x magnification setting and 4.4 μm/pixel with the 1x magnification setting.

2.2.3 Accuracy in tendon, single fibers, and cornea.

We evaluated the accuracy by comparing the PLM measurements of fiber orientation with those from manual tracings. Manual tracing is a relatively common method used to determine fiber orientation in soft collagenous tissues (Franchi et al., 2007; Hill, Duan, Gibson, Watkins, & Robertson, 2012; Stokes, McBride, Aronsson, & Roughley, 2011), and permits comparing with a reference set by an expert. We conducted three test cases: loaded tendon fibers, a single curved silk fiber, and a sample of cornea from an eye at high intraocular pressure.

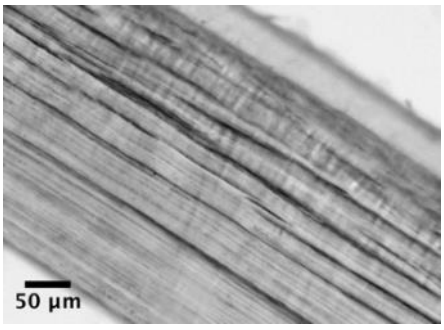

Figure 10. Image of a sagittal section through the cornea of an eye fixed at 50mmHg.
Analysis focused on the inner cornea region where the fibers displayed least undulations (bottom left).

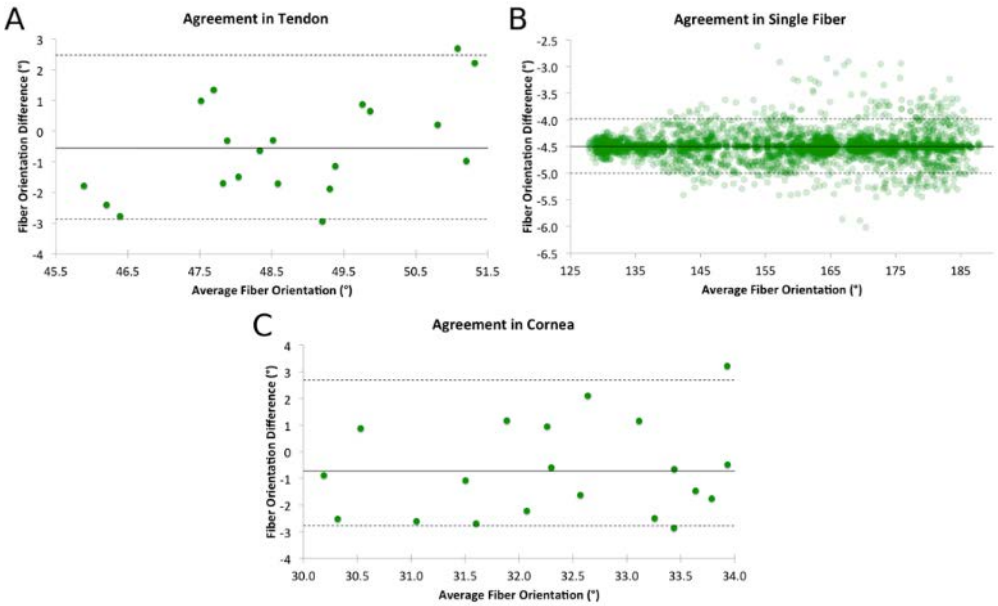

Figure 11. Bland-Altman plots of the agreement between manual markings and PLM orientation measurements in tendon (A), a single curved fiber (B), and cornea (C).

For the tendon and cornea tests, the mean PLM orientation for each line was used to construct the plot whereas every point was used for the single fiber. The dotted lines represent the 2.5th and 97.5th percentiles of the orientation differences. We note that since our goal was to determine whether the two measurement methods (manual and PLM) produced the same results, a mixed effects model was not the appropriate analysis tool. Using a mixed effects model would have required us to define apriori a criteria for measurements to be the same. Instead of making such an arbitrary call, we present the results as obtained and show agreement.

In the first and simplest case, Achilles tendon fibers were straightened, as described in Section 2.1 above. A section through central tendon was imaged using the Olympus 10x objective. Manual measurements of the fiber orientation were obtained using 20 straight lines 6-16 μm long tracing the fibers of the tendon, and compared pixel-by-pixel with the fiber orientation determined using PLM. Absolute error was defined as the absolute difference between the manual and automated measurements. To account for systematic errors from manual tracing, we also calculated the relative error, which we defined as the difference between the automated measurements for a trace and the mean of those measurements along that trace. In straight fibers,

as long as the trace is made in the same fiber, the measurements should be the same, and therefore, large variations were considered as errors by PLM.

In the second test, we placed a single curved silk fiber onto a glass slide, allowing it to rotate freely to release torsional stresses, and imaged it using the Olympus 10x objective. One long spline trace of the fiber was used, and the interpolated angle of the spline was compared to the automated orientation calculated by PLM at all pixels along the trace. The absolute and relative errors were calculated as above.

The third case replicated the first test, using corneal tissue. We selected a region through the central inner cornea of an eye fixed at 50 mmHg intraocular pressure, to reduce the effects of collagen undulations, or crimp (Liu et al., 2014), or of transverse fibers at odd angles (Winkler et al., 2013b) and imaged it using the Olympus 10x objective (Figure 10). Similar to the first test, 20 manual straight-line traces were used. The cornea traces were 5-20 μm long. Once more, the absolute and relative errors were calculated as above.

For all three tests, Bland-Altman plots were also constructed to check for agreement between the marking and the PLM calculations (Figure 11).

2.2.4 Repeatability of orientation accounting for common variations in the imaging protocol.

Next, we evaluated the repeatability of PLM using sheep optic nerve head tissue, which is more challenging due to the complexity of the architecture, the multiple fibers packed together, and the range of fiber densities. We evaluated the repeatability under three potential sources of variation that can cause artifacts: magnification (Lowe, 2004), mosaic stitching (Preibisch, Saalfeld, & Tomancak, 2009), and tight fiber packing (Helmchen & Denk, 2005). We selected and imaged a

section through the lamina cribrosa of an eye fixed at high 50 mmHg intraocular pressure using Olympus 4x and 10x objectives. Images using the 10x objective were captured in a 2x2 mosaic (~20% overlap) to cover the same tissue region as with the 4x objective, and to evaluate the effects of stitching. Three image sets were acquired with each objective, yielding three measures of orientation at each pixel for each magnification. To determine repeatability, we registered the images of a given magnification and calculated at each pixel the fiber orientation difference between the orientation in that image and the mean pixel orientation across the three image sets at that magnification. To identify any potential effects of magnification, we compared the automated fiber orientation measurements between images acquired using the Olympus 4x and 10x objectives. Some current techniques for quantifying local connective tissue orientation are affected by tissue density (Donald J. Brown et al., 2007; M. J. A. Girard et al., 2011). Hence, we also split the data into sparse (lamina cribrosa beams) and dense (sclera) collagen fibers by manually segmenting the regions. To ascertain where the measurements were most variable, we also constructed images of the fiber orientation of the 3 trials using orientation lines for a visual representation of the fiber orientation differences. These lines were computed as the mean orientation over a region 12 μm in diameter.

2.2.5 Robustness to sample translation and rotation.

Our next experiment evaluated the robustness of PLM to sample translations and rotations using optic nerve head tissue from eyes at low intraocular pressure. This is a more challenging test than those above because at low intraocular pressure the collagen fibers are crimped or wavy. Measurements of these micron-scale variations in fiber orientation are more sensitive to changes in image orientation and translation. A section through the lamina cribrosa was selected and

imaged using the Olympus 10x objective. Between each image set acquisition, the sample was rotated 5° and translated. The translations were random in the plane of the sample, while still allowing a small area of interest to remain within the field-of-view. We acquired a total of 19 image sets, each at a different angle between 0° and 95°. As a measure of robustness we compared the sample orientation change with the change measured using PLM. Only areas that overlapped in all 19 image sets were analyzed. The whole area of overlap on all images was analyzed, including areas with pigment. Pigment can be a problem for other methods currently used for fiber orientation quantification because it absorbs light reducing signal and causing artifactual edges.(Neu & Genin, 2014)

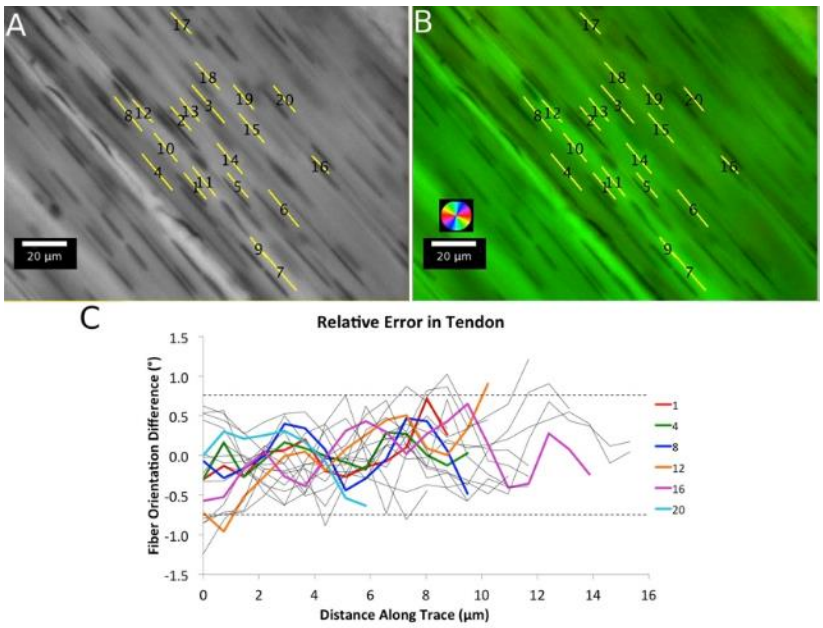

Figure 12. Accuracy in loaded tendon tissue.

Using images of loaded tendon (A), we compared PLM orientation (B) with orientation of manual traces. The relative error was small for all 20 traces (C). For clarity, six traces were highlighted in color, with the rest shown in grey. The dotted lines represent the 2.5th and 97.5th percentiles of the orientation differences.

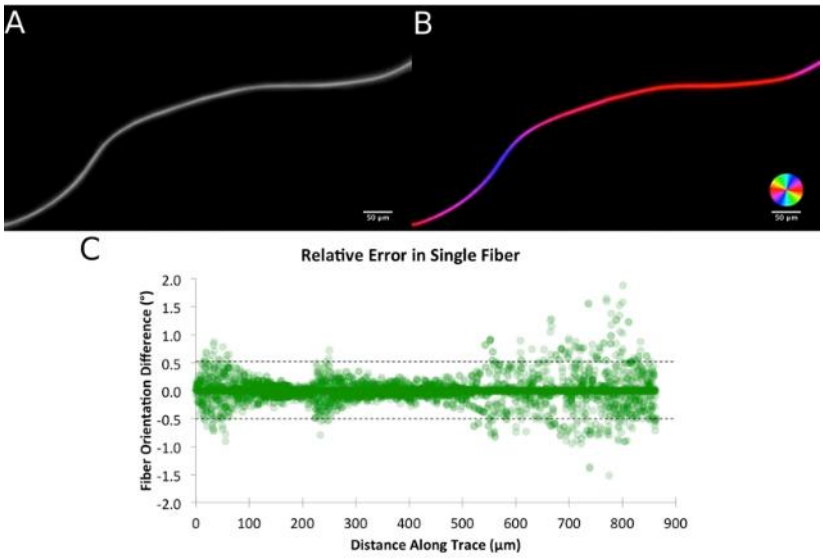

Figure 13. Accuracy in a single curved silk fiber.

Using images of a single curved silk fiber (A), we compared PLM orientation (B) with the interpolated orientation along a curved manual trace. The relative error was small along the entire trace (C). The dotted lines represent the 2.5th and 97.5th percentiles of the orientation differences.

2.2.6 Robustness to tissue fixation.

Formalin fixation has been shown to affect optical polarization properties of myocardium and liver samples(Wood, Vurgun, Wallenburg, & Vitkin, 2011), and therefore fixation could affect our measurements in ocular tissues. To quantify the effects of formalin fixation on PLM-measured fiber orientation we used the following experiment: a fresh sheep eye was cryosectioned sagittally into 30 µm thick sections. The unfixed sections were placed on glass slides and equatorial sclera was imaged with PLM (SZX16 microscope, 11.5x magnification setting, 0.8x objective), before and after immersing the section in 10% formalin for 1 hour. We then quantified the differences in local fiber orientation before and after fixation.

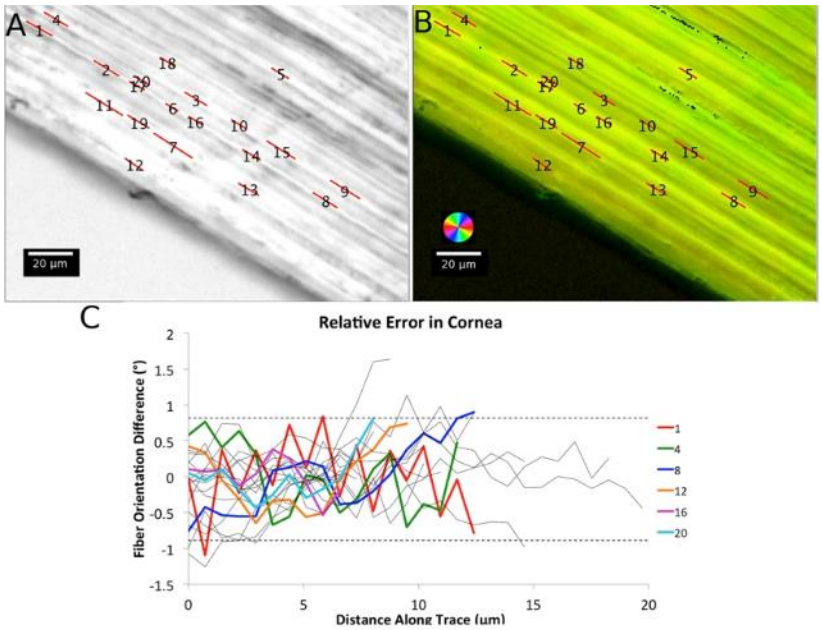

Figure 14. Accuracy in pressurized corneal tissue.

Using images of pressurized corneal tissue (A), we compared PLM orientation (B) with orientation of manual traces. The relative error was small for all 20 traces (C). For clarity, six traces were highlighted in color, with the rest shown in grey. The dotted lines represent the 2.5th and 97.5th percentiles of the orientation differences.

2.2.7 Demonstration of PLM over the globe.

We demonstrate the power of the technique over a broad field-of-view by imaging and analyzing an axial section of a whole sheep eye (~3 cm in diameter) fixed at 0 mmHg (SZX16 microscope, 1x magnification, 0.8x objective). We found this image to be clearest when masked by retardance.(Kalwani et al., 2013).

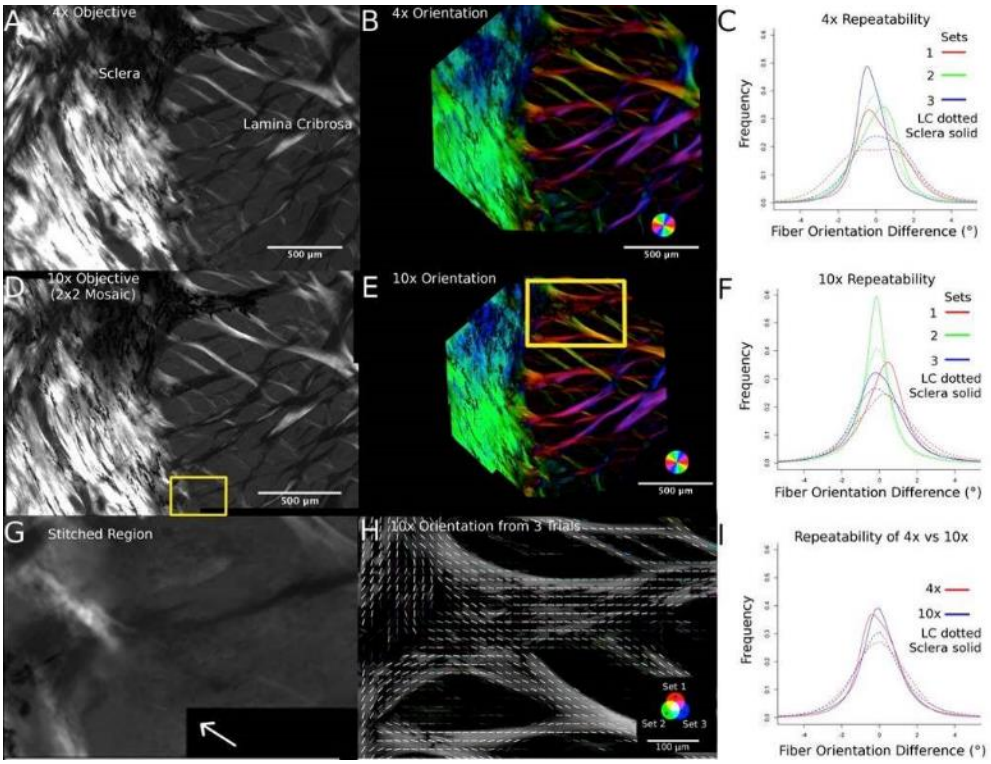

Figure 15. Repeatability in optic nerve head tissue.

Three image sets were captured using 4x and 10x objectives of a section of sheep optic nerve head tissue (A and D) and for each image set, the fiber orientation was calculated (B and E). The measurements were highly repeatable regardless of resolution (I) and tissue density (C and F) and there were no stitching artifacts (arrow in G indicates stitched region). The frequencies in panels C, F and I have been normalized to the total number of measurements. The fiber orientations from each image set were color coded and compared such that white indicated perfect agreement, and colors represented differences. The majority of the orientation lines are white (H).

2.3 RESULTS

2.3.1 Accuracy in tendon, single fibers, and cornea.

For the loaded tendon case (Figure 12) the average absolute error was 0.9°. The relative error had a standard deviation of 0.4° with 95% of the PLM measurements within 0.8°. For the single curved silk fiber (Figure 13), the average absolute error was 4.5°. The relative error had a standard

deviation of 0.2° with 95% of PLM orientation measurements within 0.5°. For the cornea at high intraocular pressure (Figure 14), the average absolute error was 1.5°. The relative error had a standard deviation of 0.4° with 95% of the PLM measurements within 0.8°. Overall the absolute error was under 5°, and after accounting for systematic error, relative errors were under 2°. Images were acquired in less than a minute, and PLM analyzed in a few seconds.

2.3.2 Repeatability of orientation accounting for common variations in the imaging protocol.

For the pressurized sheep optic nerve head, measurements were highly repeatable, even when accounting for variations between magnifications, potential stitching artifacts, and varying tissue density (Figure 15). For the images taken with the Olympus 4x objective, we found that 95% of the variability was within 3.5° (Figure 15 A, B, C), and for stitched images taken with the Olympus 10x objective, 95% of the variability was within 4.2° (Figure 15 D, E, F). Both magnifications had very similar fiber orientation variability distributions (Figure 15 I), demonstrating high repeatability across resolutions, without visible stitching artifacts in the 2x2 stitched mosaic (Figure 15 G). The orientation lines showed very few differences. When there were differences, the magnitude of the differences was small (Figure 15 H). Repeatability was high regardless of tissue density. We found that for the sparser tissue, (lamina cribrosa), the 95% of the variability was within 4.6°, whereas for the denser tissue (sclera), it was within 1.9° (Figure 15 C, F).

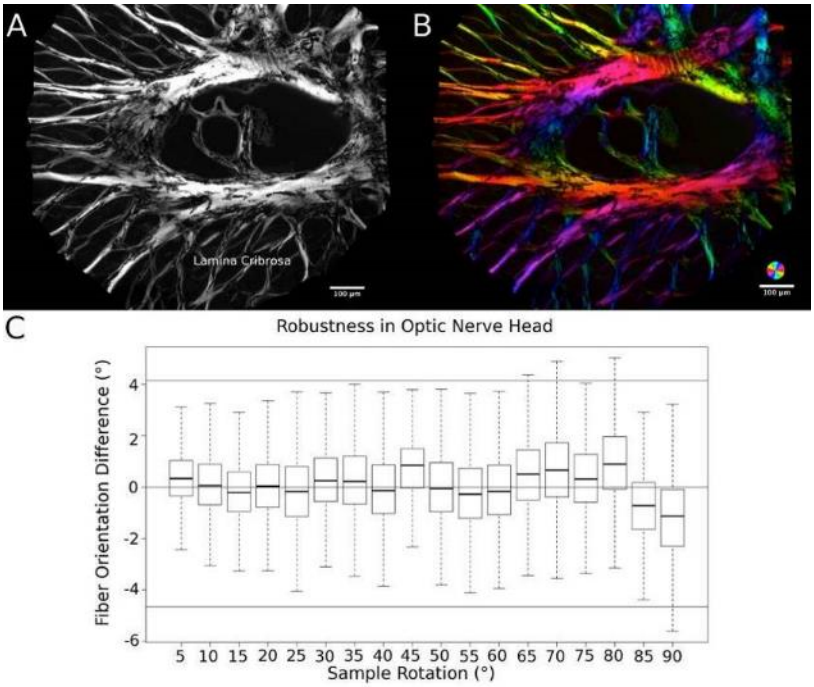

Figure 16. Robustness in optic nerve head tissue.

Image sets of sheep lamina cribrosa were taken (A) and for each set the fiber orientation was calculated (B) (see Visualization 1). The tight distributions through the different sample rotations show that our measurements are highly robust (C). The solid lines above and below represent the 2.5th and 97.5th percentiles of the orientation differences.

2.3.3 Robustness to sample translation and rotation.

The measurements for the unloaded optic nerve head were robust to sample translation and rotation. For each of the sample translation and rotations, the mean and standard deviation of the error was calculated. From these 18 error distributions, the maximum mean error was 1.1° and the maximum standard deviation of 2.9°. When pooling the error distributions, 95% of the error was within 4.7° (Figure 16) Even in areas with pigment on the lamina beams (Figure 17) (Roberts et al., 2009), the calculated orientations were smooth and continuous with adjacent unpigmented regions, demonstrating that the method was robust and produced satisfactory results.

2.3.4 Robustness to tissue fixation.

The fiber orientation measurements were robust to formalin fixation (Figure 18), with differences between fresh and 1 hour fixing of 0.58° (mean), 0.61° (median) and 2.4° (SD).

2.3.5 Demonstration of PLM over the globe

The fiber orientation was calculated using PLM over a whole globe axial section (Figure 19).

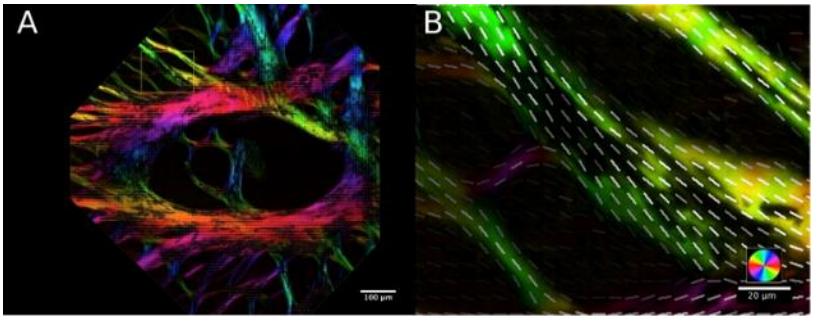

Figure 17. Using polarization microscopy in areas of low energy.

Shown is a region of the central lamina cribrosa (A), and a close-up of a couple of laminar beams with pigment (B). For clarity, in addition to color, orientation is also displayed with white lines. These lines represent the mean orientation in a square region centered at the line mid-point with size equal to half the line length. The orientations look reasonable and smooth, indicating that PLM is robust despite regions of low energy.

2.4 DISCUSSION

We have demonstrated that PLM is a powerful technique for the study of ocular tissues, producing accurate, repeatable and robust measurements of collagen fiber orientation at micron-scale over cm-scale regions, which were not affected by formalin fixation. The measurements were obtained

quickly and without the need for subjective manual tracings, or potential artifacts from staining, labeling or pigment. These results are important for the broad range of applications in which it is necessary to characterize the collagen structures of the eye, from fundamental understanding of eye physiology, to insight into the causes and changes associated with pathology and transplants.

PLM measurements of collagen fiber orientation were highly accurate, with 95% of the differences to manual tracings within 1°, and worst-case-scenario absolute differences under 5°. These differences are on the order of the repeatability in manual tracings. Differences could also be due to fiber torsion, or sub-fiber structures(Szczesny & Elliott, 2013), that are detected by PLM orientation but indistinguishable for tracing. PLM measurements were also highly repeatable, with 95% of the differences between sessions under 4°, across magnifications and mosaic stitching. Repeatability becomes increasingly challenging at higher magnifications as finer details of the structure become distinguishable, which must be consistent across images. Our method had slightly worse repeatability in higher magnification images, but measurements were still highly repeatable. Stitching artifacts can occur with image problems such as high noise, imperfect calibration, poor or irregular focus, or lack of consistent illumination. Our stitched mosaics had no noticeable edges, making for seamless mosaics, greatly extending the regions that can be analyzed from the relatively small field-of-view of a single image.

Accuracy and repeatability were not affected by collagen density, producing similarly reliable results in sparse regions, like the lamina cribrosa, and dense regions, like the sclera. Whereas other techniques of fiber analysis are challenged by either low(M. J. A. Girard et al., 2011) or high(Donald J. Brown et al., 2007) collagen densities, PLM can be used to do fair comparisons independent of density.

PLM measurements were robust to sample translation and rotation as well as formalin fixation, with differences in fiber orientation only slightly larger than repeatability. Small fixation effects were expected since immersion of the section in fixative may cause slight tissue displacement, deformation and shrinkage (Wood et al., 2011).

There is a growing number of techniques for characterizing collagen fiber architecture of ocular tissues at the micron-scale. For many years, the most common techniques relied on visual inspection of tissue sections (Jonas, Königsreuther, & Naumann, 1992). In addition to being subjective and slow, these techniques required tissue dehydration, staining and/or labeling which add variability and affect the measurements badly due to shrinkage. PLM, does not require processing the tissue in these ways, and is therefore more likely to have high fidelity. Further, sections imaged with PLM remain available for other work. For example, labeling to confirm the type of collagen (Albon, Karwatowski, Avery, Easty, & Duance, 1995).

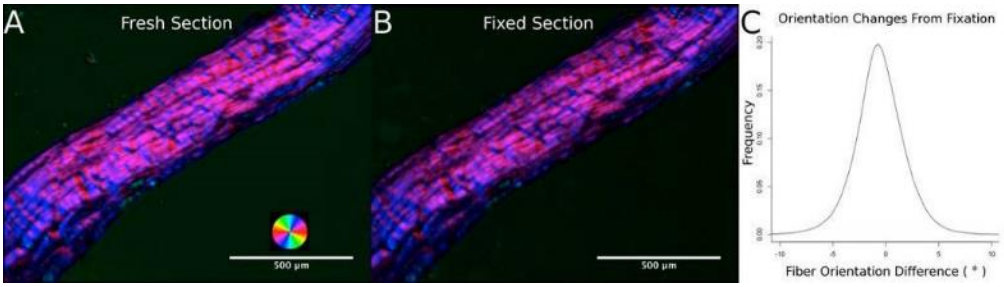

Figure 18. PLM orientation before and after fixation.

PLM Images of PLM-determined fiber orientation of equatorial sclera fresh (A) and after 1 hour fixation in 10% formalin (B). Orientations were compared at every pixel within the tissues (C).

In recent years, nonlinear microscopy has become increasingly common for the study of collagen architecture at the micro-scale, in large part due to the power of optical sectioning not available in our implementation of PLM (Jacek K. Pijanka et al., 2015; Quantock et al., 2015).

After imaging, fiber orientation is obtained through either manual tracings (Hill et al., 2012) or some form of an intensity-based method such as gradient, edge-detection, Fourier analysis, and others (Neu & Genin, 2014; Rezakhaniha et al., 2012). Intensity-based methods, while not subjective or as slow as manual tracings, have important downsides compared with PLM. Most notable is that fiber orientations can only be reliably quantified when the fibers can be clearly distinguished from one another. Hence, the effectiveness of intensity based methods decreases when the tissues are dense, when the edges of fibers cross or overlap, or in any situation where the visible edges do not represent the true orientation of the underlying collagen, such as when there is fiber torsion or twist, or fiber fractures. To reduce these problems, intensity based methods typically require higher magnifications, and much longer imaging times, than PLM. Intensity based methods also produce invalid results within or near pigment. This is important because pigments are common in several species of interest in ophthalmology research, such as non-human primates, pigs, sheep and rats. Due to the high absorbance, pigments also increase the risk of thermal damage to the tissues. In contrast, PLM measurements are objective, fast, without the risk of thermal damage and often producing excellent results even through pigmentation. Further, through energy, PLM provides a measure of signal at a pixel, which can be used to estimate the quality of a local measure.

There is also great interest in characterizing ocular collagen architecture at large scale, and several techniques have been developed to this effect, including small-angle light scattering (M. J. A. Girard et al., 2011; Yan, McPheeters, et al., 2011b), small angle x-ray scattering (Boote, Hayes, Newton, Puri, & Meek, 2003; M. J. A. Girard et al., 2011), and wide angle x-ray scattering (WAXS)(Jacek K. Pijanka et al., 2012). WAXS has recently been applied to the whole eye. (Jacek Klaudiusz Pijanka et al., 2013) Like PLM, these methods are based on the molecular characteristics

of collagen. However, these methods have substantially worse resolutions than PLM. For example, measurements using small angle light scattering had 300-500 μm transverse resolution (Yan, McPheeters, et al., 2011b), which is insufficient to capture the details of lamina cribrosa architecture. Depth resolution is also usually worse than for PLM, with noise and other problems worsening as the sample thickness decreases, such that the detriments are already substantial even for a relatively thick 50 μm thick sample.(M. J. A. Girard et al., 2011) We have shown transverse PLM resolutions on the order of 1 μm/pixel. Depth resolution in our PLM implementation is set by the thickness of the histological sections, in this study of 30 μm. In preliminary studies (data not shown) we have obtained excellent results for untreated sections as thin as 8 μm, and in 1 μm-thick sections treated with picrisirius red (to enhance collagen birefringence). Synchrotron radiation has also been used to acquire micron-scale resolution data from ocular tissues (Coudrillier et al., 2014; Keith M. Meek & Boote, 2004), but the super-specialized equipment needed makes it less widely available than PLM.

By enabling fast measurement at both macro and micro-scales, PLM promotes a multi scale characterization of ocular tissues, averting the problems of having to combine data from disparate imaging modalities, which typically have different limitations and are therefore not well suited for superposition.

It is important to consider the limitations of PLM and our analysis in this work. The orientation data obtained is only on the plane of the section, two-dimensional, while the architecture of collagen fibers in ocular tissues is three-dimensional. This limitation, however, is shared by most methods used to characterize ocular collagen. Often, methods that can, in theory, provide three-dimensional information, such as nonlinear imaging, are still used in two-dimensions due to the complexities of the tissue (Jacek K. Pijanka et al., 2012; Ian A. Sigal et al., 2014). Also,

the orientation data obtained from our PLM at each pixel represents the predominant fiber orientation at that point. It is possible that several fibers with various orientations pass through a pixel, especially at the lower magnifications. Use of thinner sections would reduce this effect. Another limitation is the use of tissue sections, which can introduce artifacts due to warping. These effects can be reduced by the use of unwarping techniques using embedded fiducial markers (Sigal, Flanagan, Tertinegg, & Ethier, 2010). Finally, we obtained good data from both microscope-camera setups, but we did not directly compare these and it is possible that the choice of camera can affect the measurements. Considering the above, we note that we see PLM as complimentary to scattering-based techniques, which have tremendous potential in ophthalmology due to their ability to obtain data from thick samples.

We have demonstrated that PLM enables a fast, objective, accurate, precise, repeatable and robust multi-scale characterization of collagen fiber orientation in ocular tissues, without the need for tissue dehydration, labeling or staining. This fiber orientation information has powerful applications in ophthalmology, including understanding the role of collagen architecture in normal physiology and aging, as well as in pathology.

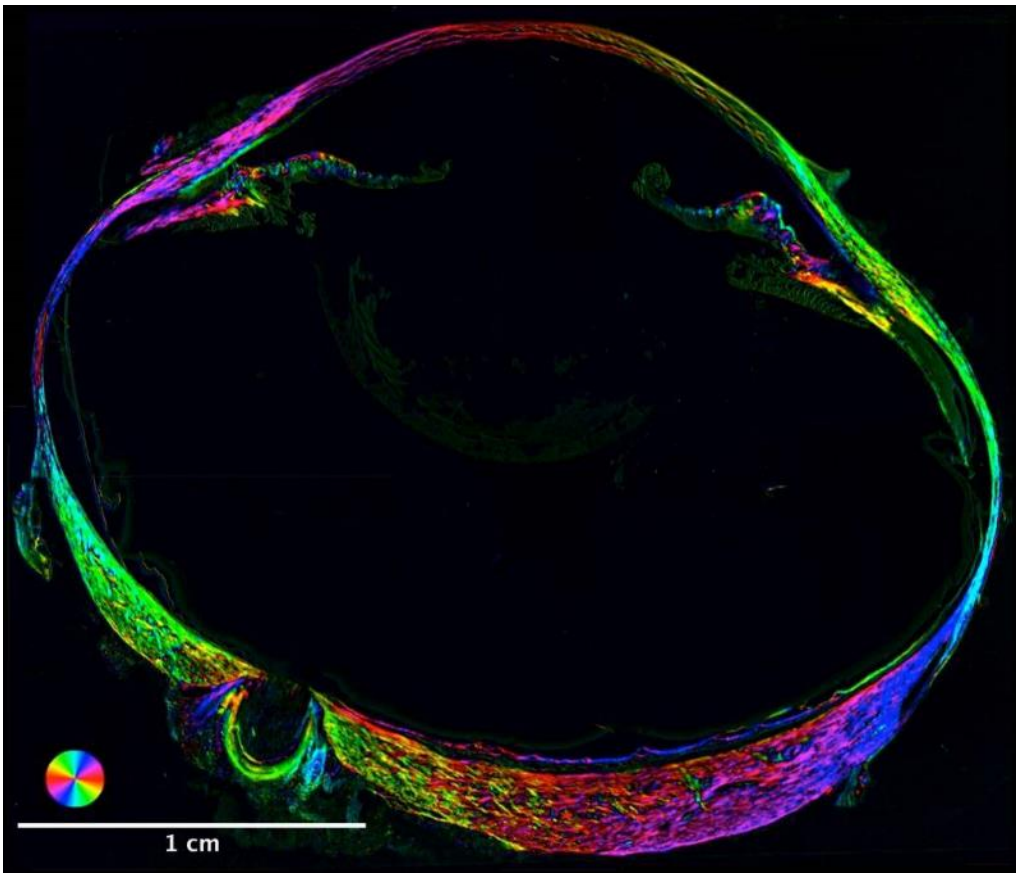

Figure 19. PLM image of a whole-globe axial eye section.

This image demonstrates the objective quantification of collagen fiber orientations over a broad field-of-view.

2.5 ADDENDUM FOR THE DISSERTATION

To further validate our PLM technique, we also compared it with polarization-sensitive second harmonic optical microscopy. This is described in Appendix A. We found an excellent correspondence between the two techniques. Interestingly, the preliminary results suggest that the combination of both techniques will reveal structural details not available to either technique alone.

3.0 RADIAL, CIRCUMFERENTIAL, AND INTERWEAVING FIBERS IN THE OPTIC NERVE HEAD

The content of this chapter was previously published in (Jan, Lathrop, & Sigal, 2017).

3.1 INTRODUCTION

The collagen fibers of the connective tissues of the eye play a central role in determining the biomechanical behavior of the globe, and are therefore central to eye physiology and pathophysiology.(Coudrillier et al., 2012b; C Ross Ethier et al., 2004) Hence, to understand the eye and preserve vision, it is necessary to characterize the architecture of collagen fibers. Multiple techniques have been deployed towards this goal, including small-angle light scattering (SALS)(M. J. Girard, A. Dahlmann-Noor, S. Rayapureddi, J. A. Bechara, B. M. Bertin, et al., 2011; Dongmei Yan, Sheridan McPheeters, Gregory Johnson, Urs Utzinger, & Jonathan P Vande Geest, 2011a), x-ray scattering(Abahussin et al., 2009; Coudrillier et al., 2013; Keith M. Meek & Boote, 2009; Jacek Klaudiusz Pijanka et al., 2013), nonlinear(Winkler et al., 2011; Winkler et al., 2013a), scanning electron,(Quantock et al., 2015; Quigley & Addicks, 1981; Quigley, Hohman, Addicks, Massof, & Green, 1983) and transmission electron(Elkington, Inman, Steart, & Weller, 1990) microscopies, and magnetic resonance imaging (MRI).(Ho et al., 2014; Ho et al., 2016) These techniques, although useful, have one or more of the following limitations, such as a small

field-of-view, low resolution, subjective and slow analysis, high expense, and introduction of artifacts. Collagen fiber architecture has also been predicted using inverse numerical modeling(M. J. Girard, J. C. Downs, M. Bottlang, C. F. Burgoyne, & J.-K. F. Suh, 2009; Grytz et al., 2011). These models are particularly useful because they can predict essential properties of the collagen fibers, such as fiber waviness or crimp, which the experimental techniques mentioned above have not provided.(Grytz & Meschke, 2009) However, inverse model predictions remain to be validated, in part because of a lack of suitable experimental techniques.

We recently demonstrated a technique based on polarized light microscopy (PLM) that can provide accurate, robust, and repeatable measurements of ocular collagen fibers.(Jan et al., 2015) Our goal in this work was to leverage PLM to visualize and quantify, with micrometer-scale resolution, the distribution and orientation of the collagen in the posterior sclera and optic nerve head (ONH), and to identify the major organizational components of these regions at the macroscopic, whole-tissue scale.

3.2 METHODS

3.2.1 Specimen preparation

Eight eyes from 5 adult (~2-year old) sheep were obtained from the local abattoir and processed within 8 hours after death. The globes were cleaned by carefully removing the fat, muscles, and episcleral tissues, using scalpels, razors, and forceps. The eyes were cannulated through the anterior chamber and fixed overnight with 10% formalin while maintaining a controlled IOP of 5 mmHg or 50 mmHg by both perfusion and immersion. A total of 7 eyes were fixed at an IOP of 5

mmHg whereas 1 eye was fixed at an IOP of 50 mmHg. Posterior pole regions centered on the ONH were excised using a circular trephine (either 8-mm or 11.5-mm diameter) and cryosectioned coronally into 30-μm-thick sections. Note that no labels or stains were applied and the tissues were never dehydrated. The tissues were not flattened, and we did not make stress-relieving cuts that could affect collagen orientations. (Jacek Klaudiusz Pijanka et al., 2013) Elsewhere we have shown that the tissue processing described above with 10% formalin followed by sectioning has minimal effects on tissue shape or size (e.g. mean ONH area changed by less than 2.5% without a change in circularity) (Tran H. et al. Minimal morphological change of ocular tissues after formalin fixation and sectioning. In Review).

3.2.2 Measuring collagen orientation

The local collagen orientation was determined from images captured using PLM following protocols previously reported.(Jan et al., 2015) Briefly, a white light source and two polarizing filters were used (Hoya, Tokyo, Japan). The birefringence of the collagen fibers causes the intensity of the detected light to vary depending on the relative orientation of the fiber and the direction of polarization of the light (Figure 20). Thus, local collagen orientation at each pixel can be determined from multiple images captured with different relative orientations.(Jan et al., 2015)

3.2.3 Image acquisition

Three imaging methods were used. Two methods used for visualization of lamina cribrosa and sclera, respectively, are described below. The third method used for further analysis of the sclera is described later in the *Methods* in the subsection on quantification

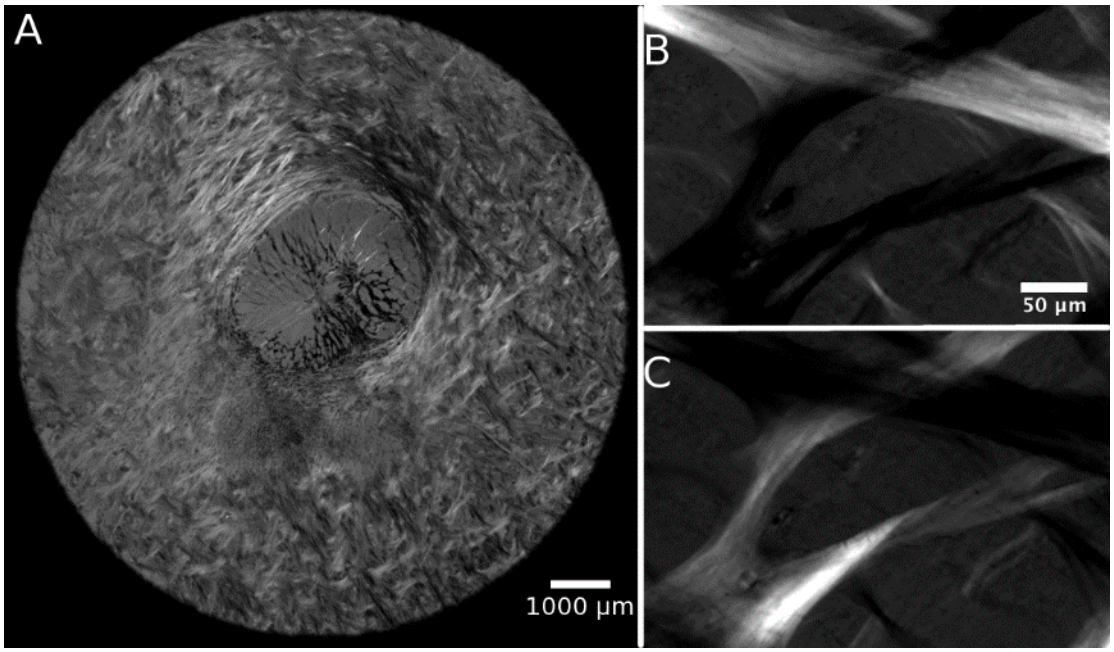

Figure 20. PLM images of the posterior pole.

Raw PLM images of a section of optic nerve head show different intensities for collagen fibers oriented in different directions (A). Two PLM images of lamina cribrosa beams with the polarizer changed by 45° (B, C).

. The rationale for the choices and merits of each method are presented in *Discussion.*

The lamina cribrosa was captured using a 10x objective (numerical aperture 0.3) on a model BX60 microscope (Olympus, Tokyo, Japan), using an RT Slider camera (SPOT Imaging Solutions, Sterling Heights, MI, USA). Sections from 2 eyes, 1 fixed at 5 mm Hg IOP (11.5 mm diameter trephine) and 1 fixed at 50 mm Hg IOP (8 mm diameter trephine), were imaged (12-bit grayscale, 0.73 µm/pixel). To capture the whole lamina cribrosa, 20 to 35 images with 20% overlap were captured for each section using a manual stage and stitched into mosaics using FIJI. (Preibisch et al., 2009)

The peripapillary sclera was imaged using a 10x objective (numerical aperture, 0.5) on a Nikon Eclipse Ti microscope (Nikon, Melville, New York), with a Cascade 1K camera (Roper Scientific, Sarasota, FL). Sections from two eyes fixed at 5 mm Hg IOP (11.5- mm diameter

trephine), were imaged (16-bit grayscale, 0.80μm/pixel). To capture the whole section in submicrometer-resolution, we used MetaMorph software (Molecular Devices, Sunnyvale, CA, USA) paired with a motorized *x-y* stage to capture a mosaic. For each section, stitched image sets of 80 to 125 images were automatically captured and stitched.

3.2.4 Image presentation

The ability to understand collagen fiber organization and identify the main features of their architecture depends on the methods used for visualization. Below we describe several tools used toward this goal.

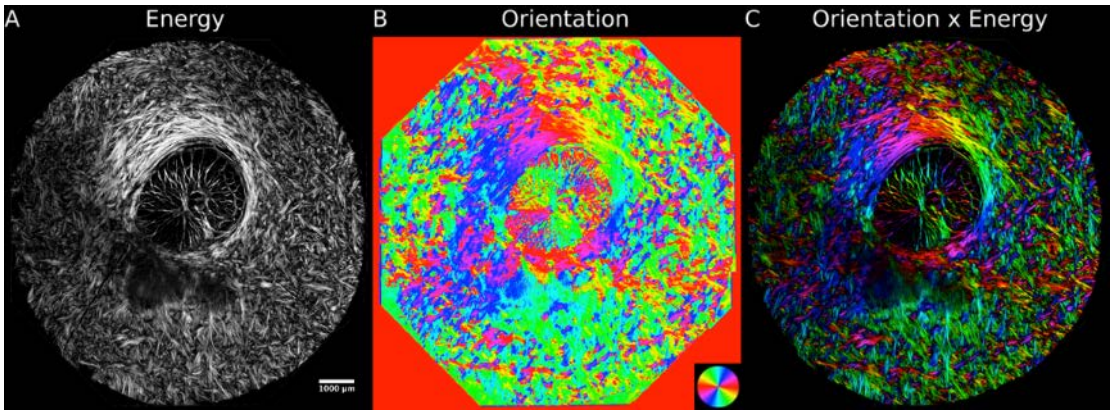

Figure 21. Improving collagen structure visualization by applying a mask.
Scaling intensity by energy (A) helps distinguish the collagen regions outside the tissues. By using this energy intensity scaling to "mask" color maps of the collagen fiber orientation (B), the architecture of the collagen fibers can be better understood (C).

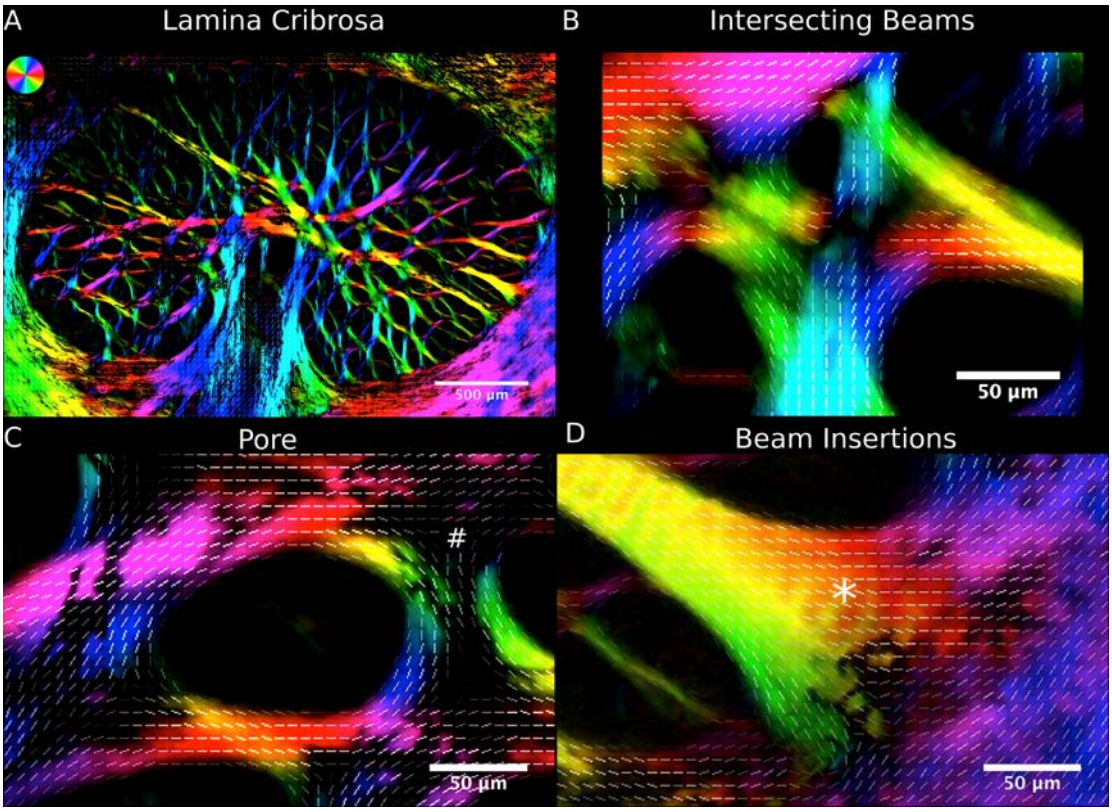

Figure 22. The lamina cribrosa visualized on the submicrometer-scale using PLM.

The collagen micro-architecture of the lamina cribrosa (A) is complex, with "knots" of intersecting beams (B), fibers wrapping circumferentially around pores (C), and anchor points where the lamina cribrosa inserts into the scleral canal (D). Dark regions of low energy due to pigment can be seen within the sclera ([A], top right) and beams ([C], hashtag) and sclera, but did not impede orientation calculations (white overlaid orientation lines, averaged over 3x3 µm2). High spatial and angular resolution allows identification of crimp, or the natural waviness of the collagen fibers, as color oscillations, such as the yellow and red bands in the beam insertion ([D], asterisk). These images were acquired from sections of an eye fixed at 5 mm Hg.

A masking technique was applied to help distinguish tissues in which the local fiber orientation at a pixel is weighted by an "energy" parameter, as described elsewhere.(Jan et al., 2015) Energy was defined by the equation $energy^2 = (I_{90} - I_0)^2 - (I_{135} - I_{45})^2$, where I_α was the pixel intensity at relative angle α between sample and polarizing filters. Energy is large when there is substantial information on collagen fiber orientation, and small when there is little information. Little information would occur, for example, in regions without tissues, or where pigment blocks

the signal. Energy weighting substantially improved structure visualization at large (Figure 21), medium, and small scales (Figure 22). Unless indicated otherwise, images of orientation are shown with energy weighting. Quantitative analyses were done without weighting.

Visualization of local fiber orientations was also enhanced by plotting short line segments to indicate the mean collagen fiber orientation within a small region (also referred to as a kernel). These were particularly helpful when also weighted using the energy parameter mentioned above, as this makes lines more intense and visible in areas with high signal quality and fade to dark in areas outside the tissues or occluded by pigment (Figure 22).

Visualization of the larger scale organization of the collagen fibers was enhanced with a "tracing method" similar to the nerve fiber tracings used in MRI-based diffusion tensor imaging (Figure 23).(Ho et al., 2016) The traces started by generating a set of seed points. From each seed point the algorithm produced a trace using local collagen orientation following a Euler integration scheme(Heermann, 1986) with step size an order of magnitude smaller than pixel size. Tracing stopped if local energy decreased under a set threshold (usually approximately 0.1) or if the trace were to take a sudden change in direction greater than 45° over a few pixels. In addition, after a specified maximum length, the trace ends in order to avoid overcrowding. Note that this tracing algorithm was only intended as a visualization aid and that there should be no expectation that it is following a single fiber, fiber bundle, or lamella.

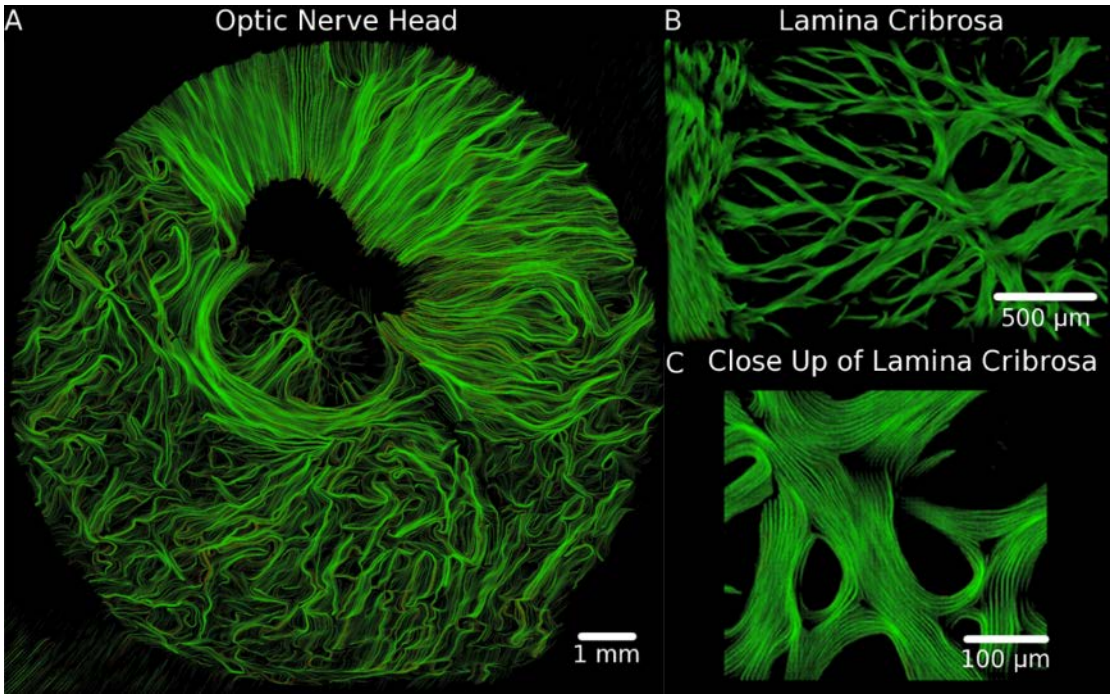

Figure 23. Traces of the collagen fibers in the optic nerve head at different magnifications help visualize the continuity of the fibers and their regional anisotropy.

Longer, more aligned lines indicate a region of higher anisotropy. (A) Highly anisotropic regions in the sclera appeared as well organized fibers that either wrapped circumferentially around the canal or extended radially from the canal to the edge of the section. (B) In the lamina cribrosa, the traces revealed the complex network of collagen fibers and (C) show how the fibers intersect and wrap around the lamina cribrosa pores. These images were acquired from sections of an eye fixed at 50 mm Hg. Because this coronal section is slightly tilted, the top right part of the section is more anterior while the lower left part of the section is more posterior. The black region next to the canal is an area anterior to the sclera, with high content of pigment and either low or no collagen.

3.2.5 Quantifying peripapillary scleral collagen architecture

While inspecting the maps of peripapillary sclera collagen fiber orientation, we noticed that there appeared to be 3 distinct regions according to the fiber architecture: i) the collagen in the sclera canal immediately adjacent to the lamina cribrosa oriented circumferentially around the canal forming a ring of fibers(Jacek Klaudiusz Pijanka et al., 2012); ii) a thin layer in the innermost sclera with collagen fibers oriented radially from the scleral canal perpendicular to the ring; and

iii) the rest of the sclera formed by interweaving collagen bundles that did not have a clear main orientation (Figure 24). Hence, we set out to determine whether these apparently different regions were indeed significantly different and whether they are present in all eyes.

Analysis of sclera was conducted using images captured using the 1x objective (NA 0.1) of a model SMZ1500 microscope, paired with a DXM1200 camera (Nikon). This microscope-camera pair allowed imaging of the whole section without mosaicking. An average of 75 serial sections (range, 42-154 sections) from 7 eyes from four sheep fixed at 5 mm Hg IOP were imaged (32-bit RGB, 4.1 μm/pixel). From these images, rectangular areas (300- to 600-μm side length) representative of each of the three regions were manually marked in every section image, when discernible. For analysis, the orientations were converted into polar coordinates based on a manually identified center of the scleral canal. In this system, 0° represented a radial orientation and 90° a circumferential orientation. For this study, we took deviations from radial in either direction to be equivalent. For each area marked (674 total), we computed the mean fiber orientation and the circular variance using directional statistics as a measure of degree of alignment or anisotropy.(Jammalamadaka & Sengupta, 2001) To simplify interpretation, the anisotropy was normalized, by the value of a uniform distribution, and the value subtracted from 1. Thus, an anisotropy of 1 represents perfectly aligned fibers, whereas an anisotropy of 0 represents fibers perfectly splayed in all directions, such as in a random distribution. Directional statistics of this type are well established and common in the study of orientation parameters.(Püspöki, Storath, Sage, & Unser, 2016b)

3.2.6 Statistical analysis

A linear mixed effects model was fit to test whether mean angle and fiber anisotropy were significantly predicted by region, accounting for autocorrelations between measurements taken from the same sections, eyes, and individuals.

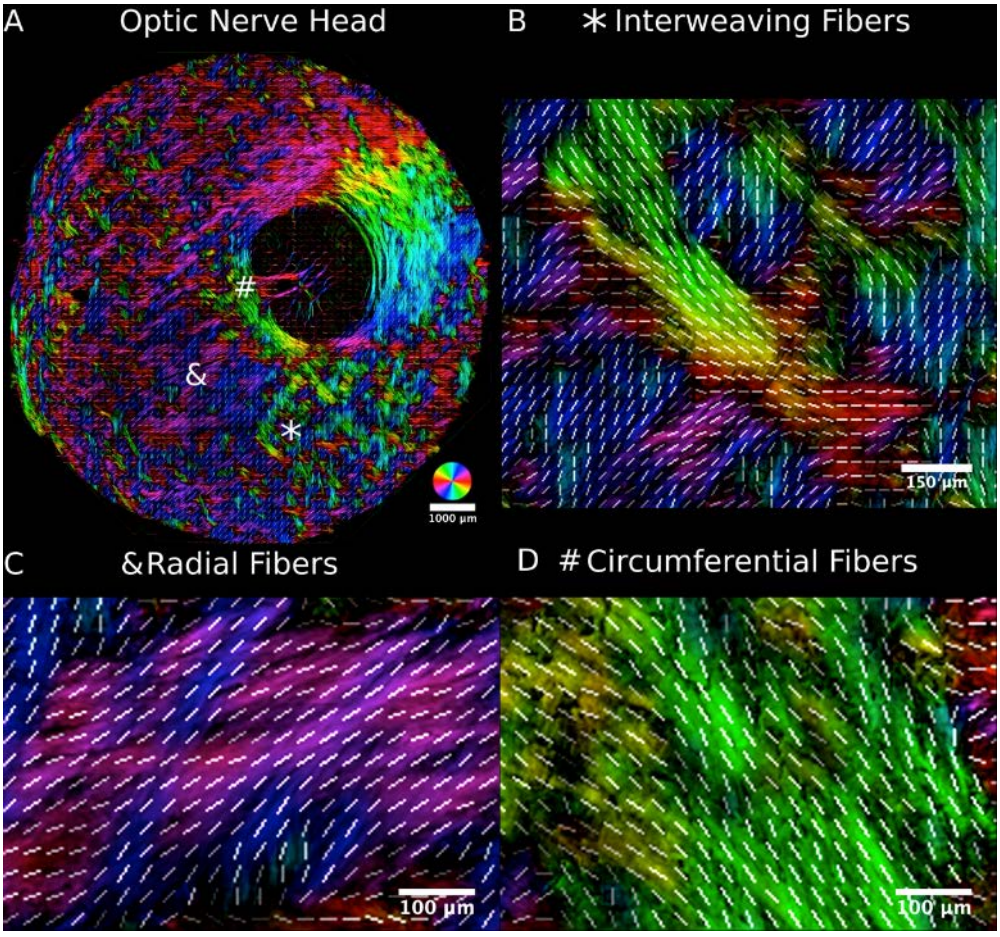

Figure 24. The peripapillary sclera visualized on the submicrometer-scale using PLM.

Three major organizational patterns were identified and marked an asterisk (A), an ampersand, and a hashtag: i) interweaving fibers that formed a basket-weave pattern ([B], asterisk), ii) fibers oriented radially from the canal ([C], ampersand), and iii) fibers wrapped circumferentially around the canal ([D], hashtag). The radial and circumferential regions form rainbow-colored patterns in their respective directions, making them easily identifiable in the images. As in **Figure 22**, white lines representing orientation averaged over 20x20 μm^2 were overlaid to aid discerning the fiber organization.

3.3 RESULTS

Figure 22 shows example images of the beautiful architecture of the lamina cribrosa. Collagen fiber microarchitecture can be seen, including beam intersections where the fibers form “knots” with multiple bundles intersecting (Figure 22B) and fibers that wrap around pores (Figure 22C). On the lamina cribrosa periphery we observed two types of lamina cribrosa beam insertions into the sclera (Figure 22D). Some insertions were narrow, formed by fibers that run perpendicular into the scleral canal. Other insertions were wide, appearing much like old trees, with some fibers running directly into the canal wall and others turning smoothly to integrate with the circumferential fibers of the sclera immediately adjacent to the canal. Note also how robust the PLM technique is able to measure fiber orientations despite substantial pigment (Figure 22C, D), and submicrometer resolution of our imaging and analysis allows direct visualization of the natural waviness of the collagen fibers, or crimp (Figure 22D). Tracings (Figure 23) displayed a larger scale collagen organization on the lamina cribrosa, in which some fiber bundles could be traced over distances of up to a millimeter. This is important as it provides a means to study how the lamina cribrosa beams carry and distribute forces. At the pore scale, the tracings showed collagen fibers wrapped circumferentially around the pores.

Wide-field micrometer-scale maps of collagen fiber orientation over the whole section are shown in Figure 21, Figure 23, Figure 24, and Figure 25, and the quantifications of the fiber orientations in these regions, from eyes fixed at 5 mm Hg IOP, are shown in Figure 26 and Figure 27. The scleral canal and the lamina cribrosa are evident in all images, although the energy masking makes the various structures obvious and interpretation simpler (Figure 21). Tracings show that

different regions of the sclera have specific patterns of collagen fiber orientation, like fibers that extend from the edge of the canal across the whole section (Figure 23). In Figure 24, three distinct regions of the sclera are discernible: i) regions of interweaving fibers without a clear orientation, ii) circumferential fibers immediately adjacent to the scleral canal, and iii) fibers aligned radially to the scleral canal, visible in the most anterior regions of the sclera, which were estimated to be 60 to 180 μm thick and extended at least 3 mm from the canal, the edge of the trephined region, clearly seen with long continuous radial fibers in Figure 23.

These different regions manifested most commonly at different depths in the posterior pole (Figure 25). To understand the depth-dependence of the fiber architecture, an image stack was formed by manually registering images from all sections of the posterior pole of an eye.(Sigal et al., 2010) We manually selected two 467μm x 566-μm regions, one proximal to the canal, immediately adjacent to the canal, and another distal, outside the circumferential ring. We then calculated the distribution of fiber orientations in these regions in each section across the tissue depth (Figure 26). In the anterior-to-posterior direction, radial fibers appear first. In proximal regions, circumferential fibers were directly posterior to the radial fibers (Figure 26A), and in distal regions, the alignment was much more complex and variable, with interweaving fibers posterior to the radial fibers (Figure 26B).

Quantitative analysis of the orientation characteristics of the three scleral regions showed distinct differences in collagen fiber orientation distribution (Figure 27). Each region was consistently discernable in all eyes and had significant differences in mean orientation and anisotropy ($P < 0.0001$). The radial and circumferential regions were highly anisotropic, differing only on the mean orientation (Figure 27A), whereas the region of interweaving fibers was much less anisotropic (Figure 27B) with a corresponding spread mean orientation.

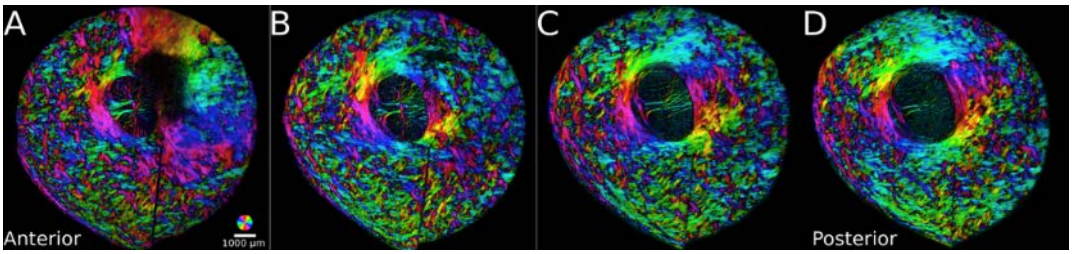

Figure 25. Serial optic nerve head sections ordered from anterior to posterior.
The radial fibers were found in the most anterior sections (A), whereas the interweaving and circumferential fibers appeared directly posterior and persisted through the sclera (B, C, D). The radial and circumferential fibers are easily distinguishable by the large regions with "rainbow" colors (note the orientation key at the bottom right of [A]). The extent of color variations gives an indication of the spatial anisotropy, such that large regions of uniform coloring indicate higher anisotropy than regions with much color variations, which suggest more isotropy.

3.4 DISCUSSION

Collagen is the main load-bearing component of ocular tissues, and collagen organization has important implications for the ability of the tissues to bear forces, in turn affecting their physiology, robustness, and susceptibility to disease. We have presented images of the collagen fiber architecture with micrometer-scale resolution over centimeter-scale regions of the posterior pole including the ONH. With PLM, the various structural components of the ONH and posterior sclera were clearly discernible and could be analyzed with high detail and revealed some characteristics of the collagen architecture that have not been described, and improved clarity of previously described features. Below we discuss some salient examples of our findings, followed by a discussion of the advantages and limitations of the study and of PLM.

The images revealed details of the peripheral lamina cribrosa and of the beam insertions into the scleral canal wall that were either unreported or that had not been characterized in detail.

It is through the lamina cribrosa beam insertions into the canal wall that the sclera provides boundary conditions to the lamina cribrosa, transferring forces that can contribute to insult or that provide anchor and support. Hence, the lamina cribrosa beam insertions are critically important for understanding lamina cribrosa biomechanics and biomechanical sensitivity. To the best of our knowledge, there have been no studies that have shown the lamina cribrosa insertions into the scleral canal wall in the way we have shown here. Some studies have addressed the insertion of the lamina cribrosa as a whole.(Sigal, Flanagan, Lathrop, Tertinegg, & Bilonick, 2012; Sigal et al., 2010; H. Yang et al., 2011) Others studies have described fibers of the lamina cribrosa inserting into concentric circumferential fibers in the sclera,(M. R. Hernandez, X. X. Luo, W. Andrzejewska, & A. H. Neufeld, 1989; M. R. Hernandez, X. X. Luo, F. Igoe, & A. H. Neufeld, 1987; Morrison, L'Hernault, Jerdan, & Quigley, 1989; Thale, Tillmann, & Rochels, 1996b) or with fibers running longitudinally within the core of laminar beams.(Morrison, Jerdan, Dorman, & Quigley, 1989) We showed that some insertions were wide and robust in appearance, with collagen fibers that turned and integrated with those of the sclera resembling old trees. Other insertions were thin and frail-looking, inserting perpendicular to the canal wall. These two beam insertion types may provide different biomechanical support to the adjacent neural tissues and to the capillaries within the beams.(Hayreh, 1969) Insertion types may also be relevant to understand lamina cribrosa disinsertions,(Faridi et al., 2014) hemorrhages,(Lee et al., 2014) and progressive remodeling of the lamina cribrosa into the pia mater.(Sigal et al., 2012; H. Yang et al., 2011)

Within the sclera, PLM shows that there are three distinct regions of sclera: circumferential fibers adjacent to the canal, radial fibers on the most anterior sclera, and a less aligned region of interweaving fibers elsewhere. The region of circumferential fibers, often also called the “ring”,(Jacek Klaudiusz Pijanka et al., 2012) has been described by several studies using a variety

of methods, including wide-angle X-ray scattering (WAXS),(Jacek K. Pijanka et al., 2015) SALS,(M. J. Girard, A. Dahlmann-Noor, S. Rayapureddi, J. A. Bechara, B. M. Bertin, et al., 2011) second harmonic imaging (SHG),(Winkler et al., 2010) scanning electron microscopy,(Thale & Tillmann, 1993b; Thale, Tillmann, & Rochels, 1996a; Thale et al., 1996b) immunofluorescence,(M. R. Hernandez et al., 1989; M. R. Hernandez et al., 1987; Morrison, Jerdan, et al., 1989) and has been predicted using inverse modeling.(Grytz & Meschke, 2009) Our observation of regions of radial fiber orientation in the sclera confirms a recent report from Pijanka et al. (Jacek K. Pijanka et al., 2015) The high resolution of PLM allowed us to ascertain that the radial fibers form a layer 60 to 180 μm thick, and the wide field-of-view shows that this layer can extend at least 3 mm from the scleral canal wall to the edge of the tissue sections. Last, the more isotropic regions of the sclera have previously been identified by SALS(M. J. Girard, A. Dahlmann-Noor, S. Rayapureddi, J. A. Bechara, B. M. Bertin, et al., 2011) and predicted by inverse modeling.(Grytz & Meschke, 2010) The combination of high resolution with wide field-of-view of PLM showed that the fiber bundles form a basket-weave-like pattern with more detail than can be discerned with SALS or inverse modeling. Our findings of variations in collagen architecture with depth are consistent with the descriptions of Thale et al[32,39]. and Thale and Tillmann (Thale & Tillmann, 1993b; Thale et al., 1996a, 1996b) based on images obtained with scanning electron microscopy. They described scleral collagen fibrils arranged in a reticular fashion (low anisotropy) in the external sclera, and in a rhombic pattern (high anisotropy) in the internal sclera. The significant differences in orientation characteristics between scleral regions may befit automated algorithms of segmentation. In terms of the regional biomechanical roles, the circumferential fibers surrounding the scleral canal are generally believed to provide structural strength to the ONH, (Coudrillier et al., 2016; M. J. Girard et al., 2009; Grytz & Meschke, 2010)

whereas the roles of the radial or interweaving fibers remain unclear and are the subject of current research. Less aligned or isotropic fibers may provide reliable support under a variety of loading conditions, as is observed on tissues such as skin.(Fratzl, 2008) The radial collagen fibers might help reduce mechanical insult to the neural tissues of the retina that are also organized roughly radially from the ONH.

High spatial and angular resolution afforded by PLM techniques enabled visualization of collagen crimping (Figure 22D). Collagen crimping has long been established as a key characteristic of fiber-forming collagens that plays a critical role in tissue mechanics at several scales.(Holzapfel, 2001) Nevertheless, few studies have explored crimp on ocular tissues, and most of what is known about ocular collagen crimping has been estimated from inverse modeling.(Grytz & Meschke, 2009, 2010) This is because micrometer-scale resolution is needed for visualizing and measuring the small orientation changes associated with crimping. PLM and our analysis techniques have the appropriate spatial and angular resolution, allowing direct detailed investigation of ocular collagen crimp.(Jan et al., 2015)

A valuable advantage of collagen structure analysis based on PLM is that it allows analysis of collagen architecture without the need for labels or stains, (Hernandez, Andrzejewska, & Neufeld, 1990; M Rosario Hernandez, Xing Xing Luo, Frank Igoe, & Arthur H Neufeld, 1987) dehydration, (H. Yang, Downs, Bellezza, Thompson, & Burgoyne, 2007) or flattening, (Jacek Klaudiusz Pijanka et al., 2013; Jacek Klaudiusz Pijanka et al., 2012) which can introduce artifacts. Although our technique works well on unfixed samples,(Jan et al., 2015) in this work we used tissues fixed with 10% formalin. We have shown that this fixation has minimal effects on tissue size or shape, an important advantage for morphometry over techniques known to cause substantial shrinkage.(Downs et al., 2007)

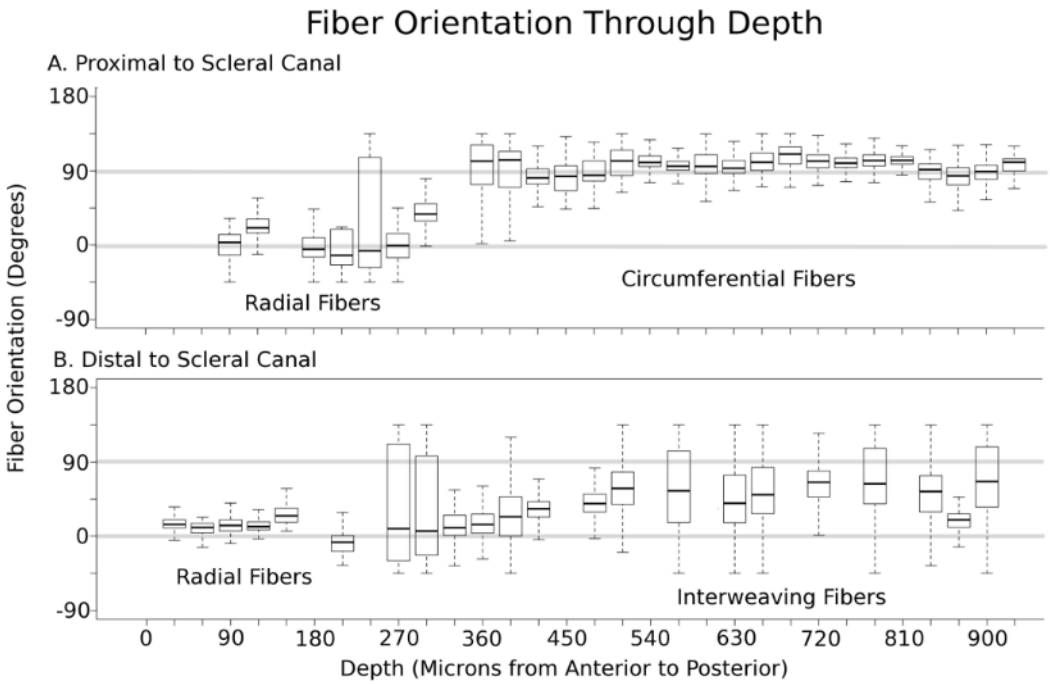

Figure 26. Box plots of the polar fiber orientations relative to the center of the canal with depth, from an eye fixed at 5 mm Hg IOP.

The circumferential fibers (orientation of 90°) were proximal to the scleral canal (A) whereas the interweaving fibers were distal to the scleral canal (B). No matter the distance from the scleral canal, the most anterior layer was oriented radially (orientation of 0°). The orientation was plotted either from -90° to 90° or from 0° to 180°, depending on which reference frame gave the least variability. Sections with low energy were excluded from analysis.

This study is not the first to identify and quantify fiber orientation in these distinct regions of the peripapillary sclera. Some imaging modalities that have been used to quantitatively measure collagen fiber orientation include WAXS, MRI, and SALS. The addition of PLM to the set of analysis tools introduces the possibility of higher resolution, which allows improved precision and accuracy. This study has ~100x the in-plane resolution and ~5x the depth resolution, as well as ~1.4x the angular resolution of a previous study using WAXS, although WAXS has a wider field-of-view in comparison to field-of-view afforded by PLM in this study.(Jacek K. Pijanka et al., 2015) Compared to MRI,(Ho et al., 2014) the resolution is ~30x the lateral resolution and ~60x the depth resolution. However, it should be noted that MRI does not require sectioning and can

potentially be used to identify collagen microstructural patterns in-vivo.(Ho et al., 2014; Ho et al., 2016) Compared to reported SALS resolutions, (M. J. Girard, A. Dahlmann-Noor, S. Rayapureddi, J. A. Bechara, B. M. Bertin, et al., 2011; Zhang et al., 2015) PLM also has ~75 to 200x the in-plane resolution and ~3x the depth resolution (using reported SALS beam diameter and thickness of the ocular tissues analyzed in published reports(M. J. Girard, A. Dahlmann-Noor, S. Rayapureddi, J. A. Bechara, B. M. Bertin, et al., 2011; Yan, McPheeters, et al., 2011a)). Note that our goal was not to do an exhaustive review or comparison of all the techniques available for characterizing collagen fiber architecture in the eye. The techniques can produce useful data, and it may be possible to overcome limitations. For example, improving resolution by changing the illumination beam characteristics.

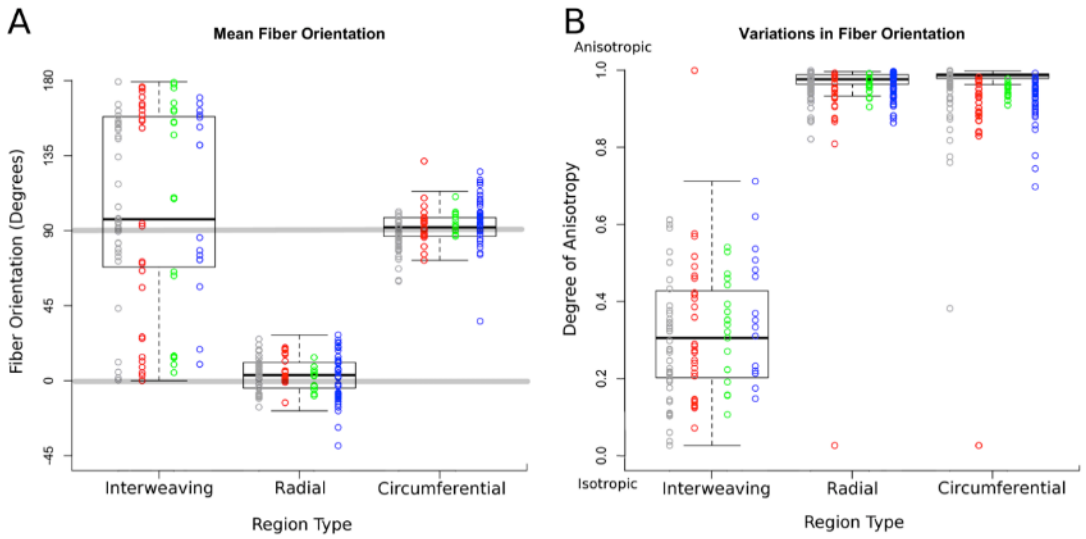

Figure 27. Box plots of the polar fiber orientations and degree of anisotropy by region type. Orientation was plotted either from -90° to 90° or from 0° to 180° depending on which reference frame gave the least variability. Data acquired from each sheep were plotted in different columns in different colors. Note that for low anisotropy, the value of the mean orientation has little meaning. Results were consistent between contralateral eyes as well as across eyes from different sheep. All eyes used were fixed at 5 mm Hg IOP.

Second harmonic imaging is a technique that produces micrometer-scale resolution images of collagen in the eye without sectioning or staining.(Kamma-Lorger et al., 2010; Teng et al., 2006; Winkler et al., 2010) Fiber orientation is typically extracted from these images using gradient-based methods, which calculate the orientation based on the texture in the image. However, high tissue density or pigment can cause artifacts. Quantifying the collagen fiber orientation with PLM is robust to the presence of pigment,(Jan et al., 2015) allowing repeatable imaging of pigmented tissues (Figure 22C, D).

PLM allows quantification of individual lamina cribrosa beams and peripapillary sclera bundles together over a large centimeter-scale field-of-view, with excellent sensitivity and resolution on both. Many of the imaging modalities listed above are more appropriate to one tissue or the other due to issues with tissue density or feature size. Jones et al., (Jones et al., 2015) for example, used SALS for quantitative analysis of the collagen microstructure of human optic nerve heads over both the lamina cribrosa and the sclera.[52] The resolution and sensitivity of SALS were sufficient to obtain measurements of the dense circumferential fibers in the peripapillary sclera. For the lamina cribrosa, however, SALS provided only rough measures of fiber density and a general radial orientation of the beams. Lamina cribrosa insertions could not be discerned or quantified. We have shown that PLM provides excellent quality of data on both lamina cribrosa and sclera, with excellent sensitivity at the critical point of the lamina insertion.

Note that in this study we used three PLM imaging systems. To visualize the fine details of the beams, the lamina cribrosa was imaged with a high-resolution system (0.73 μm/pixel) with a manual stage. The sclera, however, is much larger and using the manual stage and mosaic stitching would have been very time consuming. Hence, for imaging the sclera we switched to a system with a motorized stage and slightly lower resolution (0.8 μm/pixel). Quantitative analysis

of the radial, circumferential, and interweaving regions required imaging a rather substantial 525 sections. For this task we selected a system with which we could image a whole section without the need for mosaicking yet with excellent, resolution of 4.1 μm/pixel. We have previously demonstrated that our PLM technique is robust to changes in imaging system and magnification, (Jan et al., 2015) and we confirmed that this was the case for the three setups used in this study (results not shown).

There are several limitations to this study. Sheep eyes have similarities to those of humans, such as a collagenous lamina cribrosa, but they also have differences, such as a thick tree-like structure within the canal called the ventral groove, similar to that of pigs.(Brooks, Arellano, Kubilis, & Komaromy, 1998) It is possible that some of the structural features we have observed on the lamina cribrosa and sclera are unique to sheep and/or not shared by humans. Although learning about sheep is important to understand as an animal model,(Gerometta, Spiga, Borrás, & Candia, 2010) we are working to extend our work to other species. Another limitation is that we used histological tissue sections, which may introduce artifacts, such as warping from sectioning. These effects are small on our cryosectioning process (Tran H. et al. unpublished observations) and can, if necessary, be further reduced using fiducials and unwarping techniques. (Sigal et al., 2010) Additionally, our study is limited to 2-dimensional (2D) fiber orientations in the section plane. The eye is a complex 3D structure and measurements in 3D may be necessary to determine all the essential characteristics. This is not a limitation specific to our work. The 2D limitation is shared by all the most common techniques for studying the collagen of the eye, such as SALS and WAXS. In fact, the higher lateral and depth resolution of our implementation of PLM compared with the published implementations of SALS and WAXS, reduces errors that can arise from the 2D assumption. It is possible that the depth resolution of 30 μm in this study may still not be

enough to capture the true orientation. This is because it is possible that multiple fibers with different orientations pass through a single pixel, but our technique would only report the predominant fiber orientation at that pixel. Thinner sections may address some of this concern because higher depth resolution reduces the likelihood of multiple fibers with different orientation passing through the same pixel.

We have leveraged PLM as a powerful technique for visualizing and quantifying collagen fiber architecture in the posterior pole. Our images reveal previously unreported features of the collagen organization of the lamina cribrosa and sclera, and provide improved clarity and more details on features already described. Further work is needed to determine the generality across species of the futures identified, as well as the biomechanical roles of the two types of lamina cribrosa beams observed and of the three regions of sclera architecture.

4.0 BASELINE CRIMP DISTRIBUTION IN THE OPTIC NERVE HEAD

The content of this chapter was previously published in (Jan, Gomez, et al., 2017)

4.1 INTRODUCTION

Collagen is the main load-bearing component of soft tissues, including the eye. The organization and hierarchical architecture of collagen fibers determine tissue mechanical behavior, including key tissue properties such as anisotropy (directional stiffness) and nonlinearity (strain-dependent stiffness).(Fratzl, 2008) The influence of fiber architecture is often stronger than that of the chemical composition of the fibers.(Fratzl, 2008; Mattheck, 1998; Niklas, 1992; Wainwright, Biggs, Currey, & Gosline, 1982) Several recent studies have addressed the overall organization and orientation of collagen in the eye, focusing on the corresponding tissue anisotropy,(M. J. Girard, A. Dahlmann-Noor, S. Rayapureddi, J. A. Bechara, B. M. E. Bertin, et al., 2011; Kamma-Lorger et al., 2010; Jacek Klaudiusz Pijanka et al., 2012; Winkler et al., 2010) However, the microstructural characteristics of the collagen fibers and their role in eye tissue nonlinearity remain relatively poorly understood. In other soft tissues it is well understood that their nonlinear behavior is largely driven by the micrometer-scale waviness, or crimp, of the collagen fibers.(Holzapfel, 2001; Ottani, Raspanti, & Ruggeri, 2001) Studies in tendon and skin, for example, have

demonstrated an important inter-relationship between crimp and mechanical properties in health, aging and disease.(Bader et al., 2011; Birch et al., 2013; Franchi et al., 2008)

In the eye, studies have been limited to observations of fiber waviness and undulations in images acquired with a diversity of techniques, including brightfield,(Ostrin & Wildsoet, 2016) electron,(Andreo & Farrell, 1982) and nonlinear microscopy,(Kamma-Lorger et al., 2010; Mega et al., 2012; Midgett et al., 2016; Winkler et al., 2011) and MRI,(Ho et al., 2014) or to estimates of crimp properties from inverse numerical models.(Grytz & Meschke, 2009, 2010; Grytz et al., 2011) Employing transmission electron microscopy Liu and colleagues measured collagen fiber crimp in the cornea.(Liu et al., 2014) The numerical models point to collagen crimp characteristics playing a critical role in eye biomechanics.(Grytz & Meschke, 2009, 2010; Grytz et al., 2011; Liu et al., 2014) Nevertheless, no systematic experimental quantifications of posterior pole micrometer-scale collagen crimp have been reported.

Our goal was to quantify collagen fiber crimp in the lamina cribrosa (LC) and surrounding peripapillary sclera (PPS), compare crimp distribution between these tissues, and analyze how collagen crimp varies with distance from the scleral canal. This information will enable the development of more realistic models of ocular tissue biomechanics. Further, this study will provide a basis to understand the underlying mechanisms by which microstructure governs larger scale mechanics of soft tissues, as well as the role of microstructure on eye physiology, aging and in biomechanics-related diseases, such as glaucoma.

4.2 METHODS

One of the most natural characteristics of collagen fiber crimp is the length of a wave, or its period (Figure 28). In this first study, we characterized the distribution of the crimp period in the collagen fibers of the LC and PPS from sheep ONHs fixed at low intraocular pressures (IOPs).

4.2.1 Specimen preparation

6 adult sheep eyes ~2 years old were acquired from a local abattoir and processed within 24 hours of death. Using scalpels, razors, and forceps, the muscles, fat, and episcleral tissues were removed from each eye. The eyes were cannulated through the anterior chamber to set the intraocular pressure using a fluid column. We characterized the crimp period at normal (10 mm Hg),(Ghaffari, Shojaei, Sabzevari, & Khorami, 2011) sub-physiologic (5 mm Hg), and zero (0 mm Hg) IOPs. Two eyes were fixed at each pressure. All eyes were immersion fixed with 10% formalin for at least 12 hours while maintaining pressure. After fixation, the ONHs were excised using an 11.5 mm diameter trephine and cryosectioned into 30 μm thick coronal sections. For each eye, at least 3 sections at the level of the LC and 3 at the level of the PPS were selected for analysis. Sections were selected when they were free of artifacts, such as folds. Due to the natural eye-to-eye variability in LC position within the canal, as well as tilt during sectioning, some sections were not ideal for both tissues. A total of 26 sections were selected for analysis.

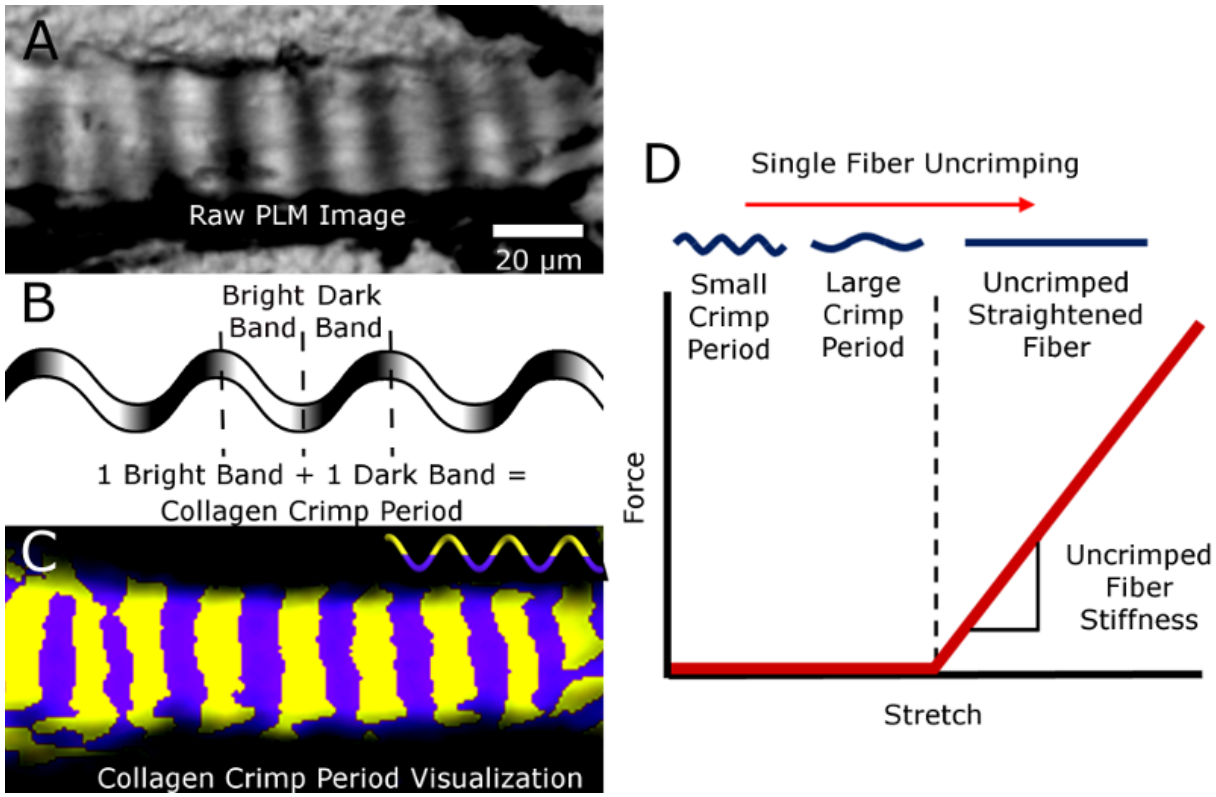

Figure 28. The collagen crimp period visualized using PLM.

A LC trabeculae beam appears banded when imaged with PLM (A). Adding the lengths of one bright band and one dark band makes one collagen crimp period (B). From processing the raw PLM images, we can pseudocolor half periods as alternating yellow and purple bands to visualize the crimp period (C). As a single fiber stretches it uncrimps, with relatively little force until it loses all crimp. The straightened fiber can only be stretched further by elongating, which requires an increasing force, and so the fiber appears stiff (D).

4.2.2 Imaging and data acquisition

The selected sections were imaged with PLM using previously reported methods(Jan et al., 2015; Jan, Lathrop, et al., 2017) in order to visualize the collagen crimp period (Figure 28). Briefly, two filters (Hoya, Tokyo, Japan) were used with the polarizer filter placed before the sample and the analyzer filter placed after the sample. Images at multiple filter orientations 45° apart were captured for optimal crimp period visualization (Figure 29). Up to four filter orientations were used in each section to quantify collagen crimp period. An Olympus SZX16 microscope was used

with an Olympus DP80 camera (36-bit, RGB, pixel shift setting), a 0.6x reducer, and 0.8x objective (numerical aperture [NA], 0.12) (Olympus, Tokyo, Japan). A manual stage was used to capture images with 20% overlap, which were then stitched into mosaics using FIJI Is Just ImageJ (FIJI).(Preibisch et al., 2009; Schindelin et al., 2012) To image the fine details of the LC, the 11.5x magnification setting on the microscope was used (0.37 μm/pixel). For each section of LC, 10-30 images were captured in order to visualize the whole LC and the scleral canal. The PPS sections were imaged using the 4x magnification setting (1.08 μm/pixel). The PPS is much larger and it would have been very time consuming to manually capture and stitch the hundreds of images that would have resulted from imaging at high magnification. For each section of PPS, 20-40 images were sufficient to visualize the whole tissue section. We have previously shown that measurements derived from intensity in PLM images are robust to changes in imaging system and magnification.(Jan et al., 2015) In the next subsection we describe the test used to verify that magnification choice did not affect the measured collagen crimp period.

4.2.3 Measuring collagen crimp period

Using FIJI,(Schindelin et al., 2012) the crimp period was manually measured from PLM images, akin to previously reported methods (Figure 28).(J Diamant et al., 1972) From the PLM images, the period was measured manually by identifying the inflection points between the bright and dark bands, where each band corresponds to half of a crimp period. A straight line was used to measure the length of 3 sequential crimp periods by identifying three bright and dark bands. This length was divided by 3 to get the average crimp period.

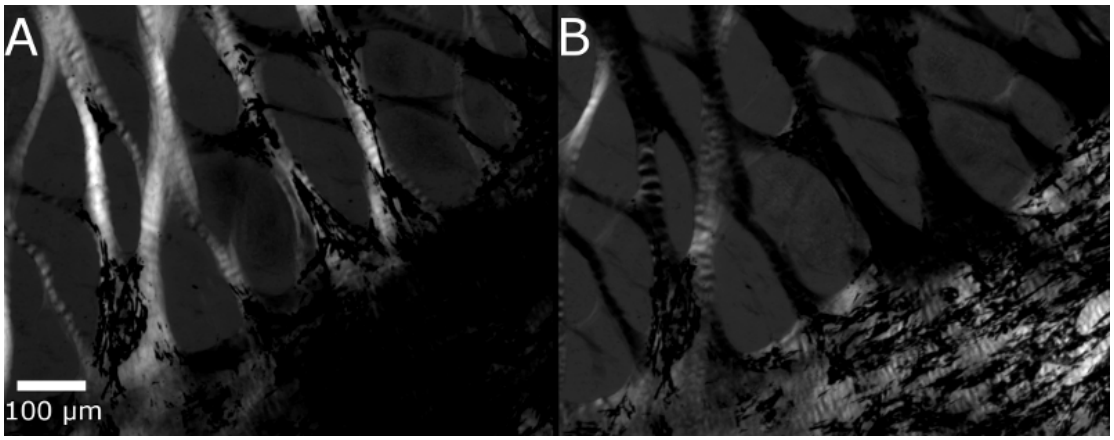

Figure 29. The same region of the ONH, imaged with two different polarized filter orientations, 45 degrees apart.

Multiple filter orientations were used in order to visualize the collagen crimp period in bundles oriented in different directions. In this case, the crimps in some LC bundles were more distinct in A, whereas those in the PPS were more distinct in B.

Due to the large number of manual measurements required, the work was split between several markers. To determine the repeatability and reproducibility of measuring the collagen crimp period, one section of the ONH fixed at 5 mm Hg IOP was imaged (12-bit, grayscale) using a Nikon Eclipse Ti microscope (Nikon, Melville, New York) coupled with a Cascade 1k camera (Roper Scientific, Sarasota, FL) and 10x objective (NA, 0.5, 0.80 µm/pixel). Nine markers delineated the same 34 fiber bundles in the image three times each.

To verify that collagen crimp period measurements are robust to acquisition magnification, one section of the ONH fixed at 5 mm Hg IOP was imaged using several magnification of the Olympus SZX16 microscope coupled with the Olympus DP80 camera, 0.6x reducer, and 0.8x objective (NA, 0.12), discussed above. A total of eight magnification settings were used to capture this series of images of a LC (2.5x with 1.75 µm/pixel through 11.5x with 0.37 µm/pixel). Below 2.5x, the collagen crimp period of the lamina cribrosa was no longer discernible, and 11.5x was

the highest setting on the microscope. Ten fiber bundles were identified in these images from different magnification settings and the collagen crimp period was measured in each bundle.

To confirm that the collagen crimp period distributions were robust to changes in imaging setup, we used alternative setups with different microscope-camera pairings to image the same sections of the 2 sheep eyes above fixed at 5 mm Hg IOP. Sections through the LC were imaged (12-bit grayscale, 0.73 μm/pixel) using a 10x objective (NA, 0.3) on an Olympus BX60 microscope (Olympus, Tokyo, Japan). This microscope was paired with an RT Slider camera (SPOT Imaging Solutions, Sterling Heights, MI). Sections through the PPS were imaged using the Nikon-Cascade microscope-camera pair with the same settings as previously described above (in paragraph detailing the repeatability and reproducibility tests). The LC and PPS collagen crimp periods were measured and the resulting distributions compared with those previously obtained from images acquired using the Olympus-Olympus microscope-camera pair.

To confirm that the collagen crimp period measurements obtained from two eyes are representative of a larger population of eyes, we repeated the measurements in an additional five eyes fixed at 5 mm Hg IOP, for a total pool of seven eyes from four animals. Collagen crimp period was measured in the LC and PPS regions using images taken using the alternative setup described above, and the resulting distributions were compared between animals and between eyes.

4.2.4 Measuring distance from the scleral canal

To evaluate how the collagen crimp period changed with distance from the scleral canal, a border between the LC and the PPS was manually drawn for each section. Measurements inside this border were categorized as on LC, whereas the measurements outside this border were categorized as on PPS. The distance of a period measurement to the canal border was calculated using custom

scripts as the shortest distance between the center of each line segment used for crimp period measurement and the manually delineated canal border.

Crimp period visualization: Some PLM images were further processed to better visualize the collagen crimp period in all fiber bundle directions simultaneously. This was done purely for visualization purposes, not for measurement. Using previously reported methods, (Jan et al., 2015; Jan, Lathrop, et al., 2017) we processed the images to determine pixel by pixel collagen fiber orientation information. This information was then used to find the difference between each pixel's fiber orientation, and the average fiber orientation in its neighborhood (10 μm radius). We then pseudo colored each pixel purple, if this difference was positive, or yellow, if this difference was negative. With this processing, crimp is easily discernible as purple and yellow bands (Figure 28) orientation. Without this processing, crimp period visibility depends on the relative orientation of the collagen bundle and the polarized light filters.

4.2.5 Statistical analyses

1) Repeatability and reproducibility of collagen crimp period measurements. To evaluate the repeatability within each marker, the standard deviation of each marker's three crimp period measurements was calculated for each fiber bundle. To evaluate reproducibility across the group of markers, the standard deviation across all marker collagen crimp period measurements for each fiber bundle was calculated.

2) Robustness of collagen crimp period measurements across magnifications. To evaluate the robustness across magnifications, the standard deviation of crimp period measurements from different magnifications was calculated for each fiber bundle.

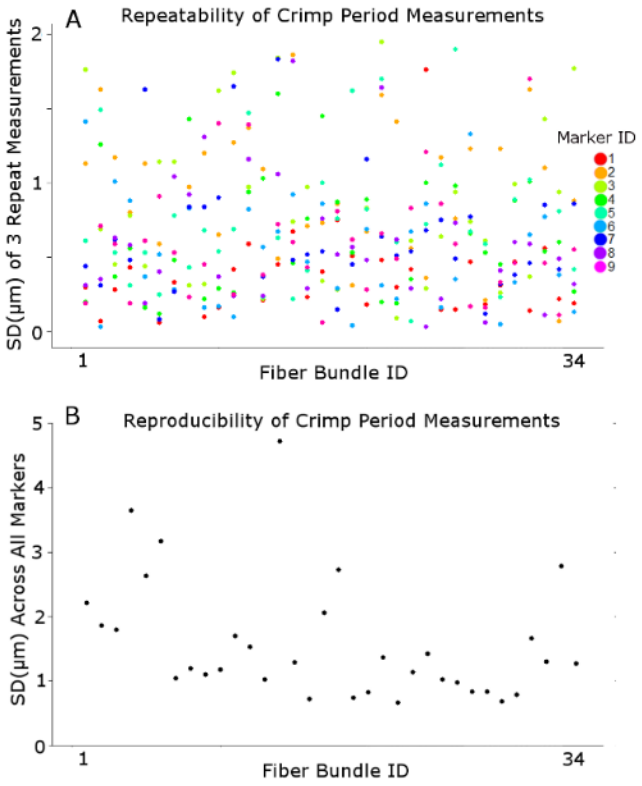

Figure 30. The repeatability (A) and reproducibility (B) of our manual collagen crimp period measurements.

A total of 9 individual markers measured the period in 34 fiber bundles 3 times to calculate the variability within (repeatability) and between (reproducibility) markers. Naturally, whether the repeatability and reproducibility are large or small, requires considering other measurements, such as those in Figure 33 and Figure 34.

3) Robustness of collagen crimp period measurements to changes in imaging setups. Linear mixed effect models accounting for autocorrelation of measurements from the same section, eye, and animal were used to test for differences in crimp period measurements between those from the standard vs alternative imaging setups.

4) Confirming measurements are representative of a larger population: From the measurements pooled across 7 eyes from 4 animals, all fixed at 5 mm Hg, linear mixed effect models accounting for autocorrelation of measurements from the same section were used to test if measurements were significantly different between those from different eyes and animals.

5) Collagen crimp period distribution. The collagen crimp period distributions in the LC and PPS were calculated. In addition, to compare the collagen crimp period of these two regions, a linear mixed effect model accounting for autocorrelation of measurements from the same section, eye, animal, and intraocular pressure was used.

6) Spatial distribution of the collagen crimp period: To determine the spatial distribution of the collagen crimp period in the LC and the PPS the collagen crimp period was first separated into groups based on spatial distance from the scleral canal. To further understand the variations in PPS crimp period with distance from the canal edge, we separated the PPS crimp period measurements into two categories: proximal (≤ 500 μm from the scleral canal) and distal (> 500 μm from the scleral canal). Linear mixed effect models accounting for autocorrelation of measurements from the same section, eye, animal, and IOP was used to determine if the PPS crimp period in these two regions were different from each other, and whether they were different from the LC crimp period. Next, linear mixed effect models accounting for autocorrelation of measurements from the same section, eye, animal, and intraocular pressure were used to find associations between collagen crimp period and radial distance from the scleral canal. The measurements from the LC and PPS were analyzed separately to determine if the collagen crimp period in each region was associated with distance from the scleral canal. When visualizing the results, we suspected that the relationship between PPS crimp period and distance from the canal was not linear. To determine the best fit, several models were fit with distance transformations (no transform or linear, logarithmic, and square root), and the model with the lowest Akaike Information Criterion (AIC) chosen. The AIC is a measure that determines the quality of the model by evaluating the trade-off between goodness of fit and model complexity. It is important to note

the AIC does not determine the significance of the model, only a relative quality of the model compared to other models of the same data.

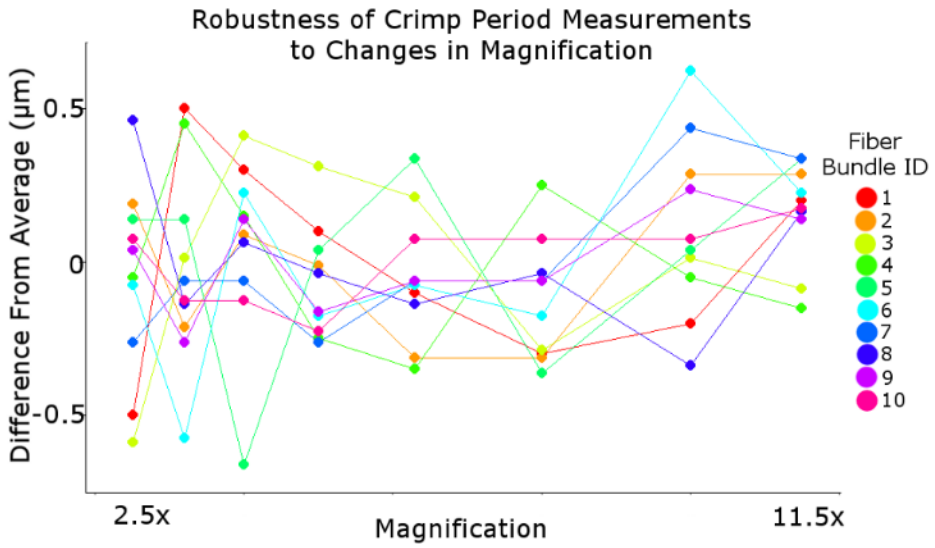

Figure 31. The robustness of our manual crimp period measurements to changes in image magnification.

One individual measured the crimp period of 10 fiber bundles through 8 magnification settings. Each crimp period measurement was subtracted from the average measurement for that bundle through the different magnifications in order to visualize the robustness. To understand whether the robustness to changes in image magnification is large or small, comparison with the actual measurements in Figure 33 and Figure 34 is needed.

4.3 RESULTS

A total of 17,374 manual collagen crimp period measurements were made in this study. Repeated measurements made by a marker had a maximum standard deviation of 1.9 µm across the 34 fiber bundles (Figure 30A). Reproducibility of measurements between markers had a maximum standard deviation of 4.7 µm across the 34 bundles (Figure 30B). Comparing measurements of collagen crimp period from images acquired with a range of magnifications between 2.5x and

11.5x the largest standard deviation was 0.4 μm across 10 fiber bundles (Figure 31). Measurements were not significantly different when using different microscope-camera pairs (P>0.1), nor were the measurements significantly different between those from different eyes and animals (P>0.1, 7 eyes from 4 animals, 12,796 total measurements) (Figure 32).

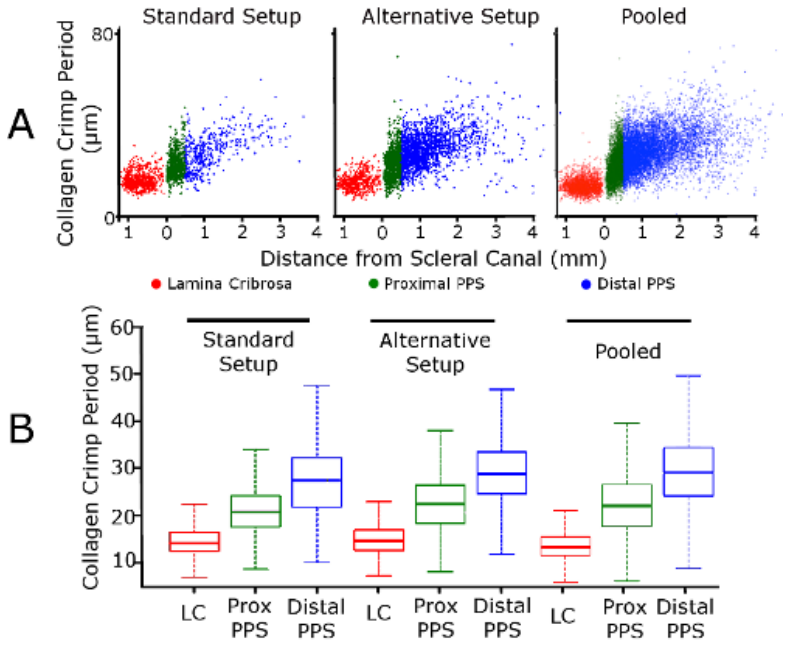

Figure 32. Collagen crimp period scatterplots (A) and box plots (B) from using different imaging setups in two example eyes, and pooled across 7 eyes fixed at 5 mmHg IOP.

The left side corresponds with the standard setup (Olympus-Olympus microscope-camera pairing), the middle with the alternative imaging setup (as defined in the main text), and the right side with the pooled distributions across 7 eyes. The period measurements were robust to using different microscope-camera pairings and similar between different eyes and animals.

To quantify the crimp period in different regions of the ONH, a total of 4,498 manual measurements were taken, with at least 450 measurements in each of the 6 eyes. The collagen crimp period distributions between all eyes were similar (Figure 33), with no significant differences between eyes fixed at the three IOPs (Figure 34). There were no statistically significant differences in crimp period between eyes fixed at IOPs of 0, 5, or 10 mm Hg (P>0.1).For every

eye and IOP the crimp periods in the LC were significantly smaller (P<0.001) and less variable (P<0.001) than crimp periods in the PPS (Figure 33, Figure 34). When pooling crimp period measurements from all pressures, the average (SD) crimp period in the LC was 13.8 (3.1) μm, and 31.0 (10.4) μm in the PPS. The median crimp period in the LC was 13.3 μm, and 30.1 μm in the PPS. The crimp period ranges were 5.2-30.0 μm in the LC and 7.3-72.0 μm in the PPS.

In the LC, the crimp period did not vary significantly with distance from the scleral canal wall (P>0.1). However, crimp period in the PPS had an interesting pattern (Figure 35), being smallest next to the canal wall – and the LC, and increasing with distance from the canal wall. The crimp period in the proximal PPS (500 μm of PPS closest to the canal) had average (SD) of 22.4 (5.8) μm, which was significantly larger (P<0.001) than the 13.8 (3.1) μm average (SD) crimp period in the LC, and significantly smaller than the 35.4 (9.5) μm average (SD) crimp period in the distal PPS (more than 500 μm away from the canal wall). The median crimp period in the proximal PPS was 21.6 μm, and 34.7 μm for the distal PPS. The increases in PPS crimp period magnitude and variability with distance from the canal wall were also significant (P<0.001) and substantial, with period more than doubling in magnitude at 2 mm from the canal (Figure 34).

Table 1. Summary of results from statistical tests.

The distance was transformed according to the model type and the AIC and P-value was calculated to determine the best model. The bolded model was best for the PPS, with the lowest AIC and a significant P-value.

Model Type	Lamina Cribrosa		Peripapillary Sclera	
	AIC	P-value	AIC	P-value
Linear	5744	0.6468	22358	<0.0001
Log	5732	0.8907	22319	<0.0001
Square Root	5737	0.7659	**22158**	**<0.0001**

All three models (linear – no transformation, log of distance, square-root of distance), showed a statistically significant association between crimp period and distance from the canal in the PPS ($P < 0.001$). The root-square model had the lowest AIC value (Table 1).

4.4 DISCUSSION

We have presented a detailed characterization of the collagen fiber crimp period in the LC and PPS at normal and low IOPs. To the best of our knowledge, this is the first systematic quantification of collagen fibers crimp properties in the posterior pole. The manual crimp period measurements were repeatable and reproducible both within and between markers. The measurements were robust to differences in the magnification used during image acquisition and to the use of different imaging setups with different microscope-camera pairings.

We quantified the collagen crimp period in the LC and PPS in eyes at normal and low IOPs. Three main results arise from this work: First, the collagen crimp period in the LC was smaller, and less variable, than the crimp period in the PPS, and did not change with distance from the canal. Second, there were no significant differences in collagen fiber crimp period in eyes fixed at IOPs of 0, 5, or 10 mm Hg. Third, in the proximal PPS, the collagen crimp period was slightly larger than in the LC, and increased non-linearly with distance from the canal wall. Let us consider each of these in turn.

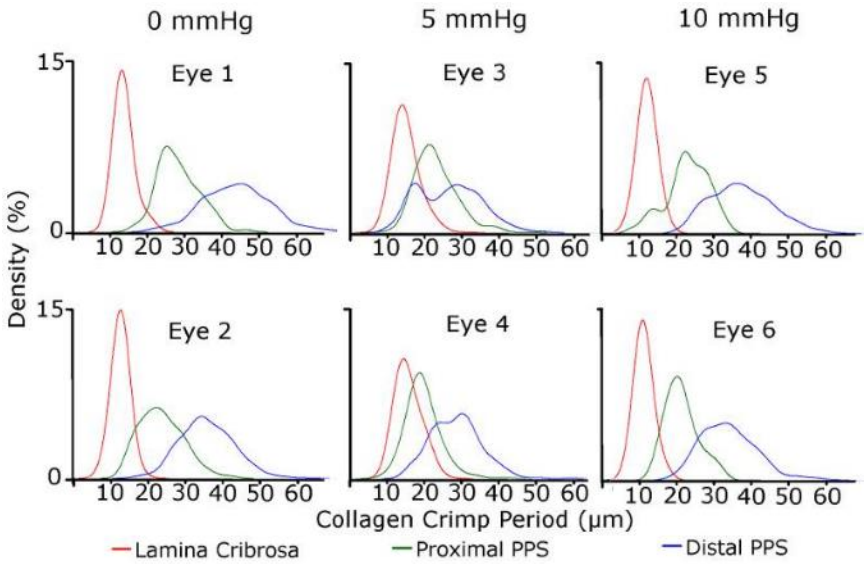

Figure 33. Density plots of the collagen crimp period distribution in each eye by LC and PPS regions.

The collagen crimp period in the LC was smaller and less variable than the crimp period in the PPS, and did not vary with distance from the canal. This indicated that the baseline crimp period in the LC was uniform. Uniform crimp morphology has been hypothesized to have a steeper (or less gradual) stiffening response to stretch than variable crimp morphology (Figure 36).(J Diamant et al., 1972) This means that the LC may have close to a step-wise stiffening response to stretch compared to the PPS. As the LC houses delicate retinal ganglion cell axons and astrocytes, this collagen crimp period distribution allows the whole LC to stiffen simultaneously, rather than allowing some parts to stiffen before others. This results in a more even response to changes in pressure across the whole LC in order to avoid concentrations of strain that could hurt the axons. Note that this still allows for local variations in IOP-induced deformations arising from the complex LC pore and beam architecture.(Ian A Sigal et al., 2014; Andrew P Voorhees, Jan, Flanagan, Sivak, & Sigal, 2016)

There were no significant differences in collagen fiber crimp period between eyes fixed at IOPs of 0, 5, or 10 mm Hg. We chose to study crimp period at these pressures to establish

the baseline characteristics of the collagen fibers, without the potentially individual-specific effects of elevated IOP. From a mechanical perspective it would be anticipated that increases in IOP would cause collagen fiber stretch, affecting the fiber crimp characteristics.(Franchi et al., 2007) Our results are important because they demonstrate that crimp period remains essentially unchanged when IOP decreases from physiologic to sub-physiologic, and even to zero. These results are consistent with the mechanical concept that at low IOP, the collagen fibers bear little load, although there may still be residual stresses in the tissue.(R. Wang, Raykin, Gleason, & Ethier, 2015) Note that these results do not imply that there were no changes in crimp with increased IOP, only that there were no changes in crimp period. IOP may result in changes in other aspects of collagen crimp.

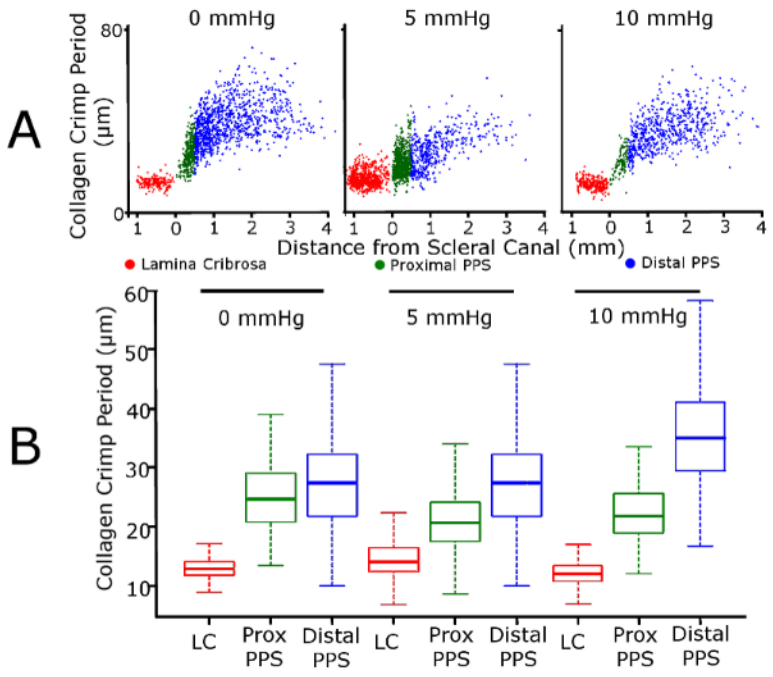

Figure 34. The crimp period distribution was similar between eyes fixed at 0, 5, and 10 mmHg IOPs. Scatterplots (A) and boxplots (B) of the collagen crimp period as a function of distance from the scleral canal pooling all sections and eyes at a given IOP.

In the proximal PPS, the collagen crimp period was slightly larger than in the LC, and increased non-linearly with distance from the canal wall. The baseline crimp period in the PPS was not uniform, indicating that the collagen fiber morphology is more variable in the PPS than in the LC. As mentioned above, the more heterogeneous the crimp morphology is at baseline, the more gradual the stiffening of the tissue is in response to stretch.(J Diamant et al., 1972) (Figure 36). Thus, our finding of heterogeneous baseline PPS crimp is consistent with the nonlinear response to mechanical loading that is well recognized in the sclera.(Woo, Kobayashi, Schlegel, & Lawrence, 1972) Based on the finding that PPS crimp period increased with distance from the canal, we predict that scleral mechanical nonlinearity will also vary with distance from the canal. This would be in addition to the already known differences in anisotropy with circumferential fibers in the proximal PPS.(Jan, Lathrop, et al., 2017) To the best of our knowledge, experiments have not yet been able to determine this. From a mechanical perspective, the canal opening in the scleral shell will result in the circumferential stresses being maximal at the canal edge, and decrease with distance from the canal. In a homogeneous thin shell, this decrease is proportional to the inverse of the square of the distance from the canal.(A. Voorhees, Millwater, & Bagley, 2011) The pattern of crimp properties observed could function to counterbalance these stress concentrations. In this way, the small differences in crimp period and variability between the proximal PPS and LC may reduce differences between the tissue stiffnesses at normal IOPs. This would alleviate concentrations of stress and strain, particularly shear, which are often harmful to tissues. At elevated IOPs, the heterogeneous crimp patterns would provide the PPS the ability to recruit additional fibers away from the canal, increasing tissue stiffness while still preventing large insult to the LC. We should note, however, that the direct mechanical relationship between crimp period and fiber recruitment and tissue stiffness remains unknown and should be investigated. One

of the main motivations for this work was to provide experimental data on the baseline crimp characteristics needed for the development of robust fiber-based microstructure constitutive models of the LC and PPS.

We are not the first to report regional collagen structure heterogeneity in the ONH. However, most studies have lacked the sensitivity and resolution, or the field-of-view for measuring the collagen crimp that we have studied. The majority of past studies have focused on the macro-scale patterns in the collagen structure. Ex vivo studies using serial block face imaging,(Reynaud et al., 2016) second harmonic generated imaging (SHG),(Albon et al., 2007; Donald J Brown, Naoyuki Morishige, Aneesh Neekhra, Don S Minckler, & James V Jester, 2007; Ian A Sigal et al., 2014) as well as in vivo studies using optical coherence tomography (OCT)(Ivers et al., 2011; Zach Nadler et al., 2013; B. Wang et al., 2013) have quantified LC trabeculae beam thicknesses and pore diameters, which was useful for understanding regional differences in the LC collagen macrostructure, but provide no information on collagen microstructure. For the PPS, studies using wide-angle x-ray scattering (WAXS)(Coudrillier et al., 2015; Jacek Klaudiusz Pijanka et al., 2012) and small angle light scattering (SALS)(M. J. Girard, A. Dahlmann-Noor, S. Rayapureddi, J. A. Bechara, B. M. E. Bertin, et al., 2011) quantified collagen fiber orientation patterns across large patches of ONH as well as for whole eye globes. Both techniques have visualized important patterns in the PPS collagen macrostructure, including a circumferential ring of collagen fibers around the scleral canal.(Jacek Klaudiusz Pijanka et al., 2013; Jacek Klaudiusz Pijanka et al., 2012; Jacek K. Pijanka et al., 2015; Quigley, Dorman-Pease, & Brown, 1991; Thale & Tillmann, 1993a) However, these studies did not address the collagen microstructure of the PPS either. One of the main reasons such modalities have not been able to detect microstructural crimp is that the orientation information that is quantified from SALS and WAXS combine the

contributions of meso-scale fiber bundle splay and microstructural crimp when measuring the collagen fiber angular distribution.(Pierlot et al., 2014) Therefore, a modality with higher sensitivity and resolution is needed to separate out these two contributions. Utilizing polarization-sensitive OCT, Baumann and colleagues noted a donut-shaped pattern of scleral birefringence in the rat PPS, formed by circumferentially organized fibers.(Baumann et al., 2014)

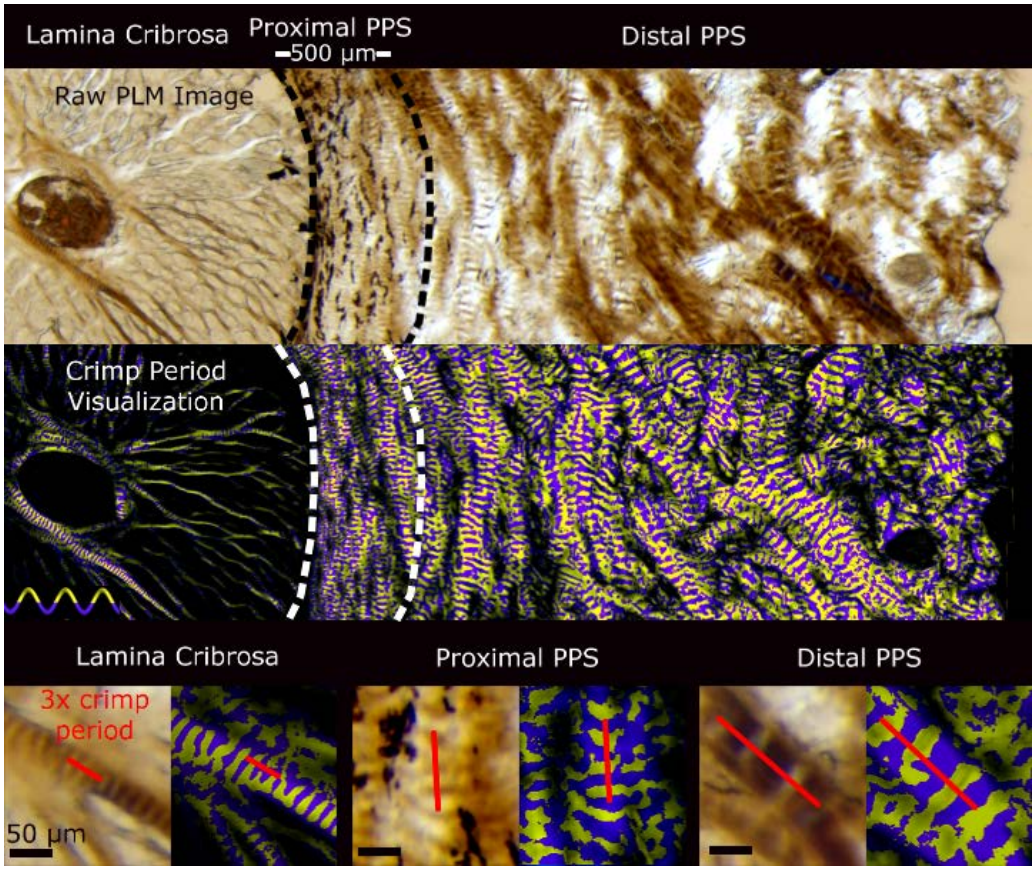

Figure 35. Crimp period visualizations of the lamina cribrosa and peripapillary sclera. Wide views spanning the lamina cribrosa and sclera under PLM (top) and visualized using the yellow and purple bands as described in the text to simplify discerning crimp period independent of the orientation (middle). The bottom shows pairs of raw PLM images and corresponding crimp period visualization images of close-ups of the LC (bottom left), proximal PPS (bottom center) and distal PPS (bottom right). An example line illustrating three periods is overlaid on each. It is easy to distinguish that the crimp period in the LC was small. In the proximal PPS the period was similar to that of the LC. The period increased with distance from the canal.

Many of the imaging techniques mentioned above are more appropriate to one tissue or the other due to large differences in the tissue density and feature size between the LC and PPS. In comparison, PLM has the appropriate sensitivity and resolution to quantify crimp in both individual LC beams and PPS collagen bundles creating a fair basis for comparison.

The relationship between crimp morphology and the overall mechanical properties of tissue is very complex. In this work we have focused on the crimp period, a natural property of the wavy or undulating collagen fibers. Nevertheless, it is important to remember that crimp period is only one aspect of the fiber undulation. Other aspects of crimp, such as the maximum deviation angle, amplitude, tortuosity and waviness can also be used to characterize the crimp, and could vary in different ways than period. For example, two different collagen fibers can have the same crimp period, but different waviness or amplitude. Because of this, a larger or smaller crimp period may not indicate tissue that is less or more stretched, respectively. However, there may be some redundancy between the parameters and not all may be needed to fully characterize the undulations. Grytz and colleagues used inverse modeling to predict the crimp maximum deviation angle in the ONH,(Grytz et al., 2011) whereas others have measured the amplitude of fibers in the pulmonary valve,(Joyce, Liao, Schoen, Mayer Jr, & Sacks, 2009) and the tortuosity of fibers in ventricular myocardium.(Omens, Miller, & Covell, 1997) Although it is generally accepted that as fibers are stretched, they will lose their crimp, each crimp parameter may have a different relationship with stretch. Further research is needed to quantify additional crimp characteristics to be able to predict local fiber recruitment and tissue properties under various levels of IOP.

The collagen in the eye has also been visualized, even if not systematically analyzed and measured.(Andreo & Farrell, 1982; Ho et al., 2014; Keith M. Meek & Boote, 2009; Mega et al., 2012; Ostrin & Wildsoet, 2016; Quantock et al., 2015) Electron micrographs revealed the wavy

collagen fiber crimp in the cornea more than 30 years ago. (Andreo & Farrell, 1982) Since then, others have visualized the crimp in the eye with other imaging modalities, including brightfield,(Ostrin & Wildsoet, 2016) nonlinear microscopy,(Quantock et al., 2015), and MRI.(Ho et al., 2014) Experimental measures of crimp characteristics exist for the cornea, using transmission electron microscopy,(Liu et al., 2014) but not for the LC or sclera.

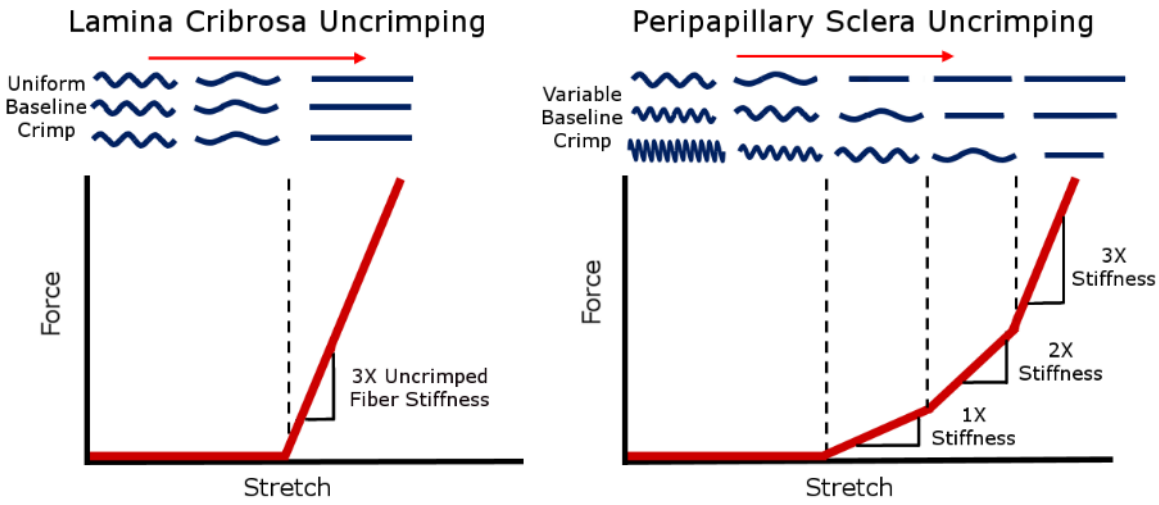

Figure 36. Schematic of how different baseline crimp distributions in the ONH can determine the nonlinear macroscopic biomechanical behavior of the tissue.

In a region with uniform, such as the LC, base crimp distribution, stretch leads to a macroscopic step increase in stiffness due to the simultaneous straightening of the fibers. In a region with variable crimp distribution, such as the PPS, the variable crimp disribution results in a macroscopic gradual increase in stiffness with stretch. It is important to note that crimp period is only one aspect of the fiber undulation and other characteristics could vary differently.

A useful property of the technique we have presented, is that the sample preparation is relatively simple. Using PLM, collagenous tissue is visible without stains or labels, avoiding time-consuming multi-step procedures. Crimp features are orientation-sensitive, so manually measuring the crimp period from sections imaged with PLM is intuitive, in comparison to measuring period from strained sections imaged with brightfield microscopy or labeled sections imaged with

fluorescence microscopy.(Downs et al., 2007; Hernandez et al., 1990; M Rosario Hernandez, Xing Xing Luo, Wieslawa Andrzejewska, & Arthur H Neufeld, 1989; M Rosario Hernandez et al., 1987; Sigal et al., 2010; H. Yang et al., 2007) Our technique also minimizes tissue processing, reducing potential artifacts. The tissues were never dehydrated, a step necessary in paraffin or plastic embedding which shrinks and warps tissue. The tissues were also never flattened, a common practice when studying scleral tissue with SALS(M. J. Girard, A. Dahlmann-Noor, S. Rayapureddi, J. A. Bechara, B. M. E. Bertin, et al., 2011) or WAXS(Jacek Klaudiusz Pijanka et al., 2013) which could affect the collagen structure and bias orientation measurements.

Along with the strengths of our method, it is important to also consider its limitations. There are potential artifacts from using ex-vivo tissues, histological processing, and cryosectioning. The tissues may have artifacts from 10% formalin fixation, though we have shown our method of fixation has minimal effects on ocular tissue size or shape. (Tran H, manuscript submitted, 2017) It is also possible that there existed some shell distortion for the eyes fixed at 0 mm Hg IOP, which could have deformed the collagen affecting the crimp period measured. However, we did not detect any statistically significant differences in crimp period between eyes fixed at 0, 5, or 10 mm Hg IOP, so the effects were small relative to the variability. Other crimp parameters may be more sensitive to these changes with IOP. Future studies could address other general structural artifacts by using fiducial markers to correct for tissue warping during processing and sectioning.(Sigal et al., 2010) Another limitation is the use of sheep eyes. Sheep eyes, like human eyes, have a collagenous LC. However, there are distinct structural differences, including a thick tree-like structure called the ventral groove in the ONH. It is possible that the microstructural crimp patterns we found in sheep may not apply to humans. It is important to

understand sheep as an animal model,(Gerometta et al., 2010) but future work should include measurements of crimp in other animal models as well as human.

Our measurements of the crimp period were done in 2D in coronal sections of the ONH. It is possible that the direction of sectioning may affect the collagen crimp period measurements. This could be addressed, for example, through the development of techniques that permit measurement of collagen orientation in 3D. (Yang B, et al. IOVS 2017; 58: ARVO E-Abstract 4825) However, in the ONH, the tissue is mainly loaded in the coronal direction. Biomechanical studies have shown that even though the IOP acts normal to the tissue, the main direction of loading (i.e. the largest forces) is in the transverse direction.(Bellezza, Hart, & Burgoyne, 2000; Norman et al., 2011; Sigal et al., 2004) Because of this preferential loading direction, the fibers oriented in this plane bear these loads and largely determine the biomechanics of the eye. Because our measurements were from coronal, or transverse, sections, in the preferred loading direction, the in-plane crimp periods are most relevant and the fibers on which these were measured are more likely to have large in-plane components. Also, the crimp period measurements we obtained may be affected by the angle of a bundle relative to the plane of the section. As such, our measurements would be projections of 3D periods, and therefore could underestimate the actual bundle periods. Thus, it seems reasonable to expect that measurements obtained in 3D would still show lower crimp periods in the LC than in the PPS. Nevertheless, this must be confirmed.

The crimp periods reported in this manuscript were cross-sectional, where the crimp in each eye was measured at a specific IOP. Because of this, the crimp trends reported are a reflection of a population of collagen fibers, rather than any specific fiber and how the crimp in a single fiber would change with pressure. To obtain this information, future studies could explore a different

type of experimental design, for example, tracking effects of loading on specific fibers or bundles. (Jan NJ, et al. IOVS 2016; 57: ARVO E-Abstract 3566)

In conclusion, to the best of our knowledge, we have presented the first systematic experimental characterization of the collagen crimp in the ONH. Crimp characteristics are important because they largely determine the nonlinear biomechanical behavior of the tissues. Our period measurements provide a basis to understand how microstructure governs larger scale tissue mechanics. This information helps reveal the role of microstructure on eye physiology, in aging, and in biomechanics-related diseases, such as glaucoma. Future directions include measuring other characteristics of the collagen crimp in addition to the period, as well as how these characteristics change with mechanical stimuli such as changes in IOP.

5.0 BASELINE CRIMP DISTRIBUTION AROUND THE EYE GLOBE

The content of this chapter was previously published in (Jan et al., 2018)

5.1 INTRODUCTION

The basic function of the eye as well as many diseases of the eye, including glaucoma and keratoconus, are intimately tied to the biomechanics of the corneoscleral shell.(Ethier et al., 2004) Corneoscleral biomechanics are, in turn, determined by the architecture of the underlying collagen. The collagen fibers of the eye, like those of other tissues, have a natural waviness known as crimp.(Andreo & Farrell, 1982; Gallagher & Maurice, 1977; Jan, Gomez, et al., 2017; Ning-Jiun Jan & Ian A. Sigal, 2018) Crimp has been noted in anatomy textbooks such as “Gray’s Anatomy”, which describes crimp as an innate property of Type I collagen fibers.(Standring, 2016) This crimp is central to eye biomechanics, as it largely determines the nonlinear (strain-dependent) biomechanical behavior of the tissues.(Fratzl, 2008; Holzapfel, 2001) Because of this importance, collagen crimp has been the focus of several studies. For example, the crimp in the cornea has been described by Andreo and Farrell,(Andreo & Farrell, 1982) and more recently by Newton and colleagues(Richard H Newton et al., 1996) and Liu and colleagues.(Liu et al., 2014) Crimp in the sclera was visualized by Ho and colleagues(Ho et al., 2014) using magnetic resonance imaging (MRI) and by Zyablitskaya and colleagues(Zyablitskaya et al., 2017) using second harmonic

imaging. We have described collagen crimp patterns in the lamina cribrosa and adjacent sclera obtained using polarized light microscopy (PLM).(Jan, Gomez, et al., 2017; Ning-Jiun Jan & Ian A. Sigal, 2018) The studies above, while useful, only describe isolated relatively small regions. Grytz and colleagues(Grytz & Meschke, 2009, 2010) used inverse modeling to estimate crimp properties in the cornea and limbus, or the optic nerve head and posterior sclera. Their models, while elegant, were still limited to regions of the corneoscleral shell. Furthermore, the models involved strong assumptions on collagen properties and globe shape, and their predictions have not been validated experimentally.

The various regions of the eye have diverse biomechanical and structural roles, and therefore the demands on the architecture and microarchitecture of the underlying connective tissues also vary. In addition, the corneoscleral shell is a continuous, cohesive envelope, in which the biomechanical behavior of one region is dependent on its own properties, and on those of other regions. The lack of experimental measures of collagen fiber properties across the globe, and specifically of collagen crimp, is a significant barrier to understanding eye biomechanics. Experimental measures of crimp are necessary to understand how the microarchitecture determines the behavior of the eye, including mechanisms related to development, aging, and pathology.

Our goals in this study were to measure the collagen fiber crimp around the entire corneoscleral shell, and to test the hypothesis that collagen crimp properties are not uniform around the globe. Specifically, we quantified the collagen crimp period, conformity, tortuosity, waviness, and amplitude across two corneal and six scleral regions.

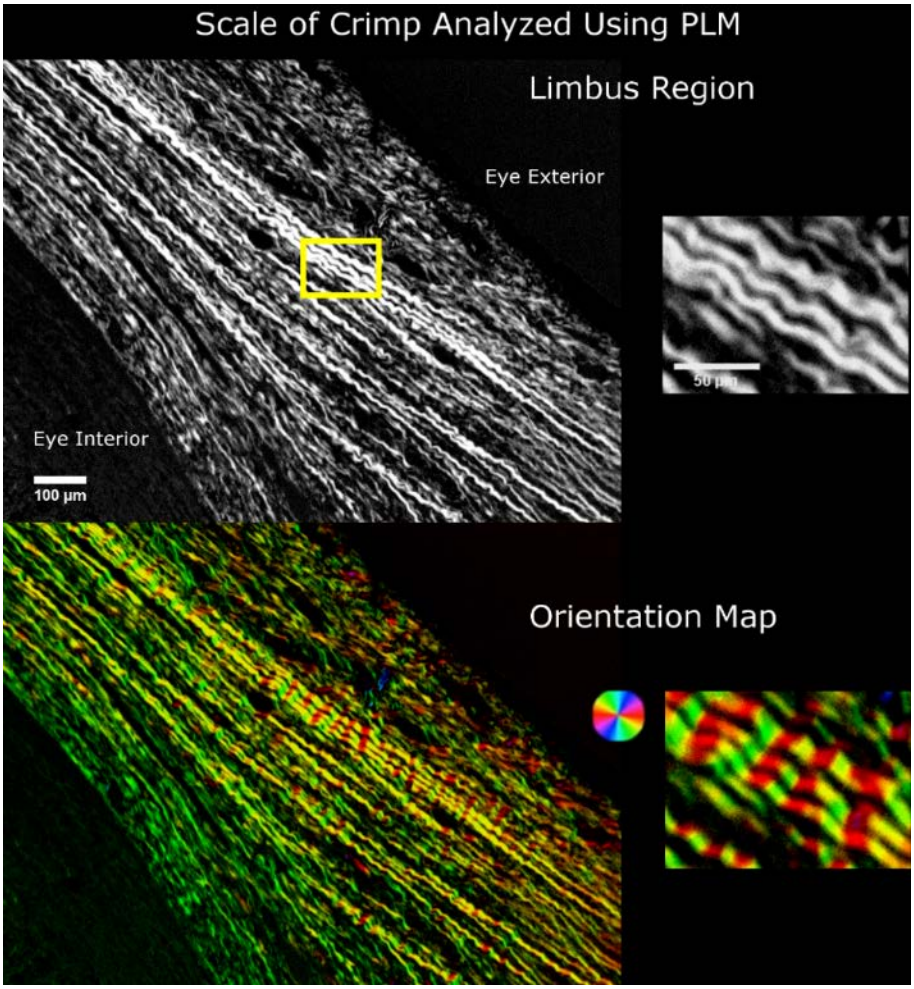

Figure 37. The scale of collagen crimp analyzed using PLM.

On the left hand side are wide-field views of the limbus region. The wavy patterns in the collagen fibers are clearly discernible and emphasized using a color map of orientation. The close up images on the right hand side show the periodic waviness analyzed in this work.

5.2 METHODS

5.2.1 On the terminology

It is imperative to recall that collagen architecture and hierarchical organization are complex and vary throughout the eye.(Fratzl, 2008) In some regions this organization has been well-characterized, such as in the cornea, which is a lamellar structure containing evenly-spaced fibrils approximately 35 nm in diameter, which are highly parallel to one-another within each lamella.(Andreo & Farrell, 1982; Gallagher & Maurice, 1977; Quantock et al., 2015) Collagen in the sclera forms what are often referred to as “bundles”. Our goal in this manuscript was not to do a detailed characterization of the collagen hierarchies over the globe. Thus, for clarity, throughout the manuscript we have used the terms “fiber bundles” or “group of collagen fibers”. With respect to our use of the term “crimp”, please see Figure 37 for an illustration of the scale of the fiber undulations studied.

5.2.2 Sample preparation

Three eyes of 2-year old sheep were obtained from a local abattoir. The eyes were processed within 8 hours of death following previously described methods, (Jan, Gomez, et al., 2017; Jan et al., 2015; Jan, Lathrop, et al., 2017; Ning-Jiun Jan & Ian A. Sigal, 2018) with slight modifications for the longitudinal sectioning of whole globes instead of transverse sections of optic nerve heads. Briefly, the muscles, fat, and episcleral tissues were carefully removed from each eye. The eyes were cannulated through the anterior chamber to a set pressure of 0 mmHg IOP using a saline reservoir. The pressure was set by first increasing the IOP slightly to 3-5 mmHg, by raising the

reservoir, to restore normal globe shape, and then lowered to 0 mmHg IOP by lowering the reservoir. The pressure was held at 0 mmHg for 15 min to allow normalization from viscoelastic effects before fixation. After the pressure had been set, the eyes were fixed by immersing them in a 10% formalin solution overnight. We have previously shown that, using formalin fixation causes only minimal changes in shape or size of ocular tissues at the macro,(Tran et al., 2017) and microscales,(Jan et al., 2015) including negligible effects on crimp. Intact whole globe eyes were embedded in such a way that all eyes lined up in the nasal-temporal and superior-inferior anatomical directions for cryosectioning. The eyes were cryosectioned into axial slices, with a thickness of 30 μm. For all eyes, the sections were obtained consecutively without loss. Sections were held flat using a standard anti-roll plate and a cold fine-tip brush before adhering the section to the histological slide. A total of 28 sections passing through both the PPS and the central cornea and free of artifacts, such as folds, were selected for imaging and analysis.

5.2.3 Imaging

The selected sections were imaged with PLM using previously reported methods (Jan, Gomez, et al., 2017; Jan et al., 2015; Jan, Lathrop, et al., 2017; Ning-Jiun Jan & Ian A. Sigal, 2018) to visualize the collagen crimp and quantify the collagen fiber orientations (Figure 37, Figure 38). Briefly, two filters (Hoya, Tokyo, Japan) were used; the polarizer filter was placed before the sample and the analyzer filter placed after the sample. Four images at filter orientations 45° apart were acquired. The relative changes in intensities at each pixel were used to determine the local collagen fiber orientation.(Shribak & Oldenbourg, 2003)

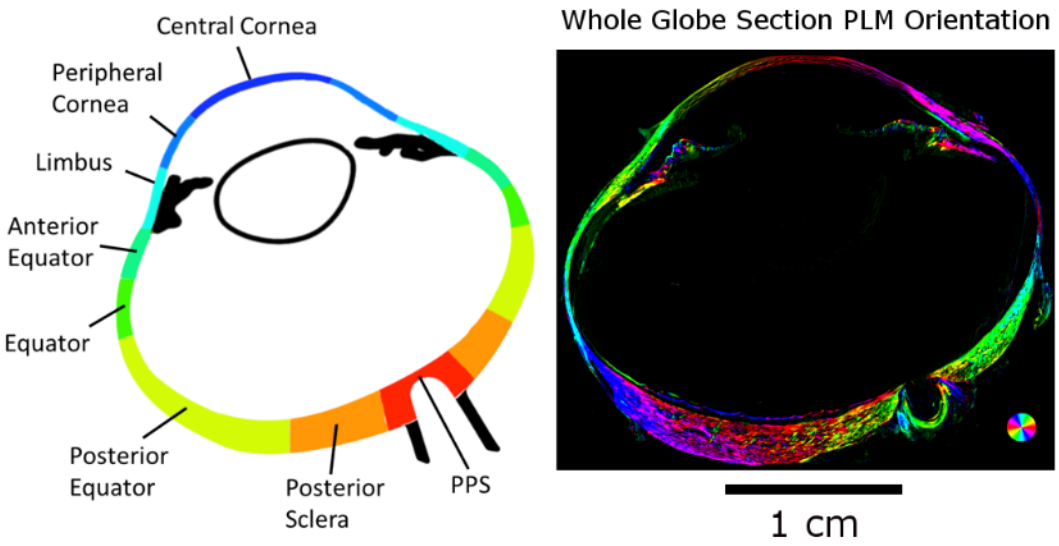

Figure 38. A map of the eye globe.

The 8 bilateral regions were analyzed for collagen crimp across the eye globe (Left). PLM images of each region were analyzed for collagen fiber orientation. PLM image of the whole globe. (Right) Colors indicate local fiber collagen fiber orientation, whereas intensity was scaled according to an "energy" measure, as explained in the main text.

The images were acquired with an Olympus SZX16 microscope (11.5X magnification setting) with an Olympus DP80 camera (36-bit, RGB, pixel-shift setting), a 0.6X reducer, and a 0.8X objective (numerical aperture [NA], 0.12) for a pixel size of 0.37 μm/pixel (Olympus, Tokyo, Japan). For analysis, the globe was divided into eight regions (Figure 38): PPS, posterior sclera, posterior equator, equator, anterior equator, limbus, peripheral cornea, and central cornea. Nasal and temporal regions were combined to focus on the anterior-posterior patterns. Each region was imaged independently. For large or thick regions, multiple images were captured to cover the entire region in a mosaic. The mosaics were obtained with 20% overlap and stitched using Fiji is Just Image J (FIJI).(Preibisch et al., 2009; Schindelin et al., 2012) We have previously shown that our collagen fiber measurements using PLM are not affected by the microscope-camera pairing, mosaics, stitching, or section orientation.(Jan, Gomez, et al., 2017; Jan et al., 2015; Jan, Lathrop,

et al., 2017) For presentation only, orientation images are presented with the pixel intensities scaled by an “energy” parameter. (Jan, Gomez, et al., 2017; Ning-Jiun Jan & Ian A. Sigal, 2018)

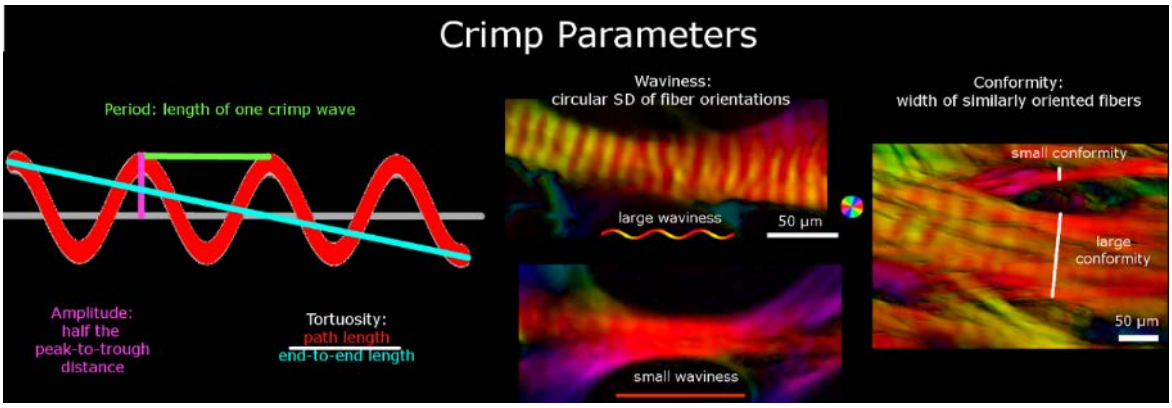

Figure 39. Crimp parameters definitions.

The crimp parameters that were quantified in this study were period, tortuosity, amplitude, waviness, and conformity. The period and conformity were measured manually, while the other parameters were measured semi-automatically using custom-scripts. The left-most panel shows an idealized collagen fiber crimp to illustrate the measurement of period, amplitude and tortuosity. The middle and right-most panel shows example PLM images presented as in **Figure 37**. The middle panel shows two collagen bundles, one with large waviness (top) and another with small waviness (bottom). The right-most panel is of a region with multiple bundles to illustrate small and large conformities. Note that this middle panel exemplifies the importance of the high angular resolution of PLM. Individual fibers and their crimp may not be directly discerned, but the orientations derived from PLM show clear evidence of undulations. Recall that the orientation analysis is done pixel by pixel and any organization and structure arise naturally. From these angles it is possible to deduce the crimp characteristics with high detail.

PLM has a high angular resolution. We have shown that PLM derived orientation measurements of ocular tissue have repeatability, reproducibility, robustness to translations, rotations, and magnification settings on the order of one or two degrees.(Jan et al., 2015) PLM, x-ray, and light scattering methods all determine orientation without detection of fiber edges.(Girard et al., 2011; Pijanka et al., 2013) Each pixel analyzed depicts the orientation of the fibers represented within that pixel, without the need for context from neighboring pixels.

5.2.4 Quantifying collagen crimp

For clarity, we start with a general description of the methods before describing in detail how each crimp characteristic was defined and quantified. We studied five crimp characteristics: period, conformity, tortuosity, waviness, and amplitude. (Figure 39) Period and conformity were measured manually from "raw" PLM images, whereas tortuosity, waviness, and amplitude were measured semi-automatically using the orientation maps derived from PLM at manually-defined places of measurement. To calculate tortuosity, waviness, and amplitude, a straight line was placed along a collagen bundle to sample the orientations obtained with PLM. (Figure 40) Using custom Fiji code, we computed the tortuosity, waviness, and amplitude from this information using Riemann sums. In a preliminary study, we verified this method by using it first to measure the parameters of simulated bundles with known crimp. Next, we used the technique on images of longitudinal sections of tendon samples fixed without load so that they exhibit large crimp, similar to those used in Jan et al 2015. (Jan et al., 2015) Tendon has large, highly regular crimp, which can be easily resolved and is therefore suitable for manual crimp tracings to compare with our algorithm measurements. Finally, we analyzed ocular crimp in regions of large and highly visible crimp near the limbus. In all of these tests the crimp parameters calculated with this technique were within 2% of the known parameters or reference measurements obtained by fiber tracing. Because we sample the orientations across a manually placed pixel line from each group of collagen fibers, we tested to see if different samplings within the same group of collagen fibers would change crimp parameters. We found that lines within 15° of the main collagen fiber group direction and spanning at least one crimp cycle produced parameters within 3% of the reference ones. Because this PLM-based technique does not require resolving fiber edges, it is not affected by image resolution in the

same way as gradient-based or edge-detection techniques such as the algorithms used in the Fiji plugin, OrientationJ.(Püspöki, Storath, Sage, & Unser, 2016a)When put together with the high angular resolution, the technique can provide more accurate quantifications of fiber crimp than trace-based techniques for images of the same resolution and pixel size. In practice, it means that it allows accurate measurement of crimp amplitudes of fractions of a micron and of fibers with small tortuosity.

All parameters were measured from lines drawn manually. However, the parameters were obtained in two different ways. For period and conformity, we directly used the length of the lines drawn to determine the parameter (divided by three for the period). For tortuosity, waviness and amplitude, the line was used to select the pixels to sample. The orientation information in the sampled pixels was then analyzed to calculate the parameters. Below we describe the measurement of each parameter. Because the lines were drawn manually, we did additional tests to quantify the repeatability and reproducibility of the parameters obtained from them. In addition, because of the large number of lines that had to be drawn manually, the work was split into three people. To ensure consistency, an additional person with several years of experience in imaging and PLM measurement of crimp properties verified the crimp measurements (NJJ).

1) Period. The period was defined as the length of the collagen crimp through one wave, and measured manually using a previously described method.(Jan, Gomez, et al., 2017) Briefly, because of the direct relationship between intensity and orientation, the period could be visually identified using the inflection points between bright and dark bands, where each band corresponds to half of a crimp period. A straight line was used to measure the length of three sequential crimp periods by identifying three bright and dark bands. The period was then calculated by dividing the length of the line by 3 to get the average crimp period. We have shown that our method for

manually measuring crimp period from PLM images of coronal sections of the PPS has excellent repeatability and reproducibility.(Jan, Gomez, et al., 2017)

2) Tortuosity. Tortuosity was defined as the ratio of the path length of a fiber trace to its end-to-end length. A perfectly straight fiber would therefore have a tortuosity of 1, and a wavy fiber would have a tortuosity greater than 1. Tortuosity is sometimes also referred to as slack, as it relates to how much a fiber can be straightened before it becomes fully straight or taut. The path length of the fiber was calculated using a Riemann sum method based on the fiber orientation in each pixel of a line segment along a collagen bundle. The end-to-end length was computed from the number of pixels in the line.

3) Waviness. Waviness was defined as the circular standard deviation of the fiber orientations along a collagen bundle. A perfectly straight fiber, or set of fibers, would have a constant angle value along the bundle, and therefore would have a waviness of 0, whereas a wavy fiber would have waviness greater than 0.

4) Amplitude. Amplitude was defined as half of the peak-to-trough distance in a wave. A straight fiber would therefore have an amplitude of 0, whereas a wavy fiber would have an amplitude greater than 0. Similar to tortuosity, the amplitude was calculated using a Riemann sum method based on the fiber orientation in each pixel of a line segment across a collagen bundle. The amplitude for each fiber bundle was averaged across two periods.

5) Conformity. The conformity was defined as the width of a group of contiguous similarly oriented fibers and recognizable as a group or bundle in the images. Whereas the other parameters are intuitive or have already been used elsewhere to describe wavy collagen, conformity requires further explanation: Collagen fibers aggregate into larger structures, such as bundles and lamellae. Initially, we considered measuring fiber bundle or lamellae width. In small regions this works well,

but over the globe things are more complex. Bundles and lamellae are interwoven, splitting and/or merging. We reasoned that measuring the width of a group of fibers of similar orientation would be a more useful representation of the collagen organization than artificially defining boundaries. Our use of conformity, thus, has the advantage of not requiring the fibers to belong to a single bundle or lamellae, and instead assumes only that they all appear together. (Figure 41) For example, in regions with wide lamellae, like the cornea, multiple collagen bundles were oriented similarily, resulting in high conformity. Other regions, like the sclera, could have interweaving collagen bundles at large angles to each other, resulting in low conformity. Thus, conformity was measured by the length of a straight line manually placed perpendicular to the main direction of the bundles.

When marking the images, care was taken to distribute the marks evenly over a region. We were also careful to place them only on well-defined collagen bundles and lamellae that were long and bright. This limits the analysis to fibers in the section plane. Elsewhere it has been shown that the signal intensity in PLM encodes information on the relative orientation of the collagen fibers and the section, and imaging, plane. (B. Yang, Jan, Lam, Lathrop, & Sigal, 2017) As such, in our PLM implementation, in-plane fibers appear brighter than fibers perpendicular to this plane. Thus, dark regions may be collagen oriented orthogonal to this plane, or other tissue components (e.g. keratocytes).(B. Yang et al., 2017)

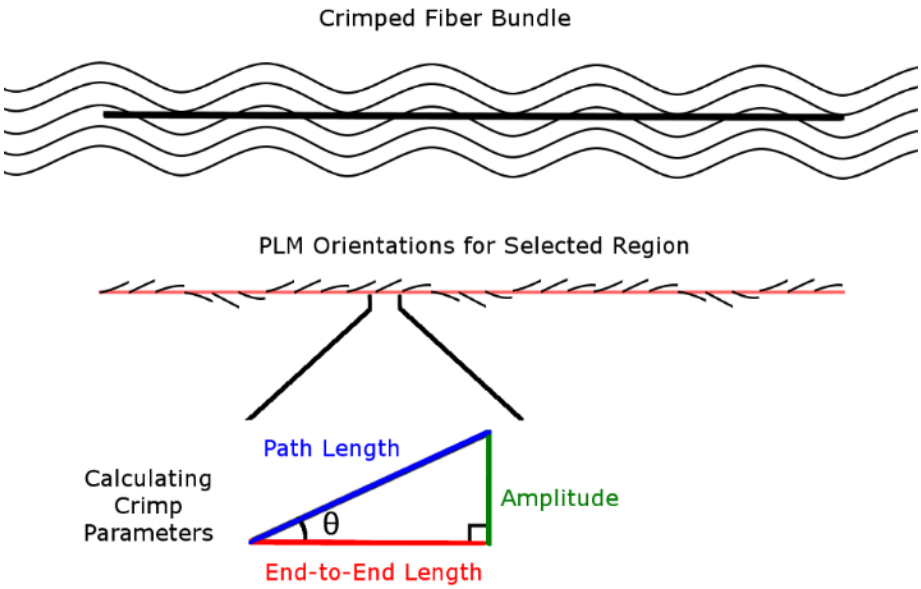

Figure 40. Calculating crimp parameters.

A straight line was marked manually along a bundle. Trigonometric identities were then used pixel by pixel along this path to calculate the local amplitude and lengths based on the orientation information derived from PLM. Local amplitude and lengths were then integrated to compute bundle crimp amplitude, path and end-to-end lengths.

5.2.5 Statistical analyses

1) Repeatability and reproducibility of manual-only collagen crimp measurements, period and conformity. To determine the repeatability and reproducibility of measuring the collagen crimp period and conformity in axial whole-globe sections of the eye, each person made manual period and conformity measurements in the same locations across the 8 regions three times. For each location, the standard deviation of each person's three crimp period and conformity measurements was calculated as well as the standard deviation of the pooled measurements. We report the largest standard deviations across all locations within each person as a worst-case measure of repeatability, and across all people as a worst-case measure of reproducibility.

2) Crimp distributions in each region. The medians, averages, and standard deviations for each crimp parameter and each region were calculated. In addition, the distributions are presented in a series of box plots in Figure 42 and heat maps in Figure 43.

3) Regional differences in crimp distributions. Linear mixed effect (LME) models accounting for autocorrelation of measurements from the same section, eye, and animal were used to determine if the period, conformity, tortuosity, waviness, or amplitude were significantly different between any two regions. Linear mixed effect models are linear models that incorporate fixed and random variables.(Gałecki & Burzykowski, 2013) Fixed variables are our variables of interest, such as period and random variables are factors that may affect the sampling population, such as whether there are different number of measurements in different regions or in different sections. We used a significance level of alpha = 0.05. Using a Bonferroni correction to account for the same test being done 28 times for each region pairing, we divided alpha by 28 for a significance level of alpha = 0.0018. The results of these tests are shown in Figure 44, with a table for each crimp parameter.

4) Bundle by bundle crimp associations in each region and across the globe. LMEs accounting for autocorrelation of measurements from the same section, eye, and animal were used to determine if there were significant associations between the crimp parameters, both pooled across all regions and within each of the 8 regions. A significance level of alpha = 0.05 was used. Applying a Bonferroni correction for the test being done 8 times for each region, we divided 0.05 by 8 to obtain a significance level of alpha = 0.00625, for the tests done within each region. In addition, the correlation coefficients, or LME slopes, were also calculated to compare the strengths of the associations. The results of the associations between tortuosity, waviness, and amplitude are shown in Figure 45.

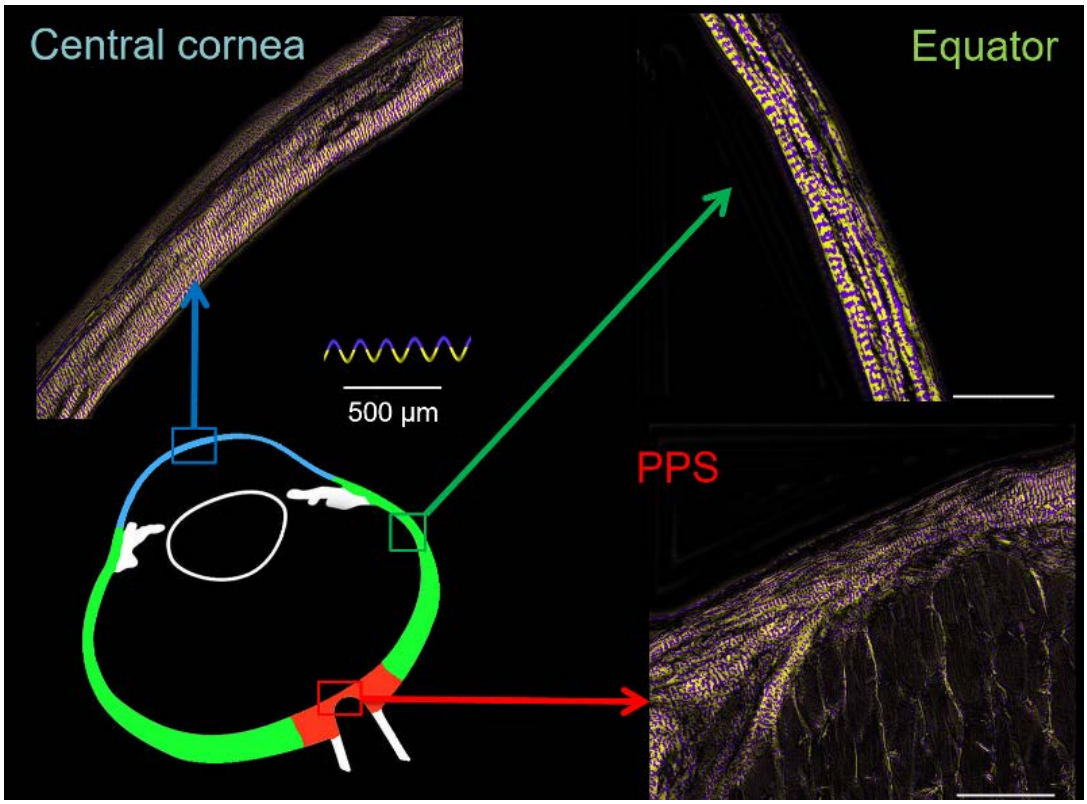

Figure 41. Crimp in different areas of the eye.

Using a yellow and purple color-scheme to highlight the collagen crimp period, we can see the collagen fibers in the cornea, sclera, and PPS had very different collagen structure. In the cornea, the majority of the collagen bundles run in the same orientation and therefore have large conformity. In the equator and PPS, the collagen bundles have more heterogeneity in their orientation, resulting in small conformity.

5.3 RESULTS

5.3.1 Crimp Distributions in Each Region

A total of 8,216 collagen fiber bundles were measured, with at least 1,500 fiber bundles per eye. The manual-only crimp parameters had small standard deviations between and across the three markers. The period measurements had a repeatability of 1.9 µm and reproducibility of 3.1 µm,

whereas the conformity measurements had a repeatability of 1.8 μm and a reproducibility of 3.3 μm.

Tortuosity, waviness and amplitude exhibited similar “double hump” or “M-shaped” distributions over the globe (Figure 42 and Figure 43). All three parameters had lower values, or “troughs” at the PPS, equator and central cornea (left, middle and right in the plots), and higher, or “peak” values in-between. However, both tortuosity and waviness had its second peak in the peripheral cornea, whereas amplitude had its second peak in the limbus. The posterior sclera region had the largest median tortuosity (1.012), waviness (17.2°), and amplitude (1.0 μm). The average±SD tortuosity was 1.028±0.060, the waviness was 20.3±13.2°, and the amplitude was 1.2±0.9 μm, respectively for this region. The equator had the smallest median (average±SD) tortuosity of 1.002 (1.008±0.045) and waviness with a median of 6.2° (8.3±8.4°) whereas the central cornea had the smallest amplitude with a median of 0.35 μm (0.59±0.69 μm).

Period and conformity did not exhibit a double hump pattern. Instead, period in the sclera increased progressively from PPS to anterior equatorial sclera, decreasing slightly to the limbus and then dropping substantially in the cornea. The anterior equator had the largest median period of 32.9 μm (31.1±9.7 μm), whereas the central cornea had the smallest, with median of 14.1 μm (14.3±2.5 μm).

Conformity exhibited a pattern roughly the opposite of the period, although the variations were smaller. Conformity changed little throughout the sclera, with a slight trough at the anterior equator and an increase at the cornea. The central cornea had the largest average conformity of 17.7 μm (20.7±12.5 μm), whereas the anterior equator had the smallest conformity of 11.7 μm (12.6±5.6 μm).

5.3.2 Regional Differences in Crimp Distribution

The matrices of comparisons between region pairings are shown in Figure 44. For every region pairing, at least one of the five crimp parameters was significantly different. Even though tortuosity, waviness, and amplitude have similar region to region patterns (Figure 42 and Figure 43), they did not have the same results when comparing between regions.

Peripheral and central cornea had significantly different collagen crimp, whereby the peripheral cornea had larger tortuosity, waviness, and amplitude than the central cornea. The period and conformity of the fibers in these two regions, however, were not significantly different.

When comparing the limbus and equator regions, we found that bundles from these two regions were not significantly different in period, conformity, and tortuosity. The limbus had larger waviness and amplitude than the equator.

When comparing the PPS and corneal regions, we found that the PPS had larger period, smaller conformity than the cornea. The PPS had smaller waviness and tortuosity than the peripheral cornea, though there was no significant difference when comparing the waviness and tortuosity of the PPS vs. the central cornea. In contrast, the PPS had larger amplitude than the central cornea, but there was no significant difference between the amplitudes of the PPS and the peripheral cornea.

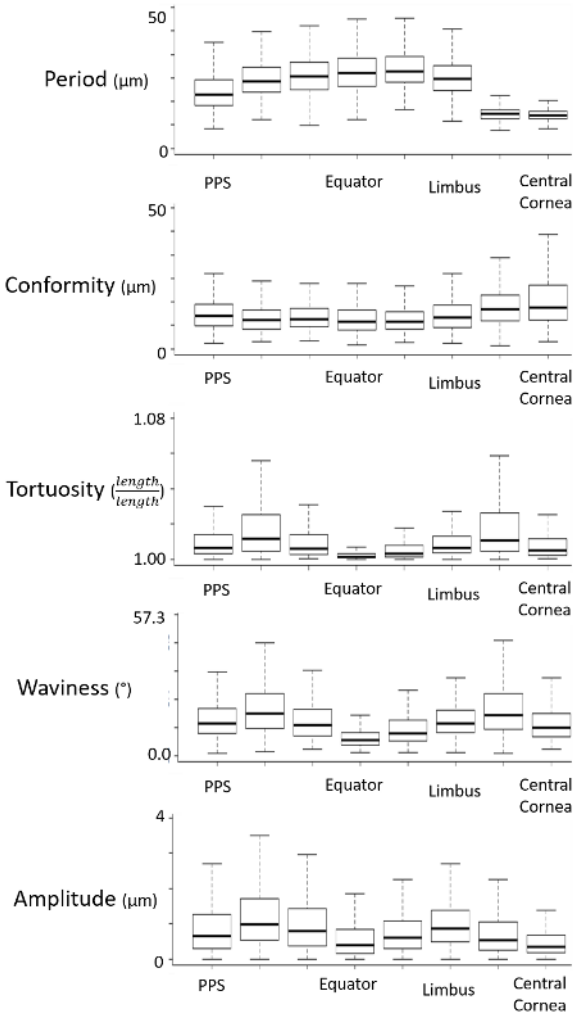

Figure 42. Boxplots of the distribution of each crimp parameter in each region.

The regions are ordered from posterior (PPS) to anterior (central cornea). Period and conformity had generally opposite trends while tortuosity, waviness, and amplitude had similar trends. Note that each box in the plots above represents between 100 and 1200 measurements.

5.3.3 Bundle by Bundle Crimp Associations

When separating the bundles by region, we found that for all the regions, tortuosity, waviness, and amplitude were positively significantly associated with one another. When measurements were pooled for all bundles across the globe, again the tortuosity, waviness, and amplitude were also positively associated with one another. Within each region and across the globe, bundles with

larger tortuosity were likely to have larger waviness and amplitude. Period and conformity relationships with other parameters were region specific, meaning that, in some regions bundles with larger period had larger conformity whereas in some regions they had smaller conformity, and in the rest they had no significant associations.

To facilitate understanding the meaning of the parameters variations measured, we constructed visualization of the variation in crimp from each region using the values of period and amplitude. (Figure 46).

5.4 DISCUSSION

Our goals were to carry out a systematic quantification of the crimp morphology over the corneoscleral shell, and to test the hypothesis that collagen crimp is not uniform over the globe, but instead that there are regional patterns. We characterized the collagen crimp properties in 8 regions of the eye, two corneal regions and six scleral regions. Three main results arise from this work. First, all the collagen crimp parameters varied substantially and significantly over the globe. Second, regions with small period were likely to have large conformity, whereas regions with high tortuosity were likely to have high waviness and amplitude. Third, fiber bundles with high tortuosity were likely to also have high waviness and amplitude. Let us consider each of these in turn.

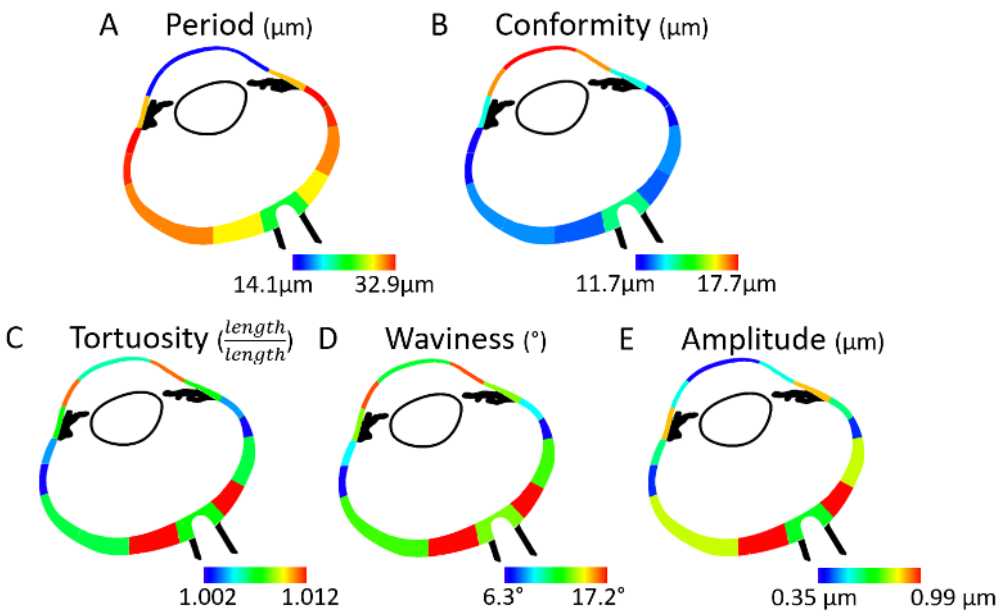

Figure 43. Heat maps of the mean of each collagen crimp parameter in each region.

Blue was used to designate the smallest value within each heat map, and red to represent the highest value.

Collagen crimp parameters varied substantially and significantly over the globe. Collagen crimp properties are a critical determinant of tissue biomechanical properties.(Fratzl, 2008; Holzapfel, 2001) Our results show that these parameters are neither uniform nor vary randomly from region to region. Instead, we found that these parameters have distinct patterns over the globe, where regions have specific combinations of parameters. (Figure 42 and Figure 43) This, in turn, points to the existence of a mechanism that controls the collagen fiber properties at the regional level.

Central corneal fiber bundles were significantly different than the peripheral fiber bundles in 4 out of the 5 crimp parameters. Only conformity was not significantly different between the central and peripheral cornea. (Figure 44) The differences in the remaining parameters indicate that the peripheral region is biomechanically distinct from the central region. Other studies have found that the peripheral cornea has a different immunohistochemistry,(Hamrah, Huq, Liu, Zhang,

& Dana, 2003) and ultrastructure than the central cornea, different thickness(Martola & Baum, 1968) and curvature,(Read, Collins, Carney, & Franklin, 2006) and different collagen fiber architecture, including density and anisotropy.(Keith M. Meek & Boote, 2009)

Regions with small period were likely to have large conformity while, regions with high tortuosity were likely to have high waviness and amplitude. As a reminder, conformity is not the width of each collagen bundle, but the width of contiguous similarly oriented bundles, which could include several collagen bundles. Generally, the larger the conformity, the more uniform and organized a region is because more of the fiber bundles are oriented in the same direction. This indicates that collagen fiber bundles that have smaller periods tend to stack together to form large groups of bundles with similar orientations. This stacking pattern may also be related to the collagen fibril diameters in these regions. Further work is needed to understand the full extent of the relationship between the crimp characteristics and the local structure. This stacking pattern may also be related to the collagen fibril diameters in these regions. Quigley and colleagues reported that the collagen fibril diameters were larger in the equator and smaller in the PPS,(Quigley et al., 1991) following a similar pattern to what we found for crimp period. The fibers of the cornea had the largest conformities and smallest periods, consistent with this region being organized more regularly compared to the sclera.(Han, Giese, & Bille, 2005; K. M. Meek & Fullwood, 2001) The sclera anterior to the equator, on the other hand, had the largest period and smallest conformity. This evidence points to the period and conformity as parameters representative of the overall level of structural organization in a tissue region.

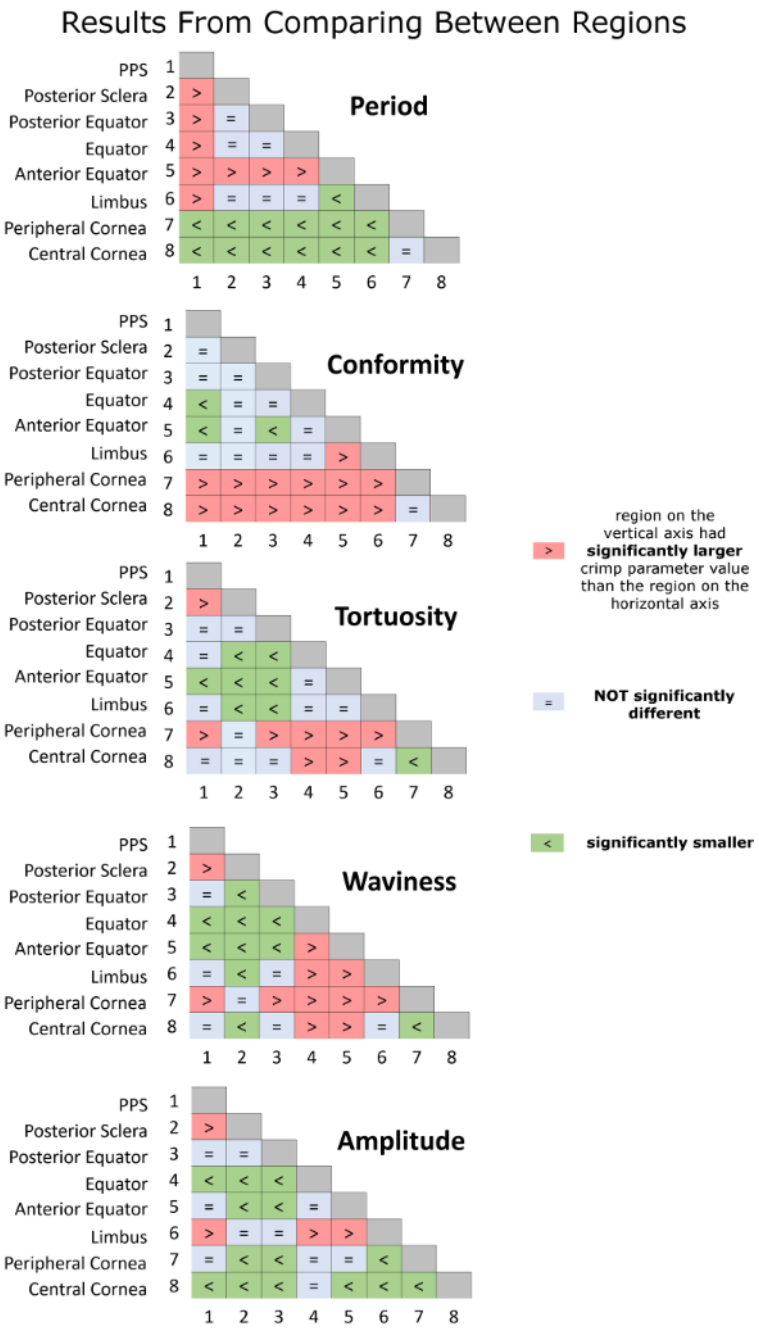

Figure 44. Matrices of LME tests comparing crimp between regions.

The distributions for each crimp parameter were compared between the 8 regions. Each matrix entry depicts a comparison between two regions. The colors and symbols indicate whether the region in the vertical axis was larger (red), smaller (green) or not significantly different (light blue) than the one on the horizontal axis.

Fiber bundles with high tortuosity were likely to have high waviness and amplitude. Fiber bundle's tortuosity, waviness, and amplitude were significantly related across the whole globe as well as within each of the 8 regions. (Figure 45) This indicates that individual fiber bundles with larger tortuosity tend to have larger waviness and amplitude, and that these associations are not region specific. For any specific fiber, tortuosity, waviness, and amplitude will vary together with stretch. (Figure 47) However, it is possible to define two fibers that have the same tortuosity, but have different waviness and amplitude (Figure 48). Even though these fibers could exist, we found that ocular collagen fibers followed a distinct pattern, in which fibers with larger tortuosity have larger waviness and amplitude. There are fewer ocular fibers with high waviness and small amplitude, high tortuosity with small amplitude, or high waviness and small tortuosity, and vice versa. This means that the individual fibers generally have similar shapes, and are proportionally larger or smaller depending on the region. (Figure 46) Further studies are needed to fully understand this relationship.

Interpreting the crimp parameters. Mechanically, stretching a crimped fiber will cause an increase in period, but a decrease in tortuosity, waviness, and amplitude. (Figure 47) Thus, studies of collagen fiber crimp typically associate larger periods with larger tortuosity, waviness and amplitude. (Diamant et al., 1972) However, two fibers can have the same period with different tortuosity, waviness, and amplitude. Hence, in a population of fibers, the period may or may not be associated with the tortuosity, waviness, or amplitude. It is therefore essential to distinguish parameters representing a population of fibers from parameters representing a specific fiber. Similarly, it is important to distinguish between parameter associations between globe regions and parameter associations within a region. Our results show that regional changes in period are more intimately related to the conformity, a structural organization parameter, rather than with the

tortuosity, waviness, and amplitude. Why the period is related to the conformity in ocular collagen fibers is still unknown and warrants further study.

LME Slopes		Tortuosity vs Waviness (1/°)	Amplitude vs Tortuosity (μm)	Amplitude vs Waviness (μ/°)
Associations in Each Region	PPS	0.15	8.24	1.84
	Posterior Sclera	0.23	5.04	1.94
	Posterior Equator	0.26	3.16	1.55
	Equator	0.25	2.62	1.02
	Anterior Equator	0.16	11.06	2.66
	Limbus	0.16	5.50	2.26
	Peripheral Cornea	0.27	3.75	1.36
	Central Cornea	0.27	4.16	1.42
Associations Across Whole Eye		0.23	4.24	1.64

color-scaled slopes: smallest slopes in green, largest slopes in red

Figure 45. The LME slopes of bundle-by-bundle crimp associations in each region.

Tortuosity, waviness, and amplitude were all significantly associated with one another for each region and across all eyes. The numbers shown on the table are the slopes of the associations obtained from the linear mixed effect models. To simplify distinguishing trends, the cells are colored according to the magnitude of the slope. Largest in red, lowest in green. For tortuosity vs waviness, the largest slopes occurred in the cornea, whereas for amplitude vs tortuosity and amplitude vs waviness, the largest slopes occurred in the anterior equator.

The similar spatial trends between tortuosity, waviness, and amplitude may indicate that these three parameters have a close-knit relationship. These three parameters are related to the amount of "slack" in a crimped fiber, which largely determines the nonlinear biomechanics of the tissue.(Fratzl, 2008; Holzapfel, 2001) Generally, stretching a straight collagen fiber requires substantially more force than straightening a crimped fiber. The process of progressive tissue stiffening due to uncrimping fibers is called recruitment. (Figure 47)

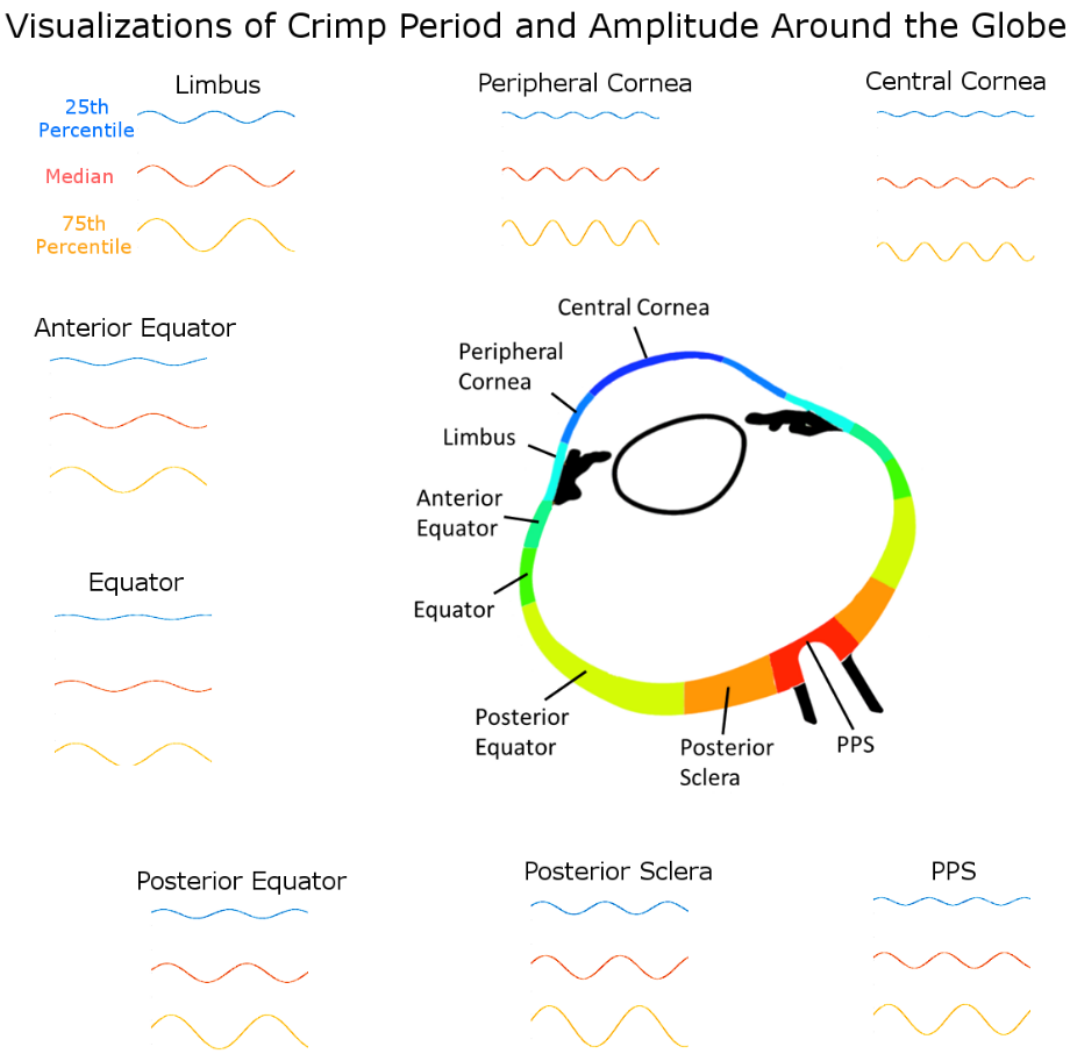

Figure 46. Comparing crimp period and amplitude across regions.

The 25th percentile, 50th percentile (median), and 75th percentile period and amplitude values were used to generate representative fibers for each region as sinusoidals. Note that these visualizations are not intended to represent any specific fibril, fiber, fiber bundle or lamellae, but are intended to visualize how the crimp differs between regions.

Although recruitment is central to the nonlinear stiffening in collagenous soft tissues, there are also other ways that collagen can stretch and stiffen, such as fiber reorientation and fibril or molecular slippage. Experimental characterization of these may require techniques other than PLM, such as the X-ray scattering, as recently demonstrated by Bell and colleagues.(Bell et al.,

2018) Fibers with more slack require more stretch to get to a straight, stiffer state. In a population of fibers with more variable slack, this stiffening is more gradual, since more and more fibers will become recruited with increasing stretch. The equatorial region had lower mean and less variable fiber tortuosity, waviness, and amplitude compared to other regions. The fibers in this region may therefore require less stretch to straighten, and would stiffen less gradually compared to other regions. The posterior sclera, on the other hand, had larger and more variable tortuosity, waviness, and amplitude. The crimped fibers in this region may require more stretch in order to straighten, and stiffen more gradually compared to those in other regions. A mechanical role for the low slack and low slack variability in the PPS and cornea is consistent with the thought that these regions would benefit from small deformations and uniform stiffening at moderate IOPs. Uniform deformations and stiffening would help maintain cornea shape and sharp optics. For the PPS, uniform stiffening and small deformations would help protect the neural tissues from excessive deformations that could cause neuropathy and vision loss. The role and potential biomechanical advantages, if any, of low slack and low slack variability in the equator is not clear and should be investigated. Our findings, however, suggest that the equator likely does not behave as a soft "mechanical absorber" to protect other regions from large acute volume or IOP increases. This is consistent a recent study in which we found that globe equatorial diameter did not change with increasing IOP.(Andrew P Voorhees et al., 2017) Alternatively, our results could be interpreted as suggesting that the posterior sclera and peripheral cornea stiffen at higher strains, perhaps serving the role of absorbers.

Crimp has been studied experimentally in several soft tissues, like tendon,(J Diamant et al., 1972) arteries,(Hill et al., 2012) and pulmonary valves,(Joyce et al., 2009) because it is recognized as a key characteristic of collagen, and central to its mechanical behavior (Figure 47).

Nevertheless, we are not aware of previous reports quantifying collagen crimp across the globe. In this study, the average corneal crimp period was 14.4 μm, consistent with past studies which have shown images of the cornea on which we estimate crimp periods of approximately 15 μm.(Andreo & Farrell, 1982; Gallagher & Maurice, 1977) This may not be the only scale at which crimp exists in the eye, as Liu and colleagues reported crimp periods ~2 μm, using transmitted electron microscopy (TEM).(Liu et al., 2014)

Reports of collagen fiber crimp in the eye go back, at least, 40 years. In 1977, Gallagher and Maurice found striations in the corneal stroma, corresponding to collagen fiber waves.(Gallagher & Maurice, 1977) Since then, others have visualized the crimp in the eye with methods such as brightfield,(Richard H Newton et al., 1996; Ostrin & Wildsoet, 2016) electron microscopy,(Andreo & Farrell, 1982) nonlinear microscopy,(Kamma-Lorger et al., 2010; Mega et al., 2012; Midgett et al., 2016; Winkler et al., 2011; Zyablitskaya et al., 2017) and MRI.(Ho et al., 2014) We have also previously visualized and quantified the collagen crimp period and waviness in the optic nerve head.(Jan, Gomez, et al., 2017; Ning-Jiun Jan & Ian A. Sigal, 2018) These studies, however, only focused on small regions. In a modeling study, Grytz and colleagues considered the globe as an integrated structure.(Grytz & Meschke, 2009, 2010; Grytz et al., 2011) Their inverse models predicted that the corneal fiber bundles had a larger crimp angle than the sclera, which agrees with our findings. Later studies with more refined modeling and highly detailed sclera deformation data have been used to make predictions of crimp changes with age.(Fazio et al., 2014; Grytz et al., 2014) However, the predictions have not been validated. We show in this study that the pattern is more complex than just a difference between anterior and posterior poles.

This study is not the first to find regional differences in collagen properties across the globe. Detailed qualitative descriptions of the collagen fiber orientation across the sclera, optic nerve head, and nerve sheath with depth were reported in 1933.(Becher & Osterhage, 1933; Fischer, 1933) There have also been studies testing strips from different regions of the sclera which showed different mechanical properties from the anterior to the posterior pole.(Curtin, 1969; Ischreyt, 1898) Norman and colleagues quantified the corneoscleral shell thicknesses through the globe in 15 equally spaced regions across the axial length of the eye and found that the sclera is thinnest at the equator.(Norman et al., 2010) Recently, a study by Whitford and colleagues used ex vivo whole globe inflation tests to find regional differences in stiffness throughout 9 regions of the corneoscleral shell.(Whitford et al., 2016) They found that the limbus and equatorial regions were the stiffest, with the stiffness decreasing progressively towards the posterior pole. These studies emphasize the importance of understanding the regional differences in the collagen structure and biomechanics across the globe. The studies mentioned above are a small subset. Many other aspects of the regional differences across the corneoscleral shell have been studied, though none of these studies experimentally quantified the collagen crimp morphology.

One possible reason for the distinct lack of experimental measures of crimp in the eye may be due to most imaging methods lacking the sensitivity, resolution, or the field-of-view for measuring the collagen crimp that PLM has.(Jan et al., 2015; Jan, Lathrop, et al., 2017) Methods like small angle light scattering (SALS)(M. J. Girard, A. Dahlmann-Noor, S. Rayapureddi, J. A. Bechara, B. M. E. Bertin, et al., 2011) and wide angle x-ray scattering (WAXS)(Jacek Klaudiusz Pijanka et al., 2013) can quantify the collagen fiber orientation across large areas of the eye with high angular resolution, similar to PLM.

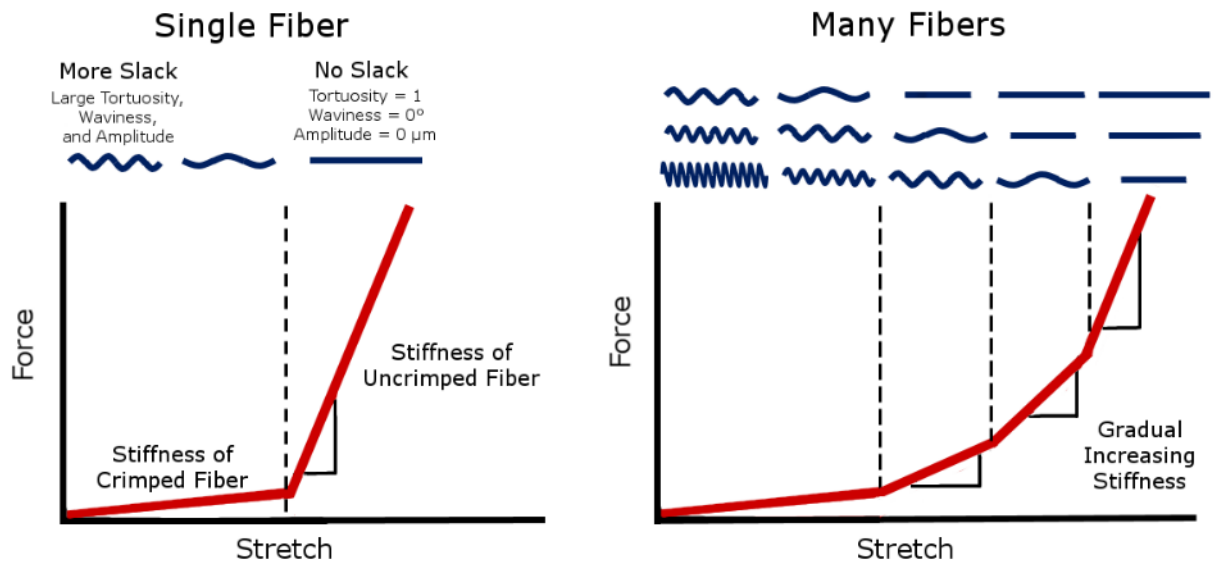

Figure 47. How crimp can influence gradual stiffening in tissue.

Stretching an uncrimped fiber usually requires a larger force than stretching the same fiber when it is crimped. (Left) The amount of stretch needed to trigger this stiffening is related to the amount of slack in the fiber. When many fibers of different slack are stretched together, more and more fibers straighten with stretch, gradually increasing the overall stiffness of the tissue. (Right) Figure modified from (Jan et al., 2017a)

In a recent study, Bell and colleagues combined these methods with digital image correlation to measure load-induced molecular tilt of fibrillar collagen in cornea.(Bell et al., 2018) However, due to its low lateral resolution this orientation information combines the meso-scale tissue anisotropy with the collagen crimp, making it very difficult to characterize the collagen crimp.(Pierlot et al., 2014) The majority of past studies have focused on the macro-scale patterns in the collagen structure.(Donald J Brown et al., 2007; Coudrillier et al., 2015; M. J. Girard, A. Dahlmann-Noor, S. Rayapureddi, J. A. Bechara, B. M. E. Bertin, et al., 2011; Ivers et al., 2011; Jacek Klaudiusz Pijanka et al., 2012; Jacek K. Pijanka et al., 2015; Ian A Sigal et al., 2014; Thale & Tillmann, 1993a) We have shown that PLM has the appropriate sensitivity, resolution, and field-of-view to quantify the crimp in ocular tissue.(Jan, Gomez, et al., 2017; Jan et al., 2015; Jan, Lathrop, et al., 2017) It has been shown that the PLM signal correlates with the orientation of

collagen fibers.(Bromage et al., 2003; J Diamant et al., 1972; Keikhosravi et al., 2017) In addition, PLM has been used extensively for quantifying crimp in other tissues, such as the vitreous, (Filas et al., 2014) tendon (J Diamant et al., 1972; Franchi et al., 2007; Hansen et al., 2001) and ligament.(Boorman, Norman, Matsen, & Clark, 2006; Shah, Jayson, & Hampson, 1977)

We quantified collagen crimp properties on eyes fixed at 0 mmHg IOP. Characterization of the crimp without IOP at 0 mmHg is essential for developing biomechanical models of the eye.(Grytz et al., 2011; I. Sigal et al., 2013) In recent studies, we characterized the crimp in the optic nerve head at baseline(Jan, Gomez, et al., 2017) as well as with increasing IOP.(Ning-Jiun Jan & Ian A. Sigal, 2018) This work presented here is the first step towards extending this understanding from the optic nerve head to the whole globe by characterizing crimp at 0 mmHg IOP. Future studies are needed to determine how the crimp parameters and their relationships change with load. This could be accomplished, for example by using PLM to track how the collagen crimp in individual bundles and a population of bundles in an ocular region change with mechanical stimuli.(Jan et al., 2016)

When interpreting the results in this work, it is important for readers to consider the complex hierarchy of architecture and mechanics of collagenous tissues. Fully understanding the behavior of the cornea and sclera requires a comprehensive approach that incorporates the structure-mechanics relationship at various scales. The crimp patterns we report represent but one of the scales that can impact tissue mechanics.

In this study, we used sheep eyes. Sheep eyes are similar to human eyes in that they have a collagenous lamina cribrosa, but differ in having a ventral groove in the optic nerve head, similar to that in pig.(Brooks et al., 1998) In addition, the sheep globe is larger and less symmetric than the human eye, with different axial lengths and equatorial diameters, as well as more variable

tissue thicknesses in the corneoscleral shell.(El‐Maghraby, Nyland, & Bellhorn, 1995; Andrew P Voorhees et al., 2017) Though it is possible that the crimp patterns found in sheep are not the same in humans, it is important to understand sheep as an animal model.(Candia, Gerometta, & Danias, 2014; Gerometta et al., 2010) Future work should include additional animal models as well as human eyes.

We did not distinguish between nasal and temporal regions of the cornea and sclera. Future studies could consider comparing more regions of the eye, including nasal and temporal, and superior and inferior quadrants. There could also be potential artifacts from using ex vivo tissues and histological processing, such as fixation and cryosectioning. However, we have shown elsewhere that our method of formalin fixation has minimal effects on ocular tissue size, shape, and crimp.(Jan et al., 2015; Tran et al., 2017)

The crimp measurements may be affected by the angle of the collagen fibers relative to the plane of the section, which could underestimate the crimp period, and overestimate conformity, tortuosity, waviness, and amplitudes. We have limited this effect by only analyzing bundles with small out-of-plane components. In addition, it is possible that the collagen crimp in the corneoscleral shell may not have the form of a 2D wave as in some tendons. (Gathercole & Keller, 1991) It may, for instance, form a 3D helix. It is also possible that the form of the crimp varies over the globe, as the cornea lamellae have different spacing and deformation constraints from bundles in the PPS. Future studies should incorporate 3D orientation information into consideration for more accurate crimp shape characterization.(B. Yang et al., 2017)

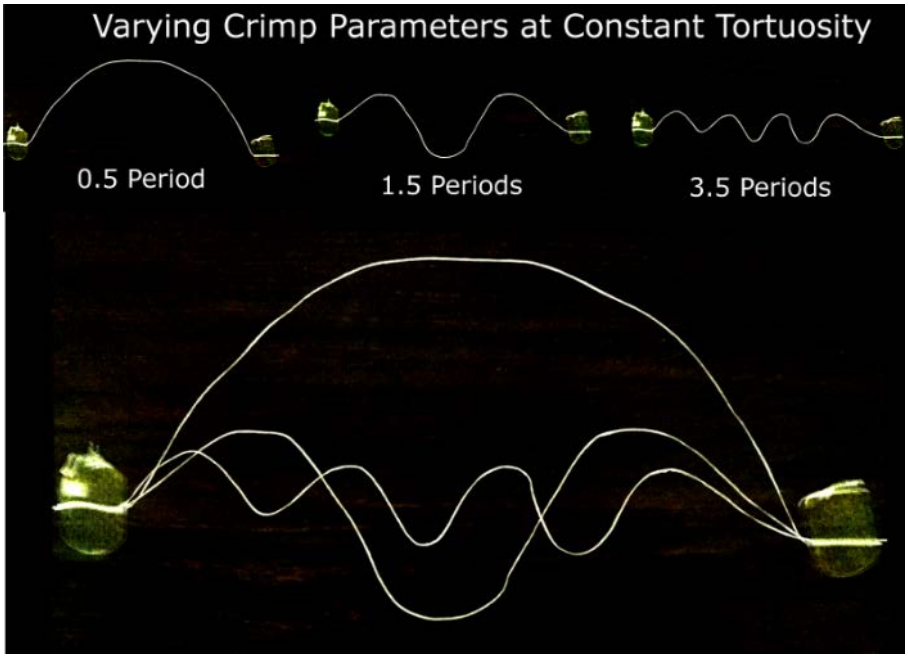

Figure 48. Demonstration of different crimp parameters that can result when the tortuosity is held constant.

Consider two fibers with the same tortuosity, one with a large amplitude but low waviness, and the other with low amplitude and large waviness. One way to visualize these different fibers is to fix the endpoints of a piece of string, with some slack, which forces the tortuosity to a constant value. Constraining the string to having a sinusoidal crimp pattern, one notices that increasing the frequency of the waves (decreasing the period) decreases the amplitude and increases the waviness. By taping the ends of a string, we held the amount of slack, or the tortuosity, of the string constant. Increasing the frequency, or number of periods, resulted in smaller periods and amplitudes, and larger waviness.

We have presented the first experimental quantifications of collagen crimp in eight regions in the corneoscleral shell. These numbers can be used to develop more accurate collagen microstructure constitutive models of the eye. These models could, for example, be used to study what type of crimp characteristics are most likely to cause pathologic deformations to the retinal ganglion cell axons in the optic nerve head, which may, in turn, allow identifying patients at a higher risk for glaucomatous vision loss.

In conclusion, to the best of our knowledge, we have demonstrated the first systematic experimental characterization of the collagen crimp properties in the corneoscleral shell. We have

demonstrated spatial patterns of collagen crimp period, conformity, tortuosity, waviness, and amplitude in 8 regions of the eye. This is important because collagen crimp largely determines the nonlinear biomechanical properties of the eye. An important motivation for this work was to provide experimental data on the baseline crimp characteristics needed for the development of robust fiber-based microstructure constitutive models of the eye. Our crimp measurements also provide a basis to understand how microstructure governs larger scale tissue mechanics. The origin and biomechanical implications of the observed collagen crimp patterns remain unclear. Whole globe regulation of collagen is likely insufficient to produce the well-defined regional patterns observed, suggesting that the mechanisms regulating these parameters must act at the regional, and perhaps, at the local levels. This information helps reveal the role of microstructure on eye physiology, in aging, and in biomechanics-related diseases, such as glaucoma.

6.0 CRIMP CHANGES OF OPTIC NERVE HEAD WITH INTRAOCULAR PRESSURE

The content of this chapter was previously published in (Ning-Jiun Jan & Ian A Sigal, 2018).

6.1 INTRODUCTION

Collagen is the main load-bearing component of the eye. The collagen fiber organization and hierarchical architecture play a central role in determining the mechanical behavior of soft tissues, often more so than the chemical composition of the fibers.(Fratzl, 2008; Mattheck, 1998; Niklas, 1992; Wainwright et al., 1982) Characterization of the collagen organization and architecture in the eye is therefore vital to understanding eye physiology, aging, and certain diseases, such as glaucoma. While substantial attention has been directed over the last two decades to characterizing ocular collagen anisotropy and the large scale nonlinear mechanical properties of ocular tissues, very little is known about the microstructural basis for the observed behavior. Thus, even though it is well established that the tissues of the eye are nonlinear at the macro scale, the underlying collagen characteristics that determine this nonlinearity remain unclear. At the microstructural level, it has been shown, by us(Jan, Gomez, et al., 2017; Jan, Lathrop, et al., 2017) and others,(Andreo & Farrell, 1982; Ho et al., 2014; K. M. Meek & Fullwood, 2001; Winkler et al., 2013a) that the collagen fibers of the eye exhibit natural undulations called crimp. Evidence in

other tissues suggests that crimp is the basis for the nonlinear behavior observed at the macroscale, in a process of stretch-induced stiffening called fiber recruitment (Figure 49). Based on this theory, Grytz and colleagues used inverse numerical models to predict ocular collagen crimp characteristics.(Grytz & Meschke, 2009, 2010; Grytz et al., 2011) Their models, while powerful, involve major assumptions on the collagen crimp shape and recruitment with intraocular pressure (IOP), and their predictions have not been validated.

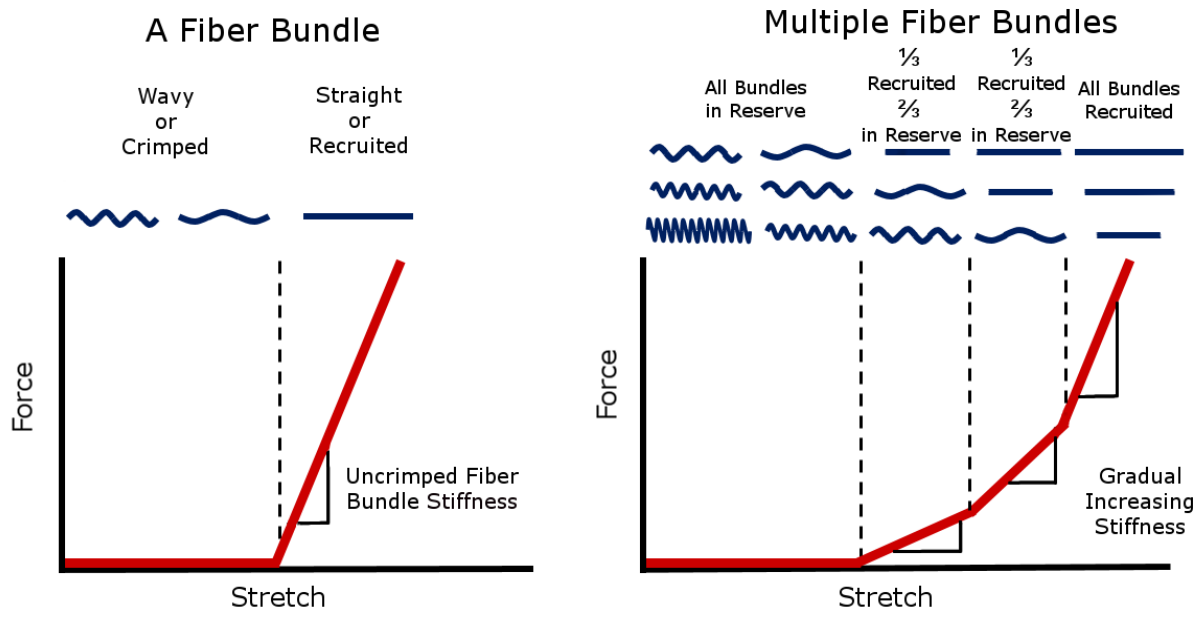

Figure 49. Idealized plots of force vs stretch differ for a fiber bundle versus multiple fiber bundles. A fiber bundle is easy to stretch when it is crimped or wavy, however after the bundle is straight or recruited, the bundle becomes much stiffer, requiring more force to elongate the bundle. (left) When many crimped fiber bundles with different amounts of slack are stretched together, the gradual straightening of the fibers creates a gradual, nonlinear stiffening, where more and more force is required to continue stretching the tissue. (right) A fiber that is straightened is referred to as recruited. Conversely, a fiber that is not recruited, but would at higher stretch, is referred to as reserved. The proportion of fibers recruited to those in reserve is directly related to the rate of recruitment. Adapted from Jan et al 2017.(Jan, Gomez, et al., 2017)

We recently demonstrated that polarized light microscopy (PLM) can be used to measure collagen fiber crimp characteristics of the lamina cribrosa (LC) and peripapillary sclera (PPS).(Jan, Gomez, et al., 2017) The study, however, only considered IOPs below normal (0, 5 and 10 mmHg),

and therefore did not provide information on normal or elevated IOPs. In addition, because the study focused on collagen crimp period, the information on stretch-induced uncrimping and recruitment was limited, compared with other parameters such as waviness.(I. A. Sigal et al., 2013; Sigal et al., 2015) To the best of our knowledge there are no other experimental measurements of collagen fiber crimp in the LC and PPS, or of the process of collagen fiber recruitment.

Our goal in this study was to quantify how ocular collagen crimp changes as IOP increases. Specifically, we quantify LC and PPS collagen crimp waviness at low, normal and elevated IOPs. An experimental characterization of the tissue recruitment at the microscale fiber-level is necessary to obtain a robust mechanistic understanding of how ocular tissues respond to loading in health and disease. Understanding uncrimping and recruitment is also useful to develop more accurate constitutive models to describe posterior pole tissue mechanics. Clinically, understanding how crimp morphology affects tissue mechanics and response to loads can augment our understanding of the biomechanical component of ocular diseases, including glaucoma. This could potentially impact diagnosis and treatment, for example through the detection or modification of sensitivity to IOP.

6.2 METHODS

6.2.1 Specimen preparation

Thirteen eyes from two year old sheep were obtained from a local abattoir and processed within 24 hours of death following the process described elsewhere.(Jan, Gomez, et al., 2017) Briefly, the muscles, fat, and episcleral tissues were carefully removed using a combination of scalpels,

razors, and forceps. Eyes were kept in 1X phosphate buffered saline (PBS) with pH 7.4 until fixation. The eyes were cannulated through the anterior chamber and IOP set using a fluid column (Figure 50). The eyes were immersion and perfusion fixed in 10% formalin for, at least, 12 hours while maintaining IOP at 0, 10, 15, 20, or 50 mmHg, with at least one eye per pressure. Normal physiologic IOP in sheep is 10-15 mmHg.(Ghaffari et al., 2011) Following fixation, the posterior poles were excised using a trephine 11.5 mm diameter and cryosectioned coronally into 30 µm thick slices. Due to the natural variability in the shape, position and orientation of the LC and PPS, as well as tilt during embedding and sectioning, some sections show better the LC or the PPS. To ensure robust analysis we made sure to have at least three good sections at the level of the LC and three good sections at the level of the PPS for each eye. Only sections free of artifacts, such as folds, were chosen.

6.2.2 Imaging

The sections were imaged using PLM following previously reported protocols.(Jan et al., 2015) Briefly, two polarized filters (Hoya, Tokyo, Japan) were used, one as polarizer placed before the sample, and the other as a analyzer placed after the sample. Four images were captured using white light illumination, with filter orientations rotated 45° between images. The relative changes in signal intensities at each pixel were used to compute local collagen fiber orientation. An Olympus SZX16 microscope was used with an Olympus DP80 camera (36-bit, RGB, pixel shift setting, Olympus, Tokyo, Japan), a 0.6x reducer, and 0.8x objective (numerical aperture 0.12). Images with 20% overlap were acquired using a manual stage, and stitched into mosaics using Fiji Is Just ImageJ (FIJI).(Preibisch et al., 2009)

To visualize the whole LC and scleral canal, 10-30 images were captured of each LC section using the 11.5x magnification setting on the microscope (0.37 µm/pixel). To visualize the PPS to the edge of the section, 20-40 images were acquired of the sections at the PPS level using the 4x magnification setting on the microscope (1.08 µm/pixel). In a previous study we demonstrated that the orientation information derived from PLM images are robust to changes in microscope-camera pairings and magnifications.(Jan et al., 2015) A lower magnification was used for the PPS to keep the number of images necessary similar to the LC.

6.2.3 Measuring collagen crimp recruitment

The collagen of the eye has a hierarchical structure, with fibrils forming fibers and fibers forming bundles. PLM is based on the optical properties of the collagen molecules, and therefore it allows accurate quantification of collagen orientation without the need to resolve and distinguish fibrils, fibers, or bundles. PLM orientation analysis is not dependent of identifying structure edges. In this work, we measured the spatial distribution of collagen molecule orientations along collagenous structures, and use these to determine waviness, and through the IOP-related changes of waviness the recruitment.

Using FIJI, straight lines were placed manually on the images along collagen bundles. When marking, attention was taken to do this only on bright clearly visible bundles. This helped ensure that the bundles were in the section plane, and minimize potential effects of out of plane orientation.(B. Yang et al., 2017) We were also careful to mark only LC beams and not the ventral tree-like or vessel walls. For each line, the PLM-derived collagen orientations of all the pixels along the line were compiled. As a measure of crimp, we computed the waviness for the line as

the circular standard deviation of the pixel angles. The wavier the fibers, the larger the spread of orientations, increasing the deviation and the waviness (Figure 51).

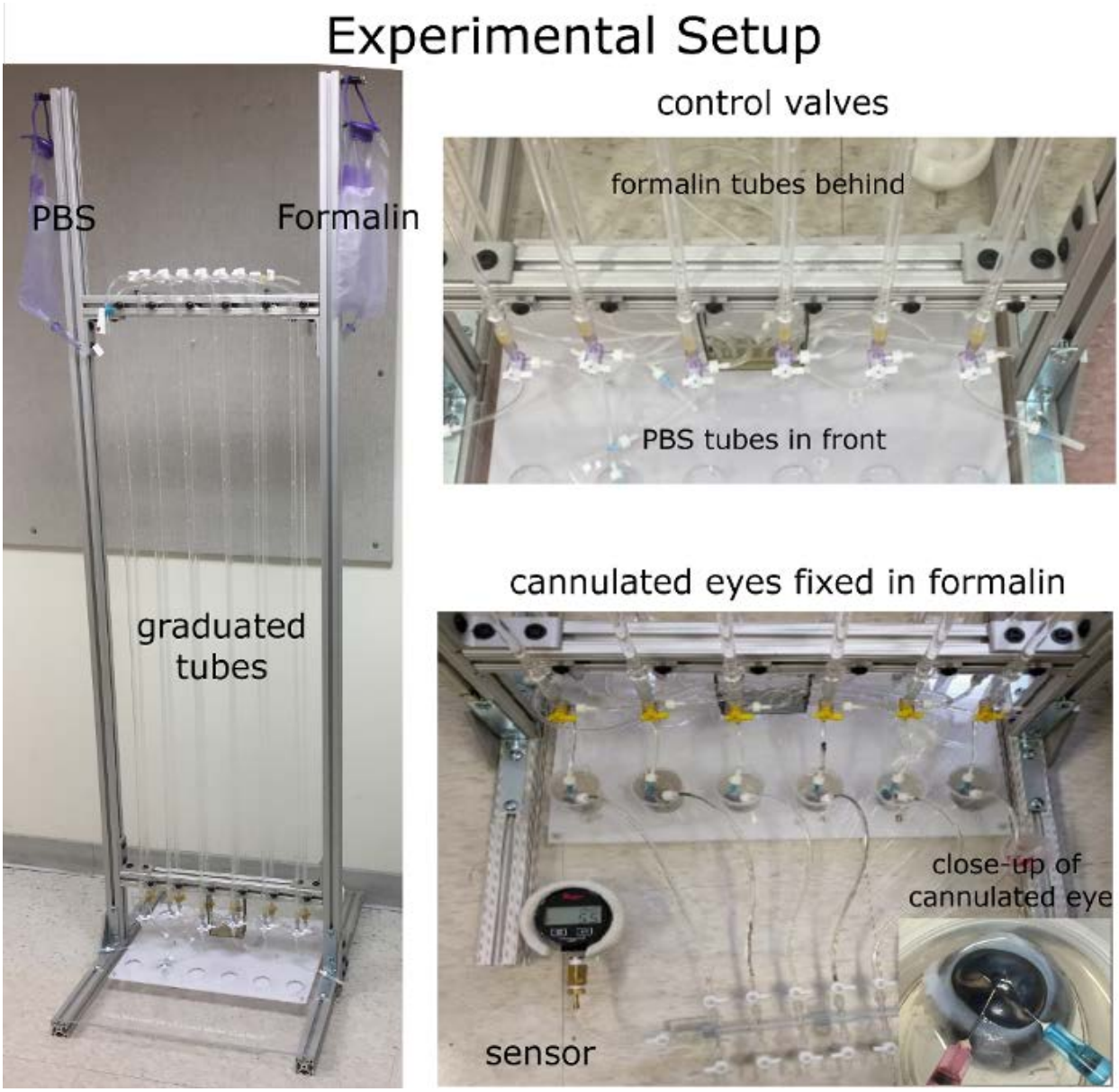

Figure 50. Experimental setup for IOP control and globe fixation.

IOP was set by controlling the height of a column of PBS from a reservoir. The system shown allows simultaneous processing of six eyes. Through the control valves we could switch the PBS to fixative, while maintaining IOP and flow. Eyes were double cannulated through the anterior chamber. Fixation is completed by also immersing the globes into fixative. The valve system also allows IOP monitoring through a sensor attached at the bottom right.

A useful property of this method to compute fiber waviness is that it is robust to the small deviations of measuring line orientation. The waviness was measured for every LC trabeculae beam and for, at least, 900 PPS collagen bundles per eye (Figure 52). In preliminary tests, we noticed that even at very high IOP levels (above 50 mmHg), the collagen was not perfectly straight, with some residual waviness due to curved bundles or beams, and fiber interweaving Quantifying this residual waviness was not our goal in this work. We were specifically focused on how the collagen crimp changes with IOP, rather than how curved or interwoven the bundles were. Therefore, based on the preliminary data observations, we defined tissue-specific waviness recruitment thresholds as the 90^{th} percentile waviness in each tissue at 50 mmHg of IOP. If the waviness decreased below the tissue threshold, the collagen fiber bundle was considered recruited. To confirm that the results presented in this work are robust to the threshold chosen for recruitment, we varied the threshold for the PPS all the way down to 10^{th} percentile.

6.2.4 Crimp visualization

Using previously reported methods, PLM images were further processed to enhance visualization of the collagen fiber crimp and their recruitment.(Jan, Gomez, et al., 2017) Briefly, the difference between each pixel's orientation and the average fiber orientation in its neighborhood (4 pixel radius, 1.5 μm for LC and 4.3 μm for the PPS) was calculated. The images were then pseudo-colored purple, if this difference was positive, or yellow if the difference was negative (Figure 53). To aid visualization, we scaled the pixel intensity by the energy, which we have described previously.(Jan et al., 2015) Briefly, energy is the signal variation when rotating the polarized filters in PLM. By scaling our images by energy, we can simultaneously discern the collagen crimp and the texture of the tissue. A crimped, unrecruited fiber shows discernible bands of purple and

yellow along the bundle. Uncrimped, recruited fibers do not have discernible bands (Figure 54 and Figure 55). This visualization was especially useful for discerning the variability in orientation remaining at elevated IOP. (Figure 55).

6.2.5 Statistical analysis

Linear mixed effect models accounting for correlations between measurements from the same sections, eyes, and animals were used to analyze how the waviness changed with pressure and the difference in waviness between the LC and PPS at each IOP. Descriptive statistical calculations such as angular mean and standard deviation were made using circular statistics.(Jammalamadaka & Sengupta, 2001) All statistical analyses were done using R.(Team, 2013)

6.3 RESULTS

A total of 20,442 measurements of collagen crimp waviness were collected, of which 13,565 were of PPS collagen bundles and 6,877 of LC beams across all eyes. From these measurements, we quantified how the waviness of the fibers and percentage of fibers recruited in the LC and PPS changed with IOP (Figure 56). We found that, while the exact fraction of fibers recruited varied with threshold percentile, the patterns and trends of recruitment did not change (Appendix B). The waviness' of the collagen fibers in the LC and PPS were different, but had similar trends with increases in IOP. At every IOP, the LC fibers were less wavy than those in the PPS ($P<0.001$) (Figure 57) The fibers in the LC also had smaller standard deviation of their waviness compared to the fibers in the PPS at every IOP, indicating that waviness in the LC was more uniform than in

the PPS. The waviness threshold above which a fiber was considered recruited was lower in the LC (3.4°) than in the PPS (6.7°), indicating that at baseline pressure the fibers in the LC are more straight than fibers in the PPS.

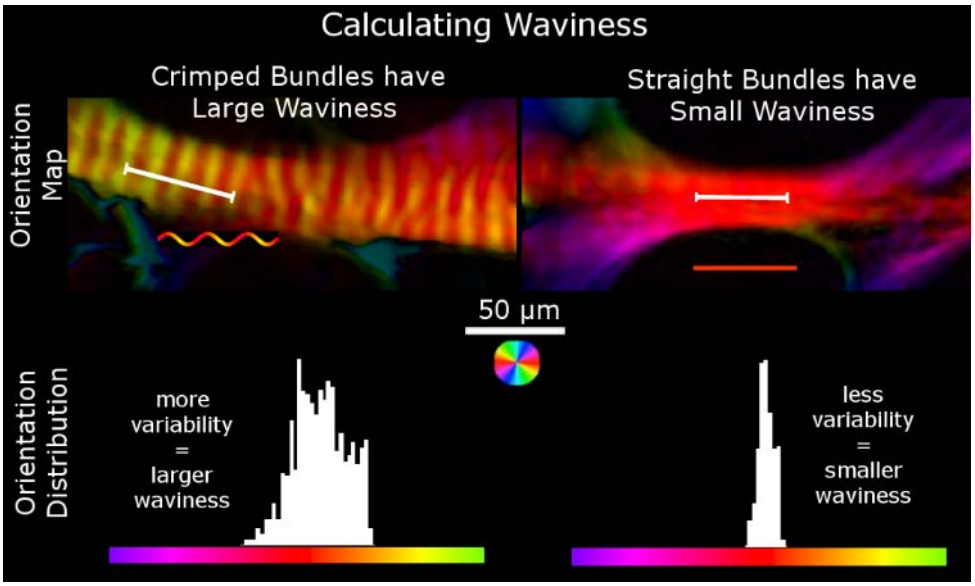

Figure 51. Orientation maps of two trabeculae beams of the LC and the orientation distributions across lines (the white line segments) drawn along each beam.

Waviness is calculated using the circular standard deviation of the collagen fiber orientations through a fiber bundle. The histograms show the distribution of orientations of the pixels under the line. In wavy crimped fiber bundles, the orientation distribution is more variable, resulting in larger waviness values (left) while in straight fibers, the distribution is less variable, resulting in smaller waviness values (right).

The recruitment curves for the LC and PPS were similar, but had important differences. Recruitment in both tissues was faster at lower IOPs (0-10, and 10-15 mmHg) than at higher IOPs (15-20, and 20-50 mmHg) ($P<0.001$). At low IOPs more sclera fibers were recruited than LC fibers, such that at 10 mmHg about half of the sclera fibers had been recruited, compared with only a third in the LC. Between 10 and 15 mmHg, recruitment in the LC was faster than in the PPS, such that, at 15 mmHg, 3/4 of the fibers were recruited in both tissues, leaving a quarter of the

fibers in reserve. Further increasing IOP to 20 mmHg caused an increase in PPS recruitment but a small decrease in the LC. These trends reversed for IOP increases between 20 mmHg and 50 mmHg as there was a slight increase in LC recruitment and a decrease in PPS recruitment.

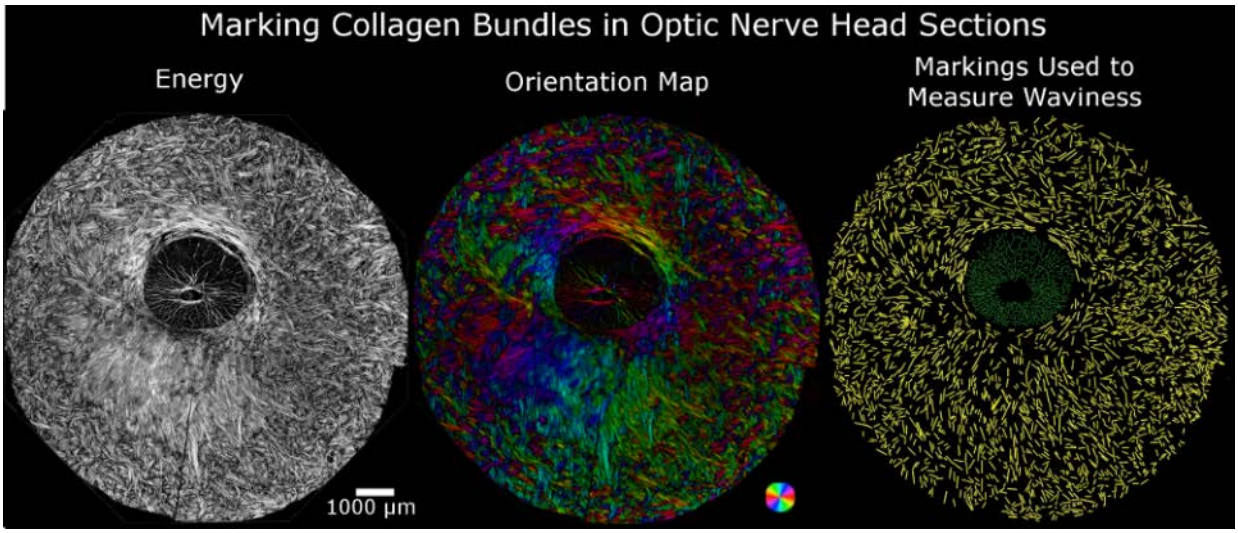

Figure 52. Manual markings of collagen bundles in images of the ONH used to measure waviness. Example energy image of a coronal section of the posterior pole centered on the optic nerve head (left). Fiber distribution and orientation are best visualized using PLM-computed orientation with intensity scaled by energy (middle). Using manually placed lines, we measured the waviness in the PPS (yellow) and the LC (green).

6.4 DISCUSSION

Our goal was to quantify the changes in LC and PPS collagen crimp waviness with IOP. Three main results arise from this work. First, the waviness of the collagen fibers decreased with increasing IOP. Second, at every IOP, the waviness of the collagen fibers in the LC was smaller and less variable than that of the PPS. Third, the LC and PPS have different recruitment curves. Let us consider each of these in turn:

The waviness of the collagen fibers decreased with increasing IOP. The decreasing waviness with increasing IOP is consistent with current theory of collagen fiber recruitment in soft tissues, in which the fibers straighten with stretch to become recruited, contributing to the local stiffening of the tissue. While this phenomenon is well recognized in other tissues, like tendon and ligament,(Hansen et al., 2001; Holzapfel, 2001; Thornton, Shrive, & Frank, 2002) this study is the first experimental evidence in the posterior pole.

At every IOP, the waviness of the collagen fibers in the LC was smaller and less variable than that of the PPS. These differences in crimp morphology suggest that there are also distinct differences between the LC and PPS biomechanical properties. In other tissues the variability of the crimp morphology is a major determinant of how gradually the tissue stiffens under tensile load. In tissues with uniform crimp morphology, fibers require the same amount of stretch to straighten, resulting in a step recruitment and a consequent sudden stiffening. Alternatively, in tissues with variable crimp morphology, fibers require different amounts of stretch to straighten, resulting in a gradual recruitment and stiffening. We have shown that the fibers of the LC have a somewhat uniform waviness at low IOPs, and a marked decrease in waviness between 10 and 15 mmHg. The fibers of the PPS, in contrast, had more waviness at low IOPs and a more gradual decrease in waviness from 0 to 20 mmHg. These results suggest that the LC stiffens abruptly between 10 and 15 mmHg, whereas the PPS gradually stiffens from 0 to 20 mmHg IOP. Experimental studies of ex-vivo inflation have not reported a steep change in strain with increasing IOP. (Coudrillier et al., 2016; Dan E Midgett et al., 2017) They observed a relatively smooth decrease in the IOP-induced strains with IOP increases, consistent with the recruitment reported in this work. Some of the differences could be due to different IOP levels studied, or could be inter-species differences. Most importantly, the relationships between strain,

stiffness, recruitment, and IOP are complex, making it difficult to make a direct quantitative comparison beyond the general trends of increasing stiffness with IOP. Future studies could correlate strain with changes in crimp and recruitment to elucidate the complexities of ONH mechanics.

It is important to note that the uncrimping or recruitment only relates to the rate of stiffening with IOP, which may be very different from overall tissue stiffness. The results above should, therefore, not be interpreted to mean that the LC is stiffer than the sclera. This study provides data that helps explain how the complex nonlinear properties of the LC and PPS arise from the collagen fibers microarchitecture and morphology. In addition to fiber uncrimping, other factors may affect overall tissue biomechanics, such as fiber reorientation and the biomechanical properties of the fibers themselves after straightening. Elsewhere, studies of collagen suggest that straight collagen fibers have a response to stretch that is close to linear up to the point of damage.(Fratzl, 2008) We did not observe any clear fiber reorientations with IOP in the tissues of the posterior pole are small, but a systematic study is needed to fully account for these effects on the tissue properties.

The LC and PPS have different recruitment curves. At every IOP an equal or larger percentage of the PPS fibers was recruited than LC fibers. Because recruited fibers are the fibers that bear load, our results reveal interesting information on the relative fraction of potentially load-bearing fibers of each tissue that are bearing load. At 10 mmHg, a low, but still physiologic IOP, twice as much of the PPS (~60%) than of LC (~30%) participated in bearing loads. Interestingly, at physiologic IOP of 15 mmHg, the same fraction (~3/4) of LC and PPS fibers was recruited, keeping ¼ of their fibers uncrimped as a reserve. This 3 to 1 ratio of loaded vs. reserved fibers at physiologic IOP for both LC and PPS, may indicate a target ratio where fibers of the LC and PPS

have remodeled their crimp morphology for optimal function in their typical biomechanical environment. At IOP of 20 mmHg, at the upper edge of the normal pressure range, we found that the PPS recruited more fibers whereas the LC recruited less. This may be a protective mechanism, whereby the PPS bears more load in order to relieve the LC and protect the retinal ganglion cell axons. It is also possible that the decrease is due to differences between eyes.

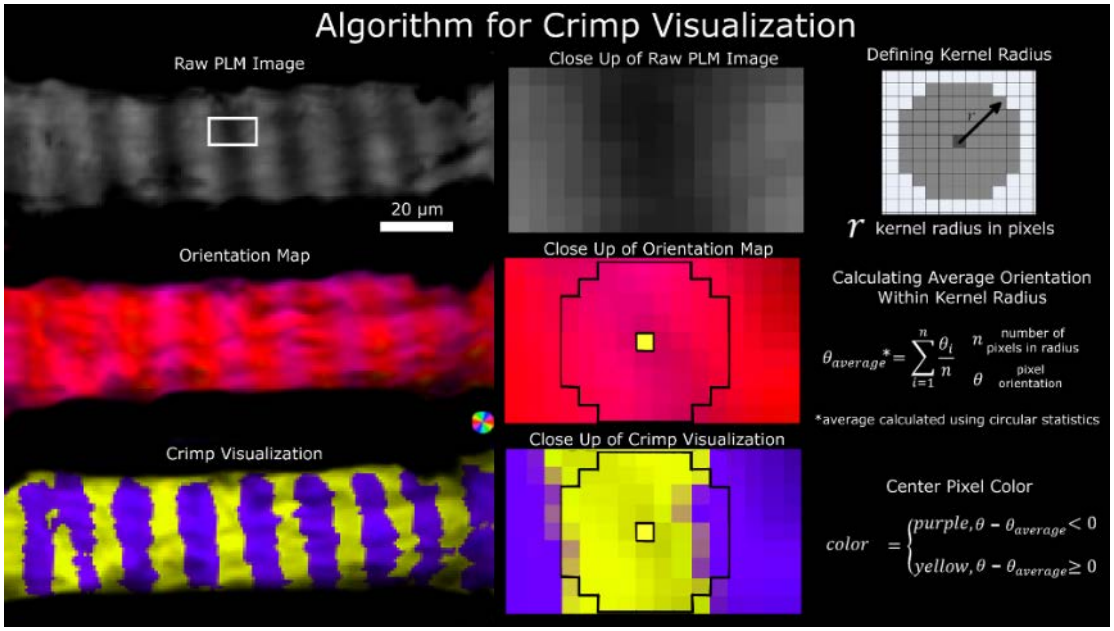

Figure 53. Crimp visualization algorithm.

A set of raw PLM images (top left) are used to calculate an orientation map (middle left). The orientations are further processed to simplify visualization of the crimp using yellow/purple bands (bottom left). The middle column shows close-ups of the LC beam region outlined in the white box in the top left panel. A kernel radius was defined (top right) and used to calculate the local average orientation (middle right). The center pixel was colored yellow or purple depending on the relative orientation of the pixel relative to the average orientation within the local kernel region (bottom right). A neighborhood of 4 pixels is shown in the close up of the orientation map and of the crimp visualization. The process is repeated for all pixels, then the pixel intensity scaled by the energy.

Studies in other tissues like arterial walls have shown similar unexplained trends where the percentage of recruited fibers drops at high strains.(Hill et al., 2012) Further studies are needed to

understand the decrease in percentage of fibers recruited in the LC from 20 to 25 mmHg and in the PPS from 20 to 50 mmHg.

The importance of collagen fiber crimp and recruitment in soft tissue mechanics has been recognized for over 40 years by several groups. The majority of studies have analyzed how crimp morphology changes with mechanical stimuli in tendon and ligament. In 1972, Diamant and colleagues quantified the crimp angle and period in tendon, and how much stretch was required to make a fiber bundle straight, or recruited.(J Diamant et al., 1972) More recently, Hansen and colleagues quantified the collagen crimp period in tendon under stretch while imaging using optical coherence tomography.(Hansen et al., 2001) For ligaments, Thornton and colleagues used PLM and scanning electron microscopy to calculate the percentage of crimped area stretched in situ under different amounts of stress.(Thornton et al., 2002) The crimp period and angle were measured for a few fibers in each area and the percentage of uncrimped area was used to track the collagen crimp recruitment. Besides tendon and ligament, recruitment curves have also recently been experimentally derived for arterial tissue and used in microstructurally-based models to predict tissue responses.(Fata et al., 2013; Fata, Zhang, Amini, & Sacks, 2014; Hill et al., 2012) For example, a study by Hill and colleagues measured the collagen crimp tortuosity, the ratio between a fiber's arc length to its chord length using manual fiber tracings of multiphoton images. (Hill et al., 2012) A collagen fiber was considered recruited if the tortuosity of a fiber dropped below a certain threshold. Manual measurements were used to fit a recruitment curve.

The importance of crimp and recruitment has likewise been noted in the ocular biomechanics community, though there is a significant lack of experimental data on collagen fiber crimp and recruitment in the eye compared to other tissues. Grytz and colleagues predicted the collagen crimp microstructure in the corneoscleral shell using stress-strain curves gathered from

mechanical tests and a constitutive model that assumed that all collagen fibers within a tissue (i.e. cornea or sclera) had uniform helical spring morphology.(Grytz & Meschke, 2009, 2010) In this model the shape of the stress-strain curve could be determined by just the crimp angle and the amplitude of the crimp relative to the fiber thickness. The crimp angle determined the inflection point in the stress-strain curve, while the amplitude relative to fiber thickness determined the nonlinearity of the curve. Grytz' model considered the nonlinearity of the stress-strain curve as arising from fiber uncrimping, rather than recruitment.

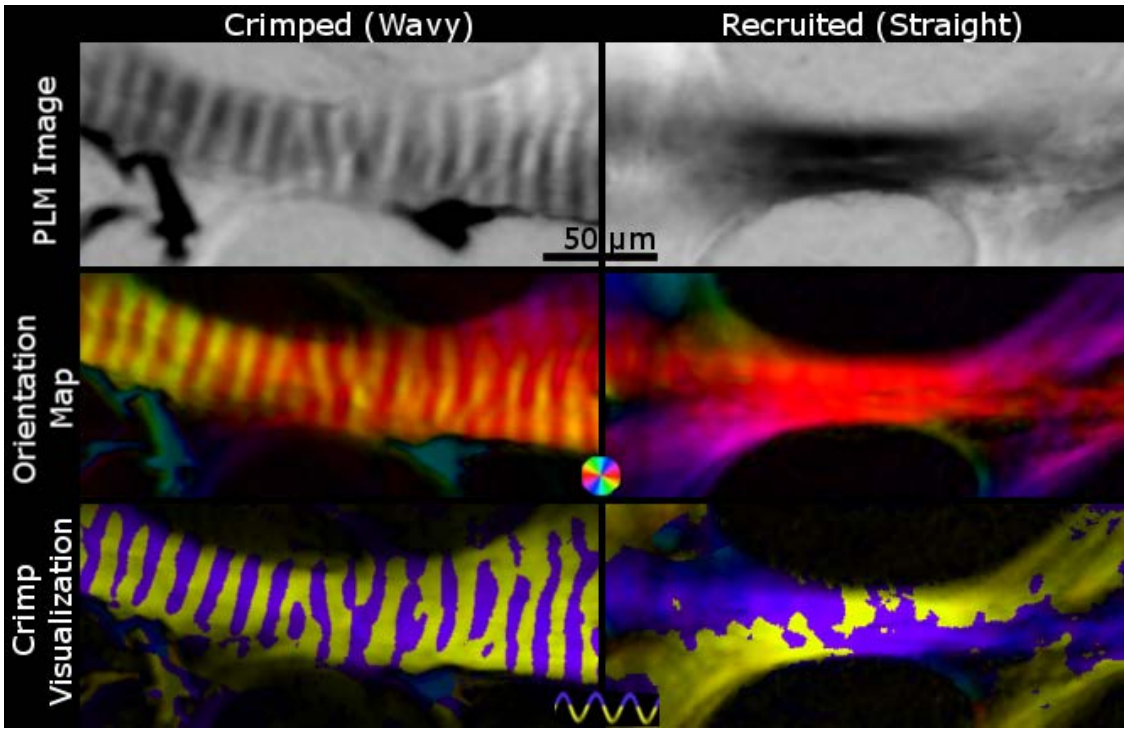

Figure 54. The crimp visualization of a crimped fiber versus a straight fiber.

Crimped, unrecruited wavy fibers (left) show changes in intensity in PLM images (top left), periodic changes in color in orientation maps (middle left), and distinct purple and yellow bands (bottom left). Recruited, straightened fibers (right), on the other hand, show a consistent intensity in PLM images (top right) and color in orientation maps (middle right), and patchy yellow and purple in the crimp visualization plot (bottom right). In addition, the crimp visualization of straight fibers fail to show clear bands of purple and yellow.

These are related, but not the same. We have found direct experimental evidence that the crimp morphology in the LC and PPS is highly inhomogeneous, and that both tissues gradually recruit their collagen fibers with increasing IOP-induced stretch. Using inverse modeling of the posterior pole Grytz and colleagues postulated that age-related stiffening in the eye is due to a changing ground matrix, though this has not been verified experimentally.(Fazio et al., 2014) The connection between tissue stiffness and aging, and age-related diseases underscores the importance of identifying the fundamental basis for changes in tissue stiffness, and the need for experimental validation of theoretical predictions.

We recently quantified collagen crimp period and its spatial distribution in the LC and PPS at low IOPs.(Jan, Gomez, et al., 2017) Consistent with this work, we found that crimp periods in the PPS were larger than in the LC. In addition, in the PPS the period increased with distance from the canal, whereas within the LC the period did not vary significantly. Liu and colleagues quantified crimp in the cornea using transmitted electron microscopy (TEM), measuring the angle of fibers in strips of cornea stretched uniaxially.(Liu et al., 2014) Others have visualized the crimp in the eye using electron micrographs,(Andreo & Farrell, 1982) second harmonic generated (SHG) imaging,(Winkler et al., 2011) and magnetic resonance imaging (MRI).(Ho et al., 2014) These studies, however, did not quantify any crimp morphology.

Studies of collagen fiber architecture of the posterior pole have typically focused on the organization at a scale larger than crimp. (Jan, Lathrop, et al., 2017) For example, for the LC, trabeculae beam and pore diameters have been described using electron microscopy,(Thale & Tillmann, 1993a) histology,(M Rosario Hernandez et al., 1987) second harmonic generated imaging (SHG),(Sigal et al., 2004) and optical coherence tomography (OCT).(B. Wang et al., 2013) The sclera macro-scale anisotropy has been quantified using small angle light scattering

(SALS)(M. J. Girard, A. Dahlmann-Noor, S. Rayapureddi, J. A. Bechara, B. M. E. Bertin, et al., 2011) and wide-angle x-ray scattering (WAXS)(Keith M. Meek & Boote, 2009; Jacek Klaudiusz Pijanka et al., 2013; Jacek Klaudiusz Pijanka et al., 2012) for the collagen orientation, and polarization sensitive OCT (PS-OCT) for collagen birefringence.(Baumann et al., 2014)

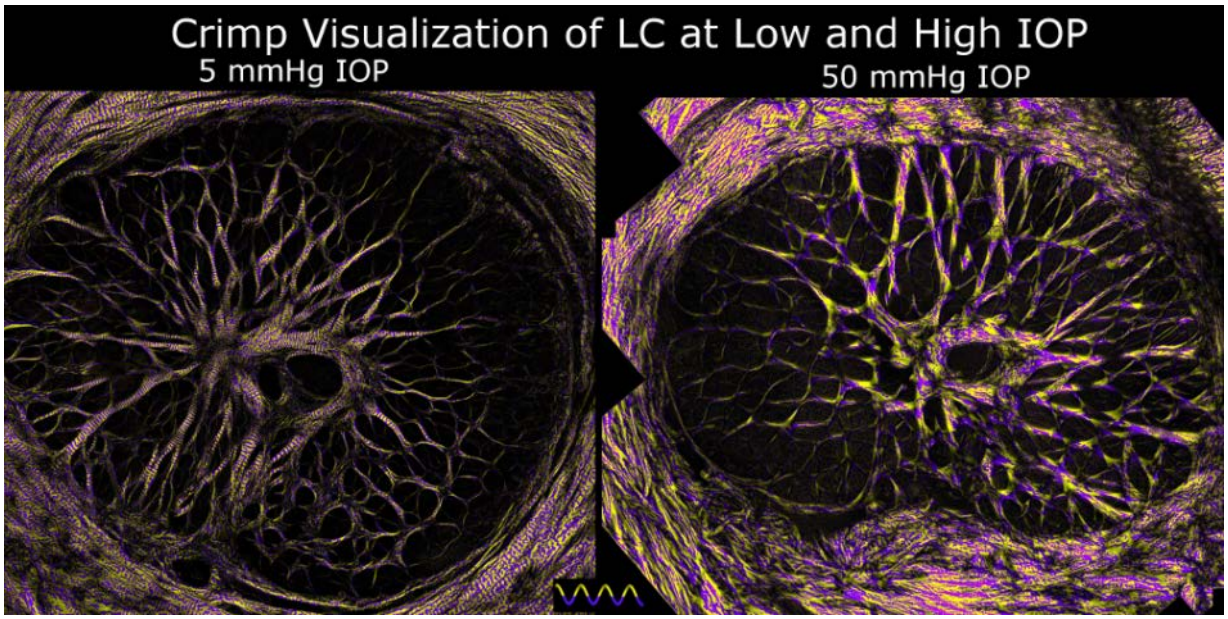

Figure 55. Crimp in LC at low and elevated IOPs.

Using the crimp visualization technique described in **Figure 53** evidences clear differences in crimp between LCs of eyes fixed at low (left) or elevated (right) IOPs. At 5 mmHg IOP, it is easy to distinguish across the whole the LC periodic purple and yellow banding perpendicular to the LC trabeculae beams. In contrast, at 50 mmHg IOP, the LC beams show patchy or noisy yellow and purple coloring, indicative of recruited fibers.

Accurate measurement of micrometer-scale crimp properties, however, requires high angular and spatial resolutions, otherwise the orientation information will encode both anisotropy and crimp.(Pierlot et al., 2014) In addition, representative characterization over the LC and PPS requires a wide field-of-view, and comparability between tissues requires a sensitivity range spanning the low density of the LC and the high density of the PPS. It is possible to quantify crimp using other modalities. For example, SHG has excellent specificity for collagen and can image

areas with micrometer-scale resolution. However, SHG protocols are more complex and the system itself is substantially more expensive. Most current methods of analyzing SHG images require resolving collagen fiber edges for tracing or for gradient-based analysis.(Fata et al., 2013; Hill et al., 2012) In areas of the ONH that have densely packed collagen with complex overlapping structures, it becomes much more difficult to ensure there are no artifacts. This is particularly difficult in areas with pigment,(Tauer, 2002) where the power of the SHG laser also increases the likelihood of thermal damage on the tissue. We have demonstrated that our implementation of PLM does not have these limitations and is suitable for characterizing ocular collagen crimp, even in densely packed areas with overlapping collagen fiber bundles.(Jan et al., 2015)

In addition, sample preparation for PLM analysis of crimp is relatively simple as the tissues can be visualized without the need for dehydration, labels or stains, reducing tissue processing and the likelihood of introducing artifacts, such as deformation. Dehydration, necessary for paraffin and plastic embedding, and for most block-face imaging, causes substantial shrinkage of the tissues. Tissue flattening via stress-relieving cuts, such as those used in some studies with SALS or WAXS(M. J. Girard, A. Dahlmann-Noor, S. Rayapureddi, J. A. Bechara, B. M. E. Bertin, et al., 2011; Jacek Klaudiusz Pijanka et al., 2013) could affect the collagen crimp. These were not necessary for PLM of cryosections.

It is important to consider the limitations of our study together with its strengths. The tissues used in this study were ex-vivo, fixed in formalin, and cryosectioned, each of which could introduce artifacts. In preliminary tests we tested fixing the eyes for 24 hours, and longer, and did not detect any differences. Nevertheless, it is still possible that the tissues were not perfectly fixed by 12 hours of formalin. If so, some crimp could “reappear” when the fixation pressure is removed, increasing the waviness observed at elevated IOP. We have previously shown that the tissue

processing steps have minimal effects on tissue size and shape.(Tran et al., 2017) The study was conducted on sheep eyes from an abattoir. This is advantageous for a first study of this type, as animals bred together for human consumption may exhibit less inter-individual variations than human donors would. Sheep eyes have a collagenous LC, but also have distinct structural differences from humans, potentially limiting the application of our findings. Sheep LC have a thick tree-like ventral groove in the ONH, which humans do not have and it is possible that the crimp patterns we have found using sheep may not be applicable to humans. In this work we analyzed only LC beams. Though understanding sheep as an animal model is important, measurements of crimp in other animals and humans are needed to understand how their microstructural crimp changes with IOP.

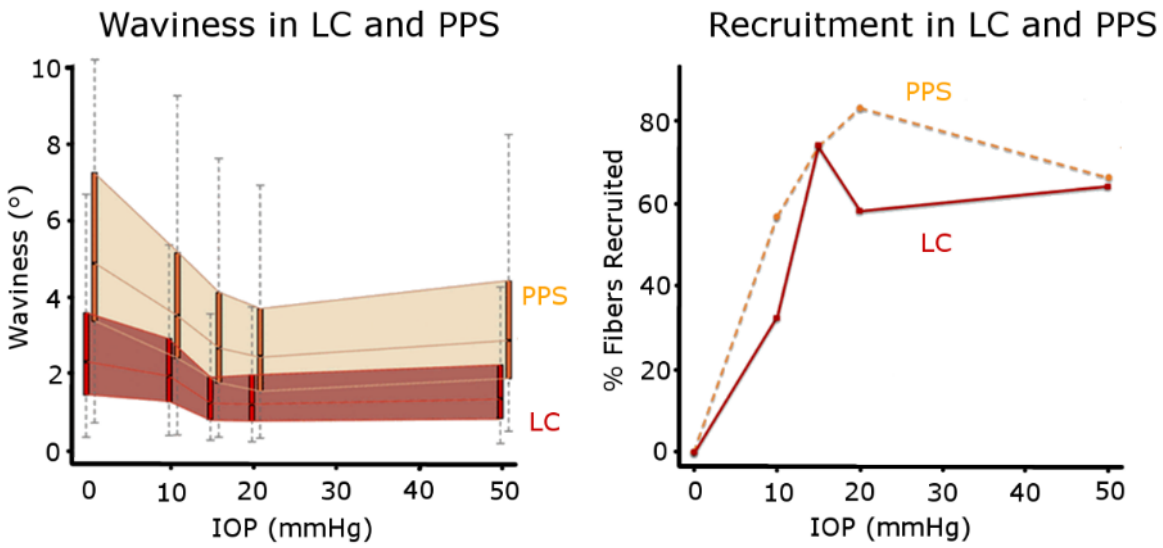

Figure 56. Waviness and recruitment in the LC and PPS.

At each IOP, we obtained the distributions of the collagen waviness in the LC (red) and PPS (orange), represented here as thin box plots.(left) The25th to 75th percentiles of the waviness as each IOP were shaded to highlight the distinct differences between LC and PPS. The resulting recruitment curves were also significantly different between LC and PPS (right). The LC consistently had lower waviness than the PPS and also reserved the same or a larger percentage of fibers than the PPS at every IOP. At 15 mmHg both the LC and PPS had ¾ of their fibers recruited and ¼ in reserve.

Another limitation of our study was that we tracked changes in collagen crimp using different samples for each IOP rather than measuring the crimp in the same sample through different IOPs. It is more akin to a cross-sectional than to a longitudinal study. It is possible that the variability between eyes may influence the recruitment trends observed, Future studies are necessary to confirm these trends, for example by using PLM to image fresh tissue at various levels of stretch, tracking individual fibers in situ(Jan et al., 2016; Wallace et al., 2017) or using SHG.(D. E. Midgett et al., 2017; Ian A Sigal et al., 2014)

Our measures of crimp waviness are based on the in-plane collagen fiber orientation derived from 2D histological sections of the ONH. The fiber orientation information can be biased depending on the direction of sectioning. However, we section the ONH coronally, which is the direction the ONH tissue experiences the majority of the IOP-induced forces. Our measurements of collagen crimp in the coronal plane would therefore be most relevant to the biomechanics of the eye. To limit our study to the in-plane fiber bundles from our coronal sections, we were careful to mark only in locations with bright well-defined bundles that appear in the section plane, In the LC, there are beams that can run oblique or even perpendicular to our plane of sectioning. These bundles would not be bright nor would they be well defined in our coronal PLM images, and therefore would not be included in the analyses. Future studies, should quantify the crimp changes with IOP in the sagittal and axial planes. Alternatively, it may be possible to do a full 3D analysis of crimp from coronal sections using more advanced PLM analysis methods.(B. Yang et al., 2017)

As mentioned previously, the waviness of the LC and PPS fibers from eyes fixed at 50 mmHg IOP was used to determine the threshold for recruitment. We assumed that at the very high pressure of 50 mmHg, the vast majority of the fibers have been recruited, so any remaining waviness was not due to the collagen crimp. By using a threshold less than the 100% percentile,

this allowed us to avoid considering beam or bundle curvature and interweaving as waviness. We recognize that there is some degree of arbitrariness in choosing the threshold percentile. Hence, we repeated the recruitment analyses using a wide range of threshold percentiles. We found that, although the percentage of fibers recruited changed with the threshold, the recruitment patterns for the LC and PPS were very similar (Appendix A). Hence, we conclude that our choice of threshold was not a determinant of the result.

We analyzed the percentage of fibers recruited for eyes fixed at 0, 10, 15, 20, and 50 mmHg IOP. The pressures were carefully chosen so that we could analyze the collagen crimp morphology in the no-IOP, physiologic, slightly higher pressure than physiologic, and extremely high pressure states. The lowest and highest pressure states were used to quantify the crimp at its waviest and least wavy. The three pressures in the middle were used to quantify the crimp at the states we suspected most of the recruitment would happen, which would be the transition from physiologic pressure through slightly higher pressures. This set of pressures provides a general shape of the recruitment curve. A more detailed characterization of the recruitment curve would require more pressures.

Collagen crimp waviness is but one parameter of the crimp morphology. There are other crimp characteristics that may also be important in determining how the crimp changes with stretch. For example, the amplitude, tortuosity, period, and maximum deviation angle can also be used to describe the crimp. In a previous study, we quantified the collagen crimp period in the posterior pole at low IOPs.(Jan, Gomez, et al., 2017) Grytz and colleagues predicted the maximum deviation angle using inverse modeling,(Grytz & Meschke, 2010) while Robertson and colleagues manually measured the tortuosity of the collagen fibers from SHG images(Hill et al., 2012).

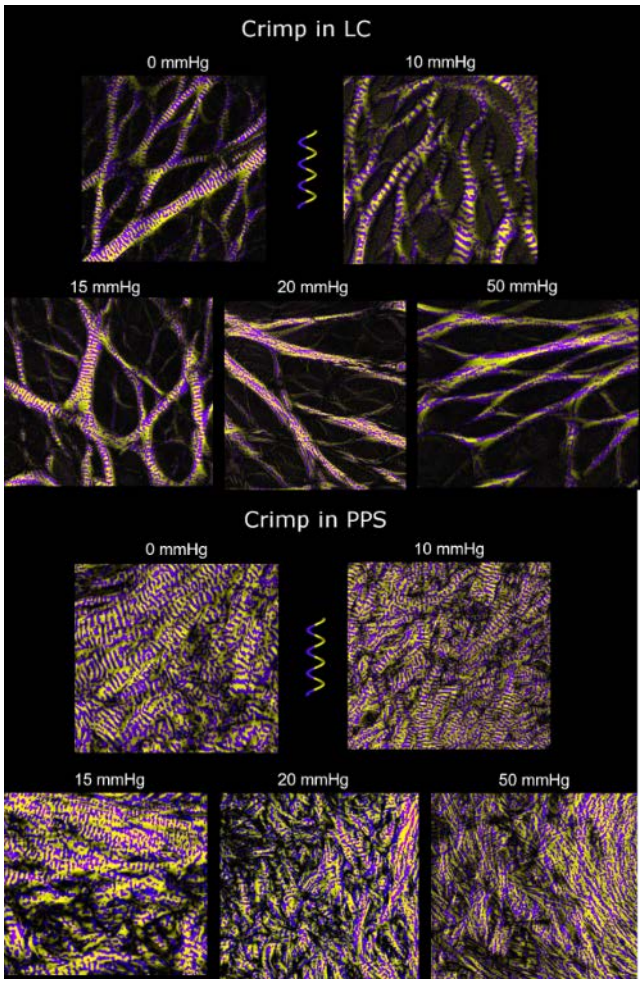

Figure 57. Crimp visualizations of LC and PPS at various IOPs.

The LC trabeculae beams gradually lose their crimp with increasing IOP. At 50 mmHg IOP, essentially all LC beams have been recruited. The PPS crimp gradually disappears with increasing IOP, though even at 20 mmHg IOP, some crimp is still apparent. Compared to the LC, the PPS had wavier fiber bundles at the same IOPs. The waviness in the LC and PPS was generally less than 10°. Midgett et al 2017 reported strains below 3% even at IOPs of 45 mmHg which agrees with the small waviness we found for the LC.(D. E. Midgett et al., 2017) For reference, in unpublished studies of sheep Achilles' tendon, we found the average waviness to be greater than 20°, which agrees with the large extensibility of tendon fibers.

Each of these parameters may potentially have different relationships with stretch. In addition, several other factors also affect tissue stiffness and response to load, including, but not limited to, fiber reorientation, fiber slip, tissue composition, collagen type, proteoglycan content and distribution and the amount and type of cross-linking between the fibers.(Birch et al., 2013; C

Ross Ethier et al., 2004; Fratzl, 2008; Holzapfel, 2001) Therefore, studies considering additional tissue characteristics are needed to fully characterize the tissue response to load. In this study we did not split the LC or PPS into regions. This may be important and necessary to detect potential region-dependent variations, which may be of importance for sensitivity to IOP or susceptibility to disease.(Z. Nadler et al., 2014)

An important goal of this work was to provide experimental measures of crimp morphology to help drive fiber-based constitutive model formulations for the posterior pole.(Coudrillier et al., 2013; M. J. Girard et al., 2009; Grytz et al., 2011; A. P. Voorhees, Jan, & Sigal, 2017) Although we obtained recruitment curves with IOP, we did not measure the stresses and strains within the LC and PPS. Our results will have to be integrated with other studies to derive the constitutive models.

In conclusion, we quantified the collagen crimp waviness in the LC and PPS at a wide range of IOPs. We derived tissue-specific recruitment curves and found that the LC and PPS have distinct crimp distributions and recruitment behaviors. Our results suggest that at a normal 15mmHg of IOP, both the LC and PPS have about ¾ of the collagen recruited or "bearing load" and about ¼ crimped or "in reserve" to bear loads and increase stiffness at higher IOPs. The recruitment curves also suggest that there may be a protective mechanism whereby the PPS relieves some tension from the LC and reduce the fraction of loaded fibers at elevated IOPs. Altogether, our findings have demonstrated a strong link between the microstructural collagen crimp properties of the LC and PPS and IOP.

7.0 CRIMP CHANGES OF EQUATORIAL SCLERA WITH UNIAXIAL STRETCH

7.1 INTRODUCTION

Collagen is a basic component of the eye and plays a central role in determining tissue biomechanics (Fratzl, 2008; Holzapfel, 2001; Wainwright et al., 1982). Changes in ocular collagen are related to some eye disorders such as myopia or diseases like glaucoma, as well as with natural processes like development and aging (Bailey, 1987; Huang et al., 2013; Rada, Shelton, & Norton, 2006; Y. Yang, Li, Yan, Cai, & Liu, 2009). Therefore to fully understand these illnesses and processes, it is important to characterize the collagen structure in the eye.

The fibrous collagen in the eye (Andreo & Farrell, 1982; Ho et al., 2014; Jan et al., 2018; Jan, Gomez, et al., 2017; Ning-Jiun Jan & Ian A Sigal, 2018; Richard H Newton et al., 1996), like in tendon and ligament (Franchi et al., 2007; Komatsu et al., 2002), have a natural waviness called crimp. Crimp is an innate property of collagen fibers, noted in anatomy books such as “Gray’s Anatomy” (Standring, 2016). Crimp has been hypothesized to be central to the nonlinear biomechanics of soft tissue through a process known as fiber recruitment (Ethier & Simmons, 2007; Holzapfel & Ogden, 2006) (Figure 58). Experimental crimp measurements from tissues like tendon (Hansen et al., 2001), ligament (Thornton et al., 2002), and arterial tissue (Hill et al., 2012) support this hypothesis, though few have experimentally characterized how the crimp recruits in the sclera. Past studies have used inverse numerical models to predict the collagen crimp structure

in the eye though these studies assumed a simplified uniform collagen crimp throughout the sclera and lacked experimental measures of crimp (Grytz & Meschke, 2010; Grytz et al., 2011). Recently, we reported the first experimental measures of scleral crimp (Jan et al., 2018; Jan, Gomez, et al., 2017) and recruitment (Ning-Jiun Jan & Ian A Sigal, 2018) in the peripapillary sclera. These studies compared the crimp from different regions of the eye characterized population crimp trends with changes in intraocular pressure (IOP). A recruitment curve was made based on the cross-sectional crimp measurements at different IOPs. These studies lacked information on how any specific collagen fiber bundle changed with stretch because the measurements were of fixed tissue, and therefore the crimp could only be quantified at one stretch state. A characterization tracking the bundle-specific changes in crimp in fresh tissue is needed to further the development of accurate fiber-based constitutive models of the eye. Hence, our goals were to use fresh scleral tissue to characterize the crimp changes with stretch and construct a recruitment curve, as well as to determine if there were any trends with tissue depth. Specifically, we tracked the changes in crimp in fresh equatorial sclera with uniaxial stretch.

7.2 METHODS

We prepared fresh sections of equatorial sclera and imaged with polarized light microscopy (PLM) at various levels of uniaxial stretch. The PLM images were used to quantify the collagen fiber orientation and track tissue deformations. Specifically, we quantified the collagen crimp waviness, micro-scale strain, macro-scale stretch, and tissue depth. We tracked the uncrimping of select collagen bundles to construct recruitment curves and tested whether the uncrimping was related to tissue depth.

7.2.1 On the terminology

It is important to note that collagen architecture is hierarchical and complex. Even in tendon, where the collagen is much more organized compared to the eye, there is confusion on the specific meaning of various terms referencing the hierarchy of the collagen (Handsfield, Slane, & Screen, 2016). This is why for the purposes of this paper, we would like to discuss what the term collagen "bundles" refers to. This term refers to the groups of highly aligned collagen fibrils of the sclera. These groupings are discernible using PLM, as we have previously shown (Jan et al., 2018).

7.2.2 Sample preparation

Three fresh goat (caprine) eyes were acquired from a local abattoir and processed within 8 hours of death following previously described methods, (Jan, Gomez, et al., 2017; Jan et al., 2015; Jan, Lathrop, et al., 2017; Ning-Jiun Jan & Ian A Sigal, 2018) with some modifications for longitudinal sectioning of fresh whole globes rather than coronal sections of fixed optic nerve heads (ONHs). Briefly, using scalpels, forceps, and razors, extraneous muscle, fat, and episcleral tissue were removed. Each eye was mounted in an embedding cryomold and filled with optimal cutting temperature (OCT) compound (Fisher Healthcare, Houston, TX). All eyes were aligned within the molds in the nasal-temporal and superior-inferior anatomical directions for sectioning. After embedding, the eyes were then flash frozen in isopentane chilled in liquid nitrogen. These molds were stored in plastic bags at -80° C and never thawed and refrozen before sectioning. Each eye was cryosectioned sagittally into 30 μm sections. Using a standard anti-roll plate and cold fine-tip brush, sections were held flat before adhering to an uncharged glass slide. Over 20 consecutive

sections through the ONH and cornea were collected for each eye. Of those, two consecutive sections free of artifacts, such as folds were used for analysis. A total of 6 sections were used for analysis. Using scalpels, forceps, and razors, centimeter long strips of equatorial sclera were carefully isolated and transferred to a modified uniaxial stretcher (Microvice, S.T. Japan, FL, USA) (Figure 58). The tissue was mounted in such a way that the superior and inferior ends of the tissue were clamped.

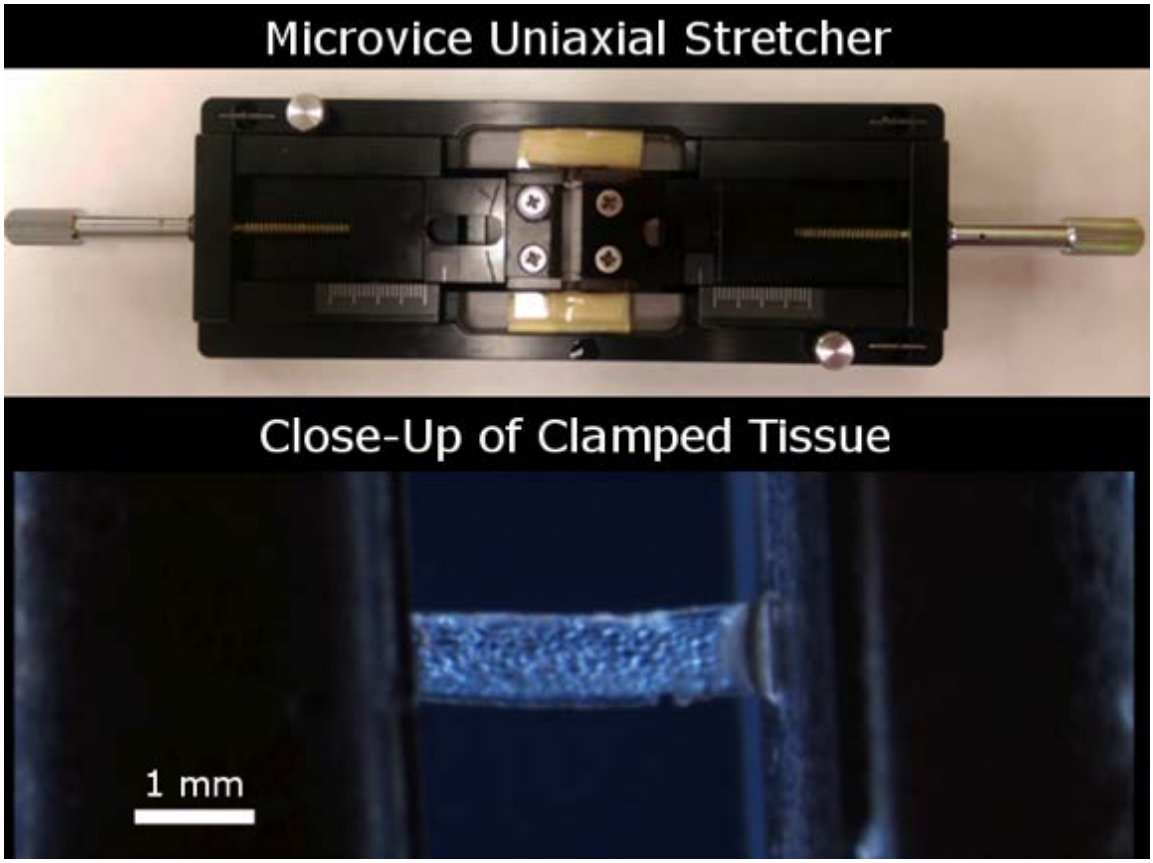

Figure 58. Microvice uniaxial stretcher was used to stretch fresh equatorial scleral sections. Above is an image of the commercial tissue stretcher. Below is a close-up of clamped tissue, imaged using transmitted light microscopy.

7.2.3 Imaging

The mounted sections were imaged at various levels of stretch using PLM using previously reported methods, (Jan, Gomez, et al., 2017; Jan et al., 2015; Jan, Lathrop, et al., 2017; Ning-Jiun Jan & Ian A Sigal, 2018) though with some modifications for imaging fresh mounted sections. Briefly, a polarizer filter was placed before the sample and an analyzer filter placed after the sample (Hoya, Tokyo, Japan). Four images were acquired, each with filter orientations 45° apart from each other. Local collagen fiber orientation was determined using the relative changes in intensity at each pixel. (Jan et al., 2015; Shribak & Oldenbourg, 2003) An Olympus SZX16 microscope (6.3x magnification setting) paired with an Olympus DP80 camera (36-bit, RGB, pixel-shift setting) was used to acquire the images. (Olympus, Tokyo, Japan) Images had a pixel size of 0.68 μm/pixel using a 0.8x objective (numerical aperture [NA], 0.12).

To stretch the tissue, the clamp holding the inferior side was held at a fixed location while the clamp holding the superior side was pulled. The clamps were fixed in such a way that they could only move in one axis. Each level of stretch was held for 15 min to allow viscoelastic effects to normalize before imaging. Each sample was stretched until failure, which we defined as when there was a visual rip in the tissue. The sample was kept hydrated with 1X neutral phosphate buffered saline (PBS) throughout the imaging session. Each section was stretched between four to six different macro-scale stretch levels before failure.

7.2.4 Crimp waviness

From the PLM-derived orientations, we measured the waviness of collagen fiber bundles. We quantified the waviness using the circular standard deviation (Jammalamadaka & Sengupta, 2001) of the collagen fiber orientations along a collagen bundle, as described previously.(Ning-Jiun Jan & Ian A Sigal, 2018) Briefly, a straight fiber bundle would have a constant angle value, and therefore the waviness would be 0°. On the other hand, a wavy fiber bundle would have oscillating angle values throughout the fiber bundle, and therefore the waviness would be greater than 0°. To measure the waviness, we sampled the orientations using line segments placed along the length of a collagen bundle. Between eighteen to twenty collagen bundles were sampled in each section (Figure 59). Only bundles that were identifiable throughout all stretch levels were used for analyses.

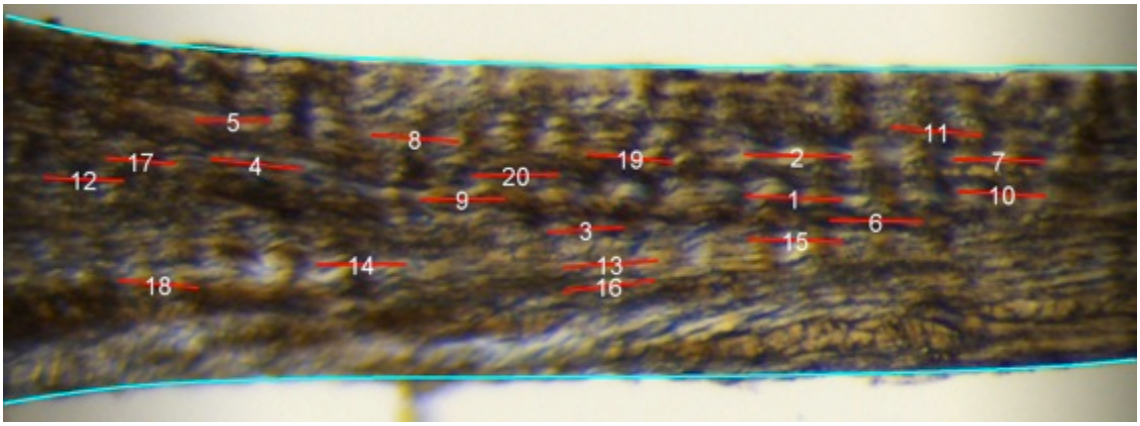

Figure 59. Tracking bundle-specific crimp changes with strain.

We marked collagen bundles in order to track the bundle-specific waviness and micro-scale strain (red lines, numbered). We also manually segmented the exterior and interior ends of the tissue in order to measure the tissue depth (cyan lines).

7.2.5 Micro-scale strain

The micro-scale strain was a measure of how the tissue locally deformed as a result of the uniaxial stretching. This was defined as the 1st principal plane strain, or how much the tissue locally stretched in the direction of the largest stretch. The strains were calculated using an image registration algorithm developed previously.(I. A. Sigal et al., 2014) Briefly, the "before" image is morphed so that it is registered with the "after" image. The strains are then calculated for each pixel based off of how each pixel was morphed to get to the final image. Specifically, we quantified the percent change in length in the direction of the largest stretch, where 0% would indicate no change in length and 100% would indicate doubling in length. This micro-scale strain was calculated at each pixel. The micro-scale strain was plotted on each pixel of the image of the tissue before each stretch (as opposed to the image of the tissue after each stretch) using color-coded strain maps. To measure the micro-scale strain in any specific collagen bundle, a line segment was used to sample the strains along the length of a collagen bundle, and the average micro-scale strain was calculated. For all of our measurements, the line segment used to measure waviness was also used to measure the average micro-scale strain.

7.2.6 Macro-scale stretch

The macro-scale strain was a measure of how much the tissue as a whole stretched. This was defined as percent change in clamp-to-clamp distance as the sample was stretched. This was measured by segmenting the border between the clamp and the tissue in each image and determining the shortest distance between the two edges for each stretch state. The percent change

in distance was calculated relative to the final distance between the clamps in the last stretch state imaged before failure. Therefore 0% would be the initial conformation before stretching and 100% would be the final conformation or last stretch before tissue failure.

Tissue depth: The tissue depth was a measure of how close a collagen bundle is to the external or internal lining of the eye. To measure this, the superficial and interior borders of the equatorial sections were manually segmented using Fiji Is Just ImageJ (FIJI). (Preibisch et al., 2009) The depth was calculated as the percent distance, where 0% would be at the exterior border and 100% would be at the interior border

7.2.7 Recruitment

Recruitment curves were made based on the changes in collagen crimp waviness, as described previously, but with a few adjustments for tracking bundle-specific changes. (Ning-Jiun Jan & Ian A Sigal, 2018) Briefly, we tracked the waviness in at least eighteen evenly spaced collagen fiber bundles in each section through at least four levels of stretch before failure. The percent of uncrimped, or recruited collagen bundles were calculated for each level of macro-scale stretch for each tissue section. We defined eye-specific waviness thresholds to determine whether a collagen fiber bundle was considered recruited. We set this threshold as the 75^{th} percentile of the waviness at the final stretch point for each eye. A recruitment curve was constructed for each section of each eye.

7.2.8 Statistical analyses

All statistical analyses were done using R. (Team, 2013)

1) **Waviness vs Micro-Scale Strain:** A mixed effect model accounting for autocorrelations of measurements from the same section and eye were used to determine whether for each collagen bundle, waviness was related to micro-scale strain. Mixed effect models incorporate fixed variable (waviness and micro-scale strain) with random variables that may affect the sampling population (what section and eye the measurement came from). (Gałecki & Burzykowski, 2013) We fit a mixed effect exponential model to the data.

2) **Recruitment Curve:** We tested if the recruitment curves of each section followed a sigmoidal curve shape. A single sigmoidal curve was fit across all sections using a mixed effect model accounting for autocorrelations of measurements from the same section and eye.

3) **Associations with Depth:** In order to test if bundles at different depths uncrimped or recruited differently, we used two linear mixed effect models, where both accounted for autocorrelations of measurements from the same section and eye. One model tested if there was an association between micro-scale strain and tissue depth, while the other model tested if there was an association between waviness and tissue depth.

7.2.9 Visualizations

Images were enhanced for qualitative visualization of the collagen crimp and tissue strains (Figure 60). To visualize the crimp changes with stretch, we used a previously described algorithm for viewing the crimp period.(Ning-Jiun Jan & Ian A Sigal, 2018) Briefly, pixels were colored purple or yellow depending on whether the orientation was larger or smaller than the local average orientation, respectively. In crimped collagen bundles, the result was clear bands of alternating purple and yellow, each corresponding to half a crimp period. In uncrimped, straight bundles, there would not be clear bands. To visualize the micro-scale strain, we pseudo-colored the pixels using

a rainbow color scheme, where small strains were violet and large strains were red. For all visualizations, the pixel intensities were scaled using energy, a parameter previously described.(Jan et al., 2015) Briefly, the energy is the PLM signal variation when rotating polarized filters. This scaling allowed us to discern the texture of the tissue.

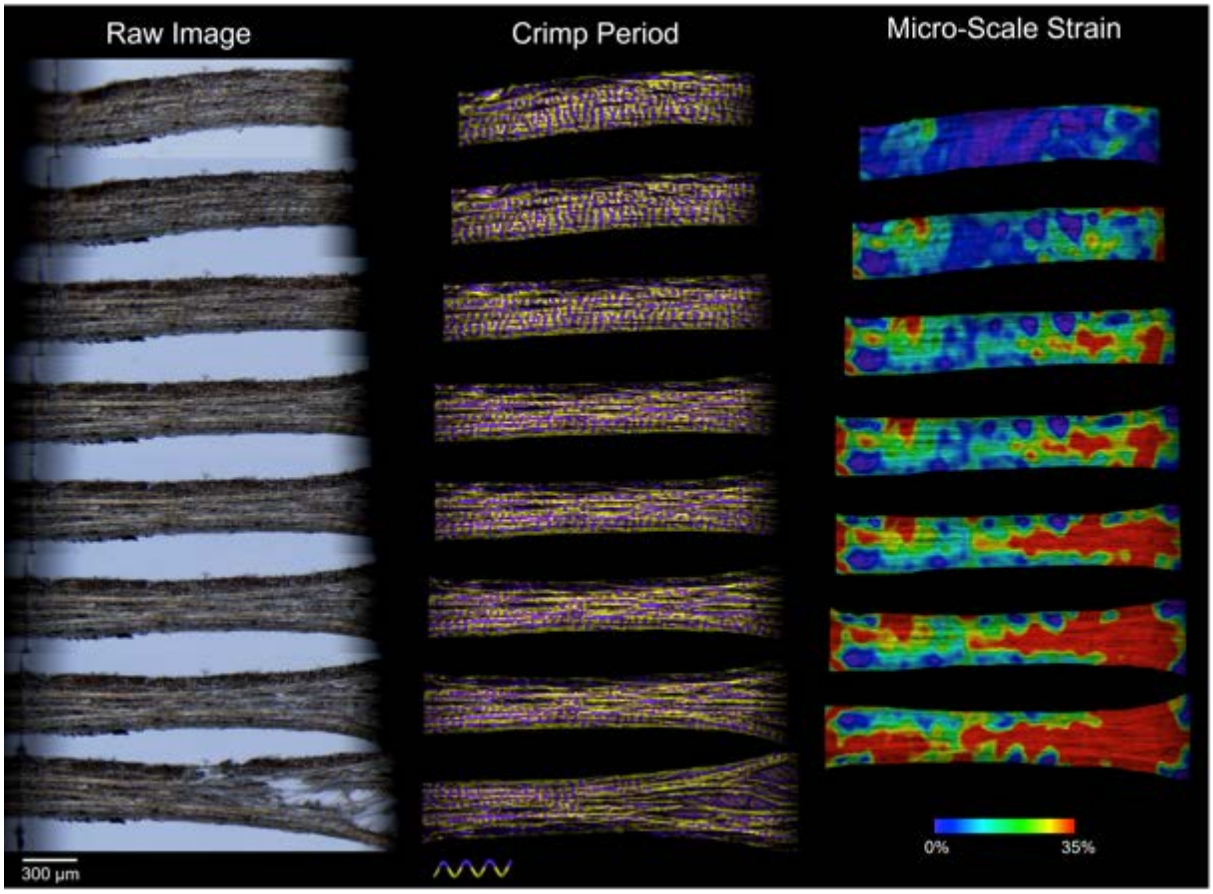

Figure 60. Equatorial sclera at various levels of uniaxial stretch.

The raw PLM images (left) are used to derive the collagen fiber orientation. From the collagen fiber orientation, we tracked the collagen crimp (middle) and micro-scale strain (right).

7.3 RESULTS

A total of 97 collagen bundles were tracked across all six sections of the three eyes. In the initial configurations before stretching, average bundle waviness was 7.5°, where bundle waviness ranged from 1.7° to 22.8°. The 75th percentile waviness values at the last stretch level before failure were 3.1° for Eye 1, 4.4° for Eye 2, and 2.8° for Eye 3 (Figure 61). The total micro-scale strain experience by a bundle before tissue failure varied, where one bundle experienced 0% strain while another experienced 36.3% strain before failure.

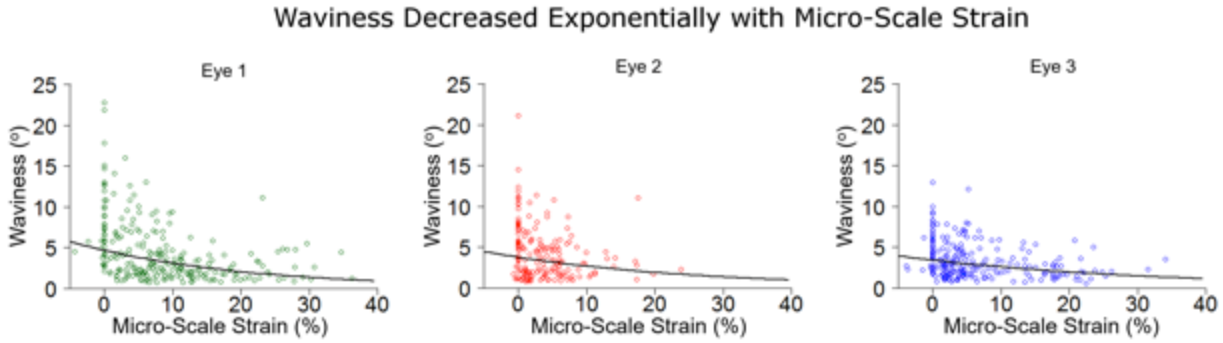

Figure 61. Waviness versus strain in each eye.

All three eyes had similar trends, where the waviness decreased exponentially with micro-scale strain. Best fit exponential lines are shown in black.

For all eyes, waviness exponentially decreased with micro-scale strain ($P<0.001$, Figure 61). The recruitment curves constructed from the waviness values for each section was also similar. The sections started with ~20% bundles recruited and ended with ~80% recruited at the final stretch state before failure. The percentage of recruited bundles with macro-scale stretch followed a sigmoidal growth pattern ($P<0.001$, Figure 62) Bundle uncrimping and recruitment was

not found to be related to tissue depth. We did not find depth to be associated with micro-scale strain ($P>0.01$) nor waviness ($P>0.01$) (Figure 63).

7.4 DISCUSSION

Our goal was to determine how the collagen crimp in fresh equatorial sclera changed with stretch and whether the crimp and recruitment varied with tissue depth. From our study, we found three main results. The first is that collagen bundle waviness decreased with micro-scale strain. The second is that the collagen bundles recruited in a sigmoidal pattern. The third is that there were no associations between tissue depth and waviness nor micro-scale strain. Let us discuss each of these in turn.

Collagen crimp waviness decreased with micro-scale strain. We found that for each collagen bundle, the waviness decreased as the strains experienced by that bundle increased. This implied that as each crimped fiber bundle was stretched, the bundle became less wavy. This supports the current theory of recruitment, which emphasizes that there exists a direct relationship between stretch and bundle uncrimping, which in turn can affect the nonlinear biomechanics of the overall tissue (Fratzl, 2008). By tracking individual collagen bundles with stretch, we experimentally showed this direct relationship. To the best of our knowledge this is the first time that individual collagen bundles have been tracked for changes in crimp waviness with stretch in the sclera. In addition, we were able to characterize this rate of decrease as an exponential, where the bundles lost most of its waviness within 10% strain and lost less at higher strains. Though this relationship is well-characterized for various tendons and ligaments throughout the body (Hansen et al., 2001; Holzapfel, 2001; Thornton et al., 2002), few have experimentally characterized the

crimp with stretch in the sclera. The only experimental study we know of, is our own previous study that measured the crimp waviness in ONHs fixed at various IOPs (Ning-Jiun Jan & Ian A Sigal, 2018). Our results agree with this previous cross-sectional study, where we found that in a population of collagen bundles, waviness decreased with increasing IOP-induced stretch.

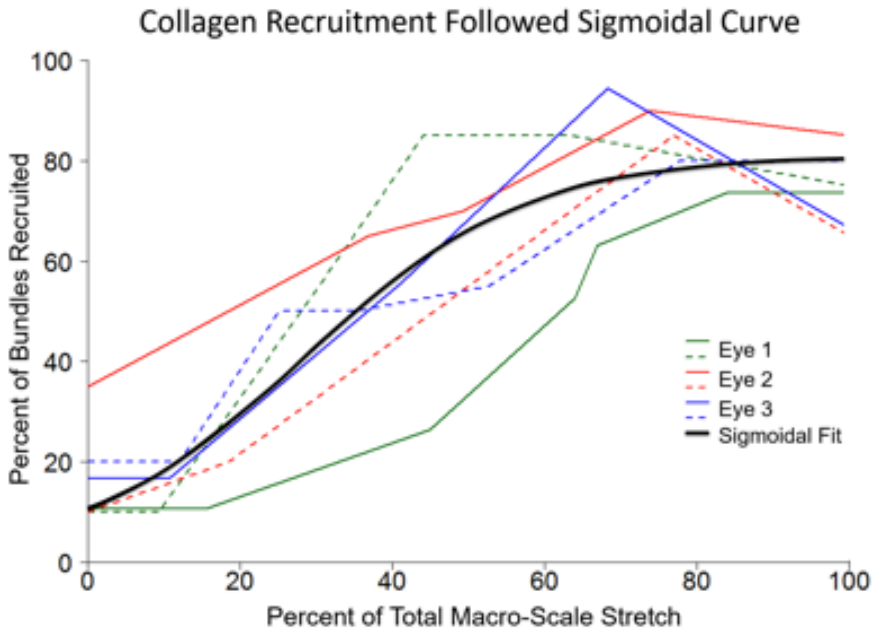

Figure 62. Constructing recruitment curves.

The percentage of recruited collagen bundles over the different levels of macro-scale stretch was plotted for each of two sections (solid and dashed lines) per eye for the three eyes (green, red, and blue). A sigmoidal function was fit across all the measurements (black line).

Collagen bundles were recruited gradually. The collagen bundles recruited over a large range of the macro-scale stretch, generally starting to recruit around 10% and leveling off at around 80% of the final tissue length before failure. This gradual recruitment agrees with our highly variable crimp waviness of the tissue before stretching. According to current theory of collagen recruitment, groups of collagen bundles with uniform crimp would recruit simultaneously, while groups with variable crimp would recruit gradually (Fratzl, 2008) (Figure 64).

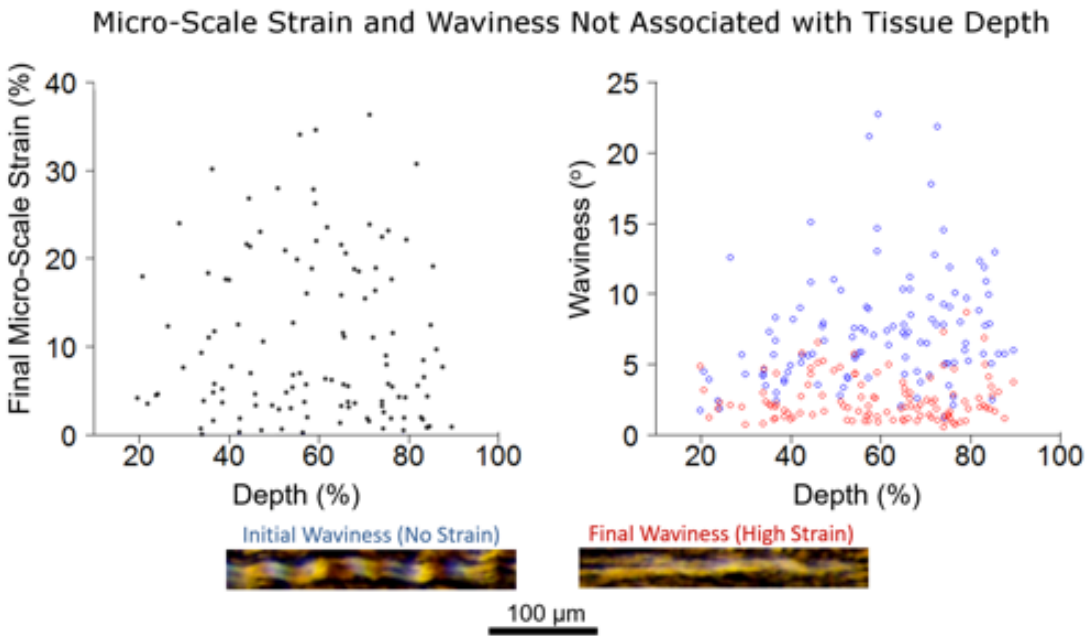

Figure 63. Associations of micro-scale strain and waviness with depth.

On the left are of the micro-scale strains in the final tissue stretch state before failure, or the total micro-scale strain experienced by each bundle, as a function of tissue depth. On the right are the crimp waviness at the initial stretch state (blue) and the same bundles at the final stretch state before failure (red). Both were plotted as a function of depth. On the bottom is an example of a bundle before stretching with high waviness and the same bundle at the final stretch state with very little waviness. We did not find depth to be associated with the micro-scale strains nor the waviness.

The collagen bundles of the equatorial sclera were found to recruit in a sigmoidal fashion with macro-scale stretch. It took a small amount of macro-scale stretch to initialize the recruitment process, giving rise to the toe-region of our recruitment curve. The rate of recruitment increased to around 50% of the final macro-scale stretch before slowing and leveling off at around 80% stretch. Again, our results agree with our previous cross-sectional study comparing the crimp of ONHs fixed at various IOPs, where gradual recruitment was also found for the sclera (Ning-Jiun Jan & Ian A Sigal, 2018).

There were no associations between tissue depth and waviness nor micro-scale strain. We found that the equatorial scleral collagen bundles did not stretch more or less depending on

tissue depth. We also found that the crimp morphology did not have any relationship with tissue depth. Superficial bundles acted similarly to those deeper in the tissue. This suggests that in a clinical setting, when usually only the surface equatorial scleral collagen fibers are visible and accessible, we still may be able to predict the biomechanical behavior of the deeper layers. For example, the use of reflected polarized light microscopy (Jacques, Ramella-Roman, & Lee, 2002) can analyze the collagen crimp in the superficial layers of the equatorial sclera, which could then be used to predict the biomechanics of the deeper tissue layers.

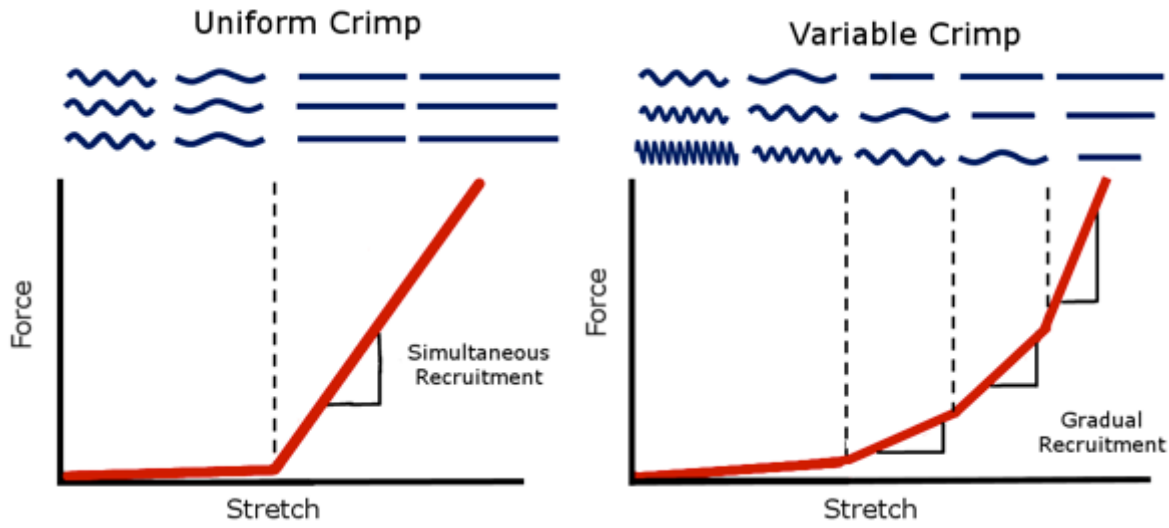

Figure 64. Recruitment of collagen bundles with uniform versus variable crimp.
When stretching collagen bundles with uniform crimp, all bundles straighten simultaneously, creating an abrupt change in stiffness. On the other hand, when stretching bundles with variable crimp, more and more bundles become recruited as stretch increases. Figure adapted from (Jan, Gomez, et al., 2017).

Collagen is known as the main-load-bearing component in soft tissues, and experimental measures of collagen crimp and recruitment are important for biomechanical analysis of soft tissue. The crimp and recruitment largely determine the nonlinear biomechanics of the tissue. This importance is evidenced not only by several biomechanics text books (Fratzl, 2008; Holzapfel,

2001), but also the numerous studies that have experimentally characterized the crimp microstructure in soft tissue, including in tendon (J Diamant et al., 1972; Franchi et al., 2007; Hansen et al., 2001; Mountain et al., 2011), ligament (Boorman et al., 2006; Komatsu et al., 2002; Shah et al., 1977; Thornton et al., 2002), and arterial tissue (Fata et al., 2013; Fata et al., 2014; Hill et al., 2012), to name a few.

In the ocular biomechanics community, the importance of crimp and recruitment has likewise been noted. The crimp in the eye has been visualized using various imaging modalities, including electron microscopy (Andreo & Farrell, 1982), second harmonic generated (SHG) imaging (Winkler et al., 2011), and magnetic resonance imaging (MRI) (Ho et al., 2014). For the cornea, the crimp has recently been quantified using transmitted electron microscopy (TEM) (Liu et al., 2014). However, few experimental measures of crimp and recruitment exist for the sclera. The only previously known experimentally derived recruitment curve for the sclera is that from earlier this year from our group (Ning-Jiun Jan & Ian A Sigal, 2018), where eyes fixed at different IOPs were compared for changes in crimp waviness. To the best of our knowledge, this study is the first to track bundle-specific changes in crimp for fresh sclera and to characterize a recruitment curve from this information. Prior to 2018, the only known studies on crimp in the sclera have been modeling studies, which predicted the collagen crimp microstructure based off of information derived from mechanical tests (Grytz & Meschke, 2009, 2010). These models were based on very general assumptions, such as uniform crimp in the cornea and sclera, which we have explicitly demonstrated as false in this study and our previous experimental studies of crimp in the ONH and around the eye globe (Jan et al., 2018; Jan, Gomez, et al., 2017).

Our study is not the first to characterize the collagen architecture and biomechanics in the eye using fresh tissue. Baumann and colleagues have quantified the collagen birefringence

and how the birefringence changes with IOP using polarization-sensitive optical coherence tomography (PS-OCT) (Baumann et al., 2014). Liu and colleagues also recently quantified how the crimp in the cornea changed with uniaxial stretch using TEM (Liu et al., 2014). Extensive histological studies have also been done on the ONH and sclera to characterize the collagen and elastin (M Rosario Hernandez et al., 1987; Quigley et al., 1991; Thale & Tillmann, 1993a).

Collagen crimp is not the only contributor to the overall biomechanics in the eye. It is true that the crimp largely determines the nonlinear aspects of the biomechanical behavior, or the rate of strain-related stiffening in the tissue, but it is important to note that many factors contribute to the biomechanics of the tissue, including but not limited to collagen fiber realignment, fiber slip, tissue density, anisotropy, and other components of the ground matrix, including elastin and proteoglycan content (Birch et al., 2013; C Ross Ethier et al., 2004; Fazio et al., 2014; Fratzl, 2008; Holzapfel, 2001). These factors may have contributed to the variability in how much the waviness changed relative to the amount of micro-scale strain experienced by any specific bundle. Some bundles lost their waviness and uncrimped at low micro-scale strains, while others experienced much larger strains before uncrimping. Some collagen bundles even never uncrimped, even at tissue failure. It is possible for example, that some of these bundles first needed to be realigned before they could uncrimp, while others may have already experienced micro-tears, and the fiber bundles slid past the others, and therefore the crimp remained unchanged.

In this manuscript, we quantified the waviness of the collagen crimp, which is but one crimp characteristic of many. Other crimp characteristics may also be important when characterizing crimp changes with stretch. For example, we could have quantified the collagen crimp period, which is a simple intuitive measure that can be made manually directly from PLM images. We have quantified this crimp characteristic previously in ONH tissue as well as around

different regions of the eye globe (Jan et al., 2018; Jan, Gomez, et al., 2017). However, as crimped fibers are stretched, the period becomes increasingly difficult to detect until the crimp disappears all together when the fibers become straight. This is one of the reasons we did not measure the crimp period with stretch. Besides period, other crimp characteristics include amplitude, tortuosity, and maximum deviation angle. We have also previously quantified the crimp amplitude and tortuosity in different regions around the eye globe (Jan et al., 2018). Using inverse modeling, the maximum deviation angle has also been predicted for the sclera (Grytz & Meschke, 2010). Each parameter could have different relationships with stretch. Future studies should consider other crimp characteristics as well as the crimp waviness when studying how the sclera responds to load.

Our study imaged fresh goat eye tissue without fixation or dehydration as these are not needed for cryosectioning. Typically, in paraffin or plastic embedding methods, the tissue needs to be fixed and dehydrated, which could shrink and warp tissue. In addition, because of the minimal tissue processing, we were able to stretch thin sections of fresh tissue to observe the crimp changes using PLM. Other studies have used imaging modalities like optical coherence tomography (OCT) (Baumann et al., 2014), magnetic resonance imaging (MRI) (Ho et al., 2015) to track changes in the eye with IOP. However these studies have not tracked bundle-specific changes with stretch.

It is important to consider the limitations of our study as well as its strengths. We used goat eyes in this study, which are similar to human eyes in general eye size and shape (Ribeiro, Santos, Campos, Teixeira, & Laus, 2010). However, there are also distinct differences. For example, goat eyes have a thicker sclera than human eyes (Al-Redah, 2016). It is possible that human tissue would have different crimp structure and recruit differently than goat tissue, though

goat is still important to understand as an animal model (Chen, Wu, Zhang, Fan, & Shen, 2011). Future work should include other animal models as well as human eyes.

Another limitation is that all PLM orientation analyses were done in 2D sections of the equatorial sclera. It is possible that there is some variability in the sectioning direction, which could affect consistency of crimp measurements between sections. Also, it is possible some of the collagen had out-of-plane components. To address this, future studies should incorporate 3D collagen fiber orientation measurements using advanced PLM methods (B. Yang et al., 2017). In addition, we did not differentiate between superior and inferior equatorial sclera. Future studies should consider comparing differences between different regions of the eye, like comparing nasal, temporal, superior, and inferior sides of the eye.

Though we have provided a thorough characterization of bundle-specific crimp changes in the sclera with stretch, we did not quantify the corresponding forces, nor did we use IOP to induce stretch. Our current set up using the commercial uniaxial stretcher did not allow us to do either of these. We intend to incorporate both of these into future studies of eye biomechanics by using a different apparatus that would allow simultaneous PLM imaging with IOP inflation.

In conclusion, this study is the first to track bundle-specific collagen crimp changes with stretch in equatorial sclera. We found that the crimp waviness decreased with micro-scale strain and that the collagen bundles recruited in a sigmoidal fashion. Our measurements provide insight into the microstructural basis of nonlinear biomechanics in the sclera. This information helps us develop fiber-based models of the eye, which could help us understand eye biomechanics in relation to aging and diseases like glaucoma.

8.0 DISSERTATION CONCLUSIONS

8.1 SUMMARY

This project established a method based on PLM to quantify collagen fiber orientation and crimp in the eye. We provided the first experimental characterization of the distribution of crimp in the ONH and throughout the eye globe, as well as the first experimental characterization of crimp-based recruitment in the ONH and equatorial sclera. PLM also revealed previously unreported aspects of the collagen structure of the posterior sclera, including a region of fibers arranged radially from the scleral canal.

Specific Aim 1. Characterize the performance of PLM for the study of ocular collagen architecture and crimp.

1A) Test the prediction that PLM provides accurate and repeatable micron-scale collagen fiber orientation and crimp measurements in eye tissue, robust to fixation, the presence of pigment, changes in magnification, and large differences in collagen density and organization between the LC and PPS.

Our method based on PLM provided highly accurate measurements of collagen fiber orientation in eye tissues. Our study also showed that our method was repeatable. For example, repeat measurements showed that 95% of the PLM-derived orientation values were within 5° of each other. PLM-derived orientation measurements were also robust to common variations in imaging protocol, including sample translation and rotation and changes in magnification. The measurements of collagen fiber orientation in eye tissue were also robust to formalin fixation, the presence of pigment, and the differences in density between LC and PPS. Our method based on PLM was fast and did not require any manual tracing of the fibers. It also did not require tissue dehydration, staining, or labeling, which are common tissue processing steps for most other histological analyses that affect the fidelity of the collagen architecture.

1B) Test the prediction that PLM can quantify the micron-scale collagen fiber orientation and crimp across large cm-scale regions of the eye.

We found that PLM can provide micron-scale orientation information across cm-scale areas of eye tissue. We demonstrated this ability by imaging cm-scale coronal sections of the ONH and axial section of whole eye globes. Stitching PLM images to form mosaics produced no noticeable edges between images. We were able to stitch more than 125 PLM images together to form

seamless mosaics that spanned cm-scale sections. From these images, we revealed previously unreported features of the collagen organization of the ONH. For example, images of the LC showed both wide robust beams that turn and integrate with the scleral canal as well as thin, frail-looking beams that insert perpendicular into the scleral canal. These images also showed that fibers of the LC beams wrapped concentrically around "pores" that contained the retinal ganglion cell axons. Images of the PPS showed three distinct regions: circumferential fibers adjacent to the canal, radial fibers in the anterior sclera, and interweaving fibers throughout the depth of the sclera. This study was the first to show micron-scale orientation maps of all three regions. From these maps we quantified the presence of each as a function of depth in the tissue. Analyzing our high resolution orientation maps, we also showed that the radial fibers could extend at least 3 mm from the scleral canal.

Specific Aim 2. Characterize the baseline crimp in the eye by testing the hypotheses that:

2A) The collagen bundles of LC trabeculae beams are crimped at baseline. Specifically, we test the hypothesis that LC trabeculae beams inserting into the scleral canal have different crimp than those that do not.

We demonstrated that the collagen bundles of the LC trabeculae beams were crimped at 0, 5, and 10 mmHg IOP and characterized the distribution of the crimp. The crimp period was not significantly different between those of collagen bundles in the LC fixed at 0, 5, and 10 mmHg IOP. We analyzed the crimp period as a function of distance from the scleral canal to characterize the spatial distribution of the crimp. We showed that there was no significant relationship, meaning that the collagen bundles of the trabeculae beam insertions did not have significantly different crimp period than that of beams that were not inserting into the scleral canal. This implied that

beam insertions may not have significantly different nonlinear properties compared to other trabeculae beams.

2B) PPS collagen bundles are crimped at baseline. Specifically, we test the hypotheses that the crimp of the PPS is different than that of the LC and that regions of the PPS farther away from the LC have larger differences in crimp.

We demonstrated that PPS collagen bundles were crimped at baseline. The PPS collagen bundles had significantly larger and more variable crimp period than that of the LC trabeculae beams. This implied that the PPS collagen bundles could stretch more before stiffening, and that the stiffening response would be more gradual than the LC. We also established that there was a spatial pattern to the crimp in the PPS collagen bundles. PPS collagen bundles proximal to the scleral canal had smaller and less variable crimp period compared to bundles distal to the canal. The crimp period of the proximal PPS collagen bundles was similar to that of the LC beams. The similarity in crimp period may serve to counterbalance stress concentrations between the LC and PPS. When analyzing the crimp period as a function of distance from the scleral canal, we found that the crimp period significantly increased with scleral canal distance. We characterized this increase to be nonlinear, with the crimp period increasing as a function of square-root of the canal distance.

2C) Collagen bundles around the whole globe are crimped at baseline. Specifically, we test the hypotheses that there are significant differences in crimp between regions around the eye globe.

We demonstrated that collagen bundles across the whole eye globe are crimped at baseline. We showed that across 8 bilateral regions around the eye globe, there were collagen bundles that were crimped at 0 mmHg IOP. We also revealed interesting regional relationships between different parameters of collagen crimp and architecture. For example, we found that central corneal fiber bundles had significantly different crimp tortuosity, waviness, amplitude, and period than the peripheral corneal fiber bundles. This suggested that the peripheral cornea had different nonlinear biomechanical properties than the central cornea.

Specific Aim 3. Characterize how ocular collagen crimp changes with mechanical loading by testing the hypotheses that:

3A) ONH crimp changes with increased IOP. Specifically, we test the hypothesis that the rate of recruitment of the PPS collagen bundles is different than that of the LC beams.

We quantified the crimp waviness of the ONH collagen bundles and demonstrated these collagen bundles become less wavy with increasing IOP. Our study revealed that at every IOP, the LC collagen bundles were less wavy than PPS collagen bundles. We also established recruitment curves for the LC and PPS from the crimp waviness measurements. The LC collagen bundles were recruited differently than the PPS collagen bundles. At low IOPs, a higher percentage of PPS bundles were recruited than LC bundles. At physiologic IOP from 10-15 mmHg, the LC recruited more bundles than the PPS. At 15 mmHg, both LC and PPS had similar fractions (3/4) of collagen bundles recruited. This common fraction suggested a target fraction of recruited bundles needed for optimal biomechanical function.

3B) Equatorial scleral crimp changes with uniaxial stretch. Specifically, we test the hypothesis that rate of recruitment of equatorial sclera is independent of tissue depth.

We quantified the crimp waviness of equatorial sclera bundles and characterized how the crimp changed with stretch. We tracked the bundle-specific changes in crimp waviness with strain and demonstrated that the equatorial collagen bundle waviness decreased exponentially with strain. We also found that equatorial scleral bundles did not recruit differently depending on tissue depth, meaning superficial collagen bundles recruited similarly to those deeper in the tissue.

8.2 LIMITATIONS

Together with the strengths of this work, it is important to consider its limitations. First, is that the collagen analysis presented herein was done on sheep and goat eyes obtained from abattoirs. Eyes from these species share some similar anatomical features with human eyes, like a collagenous LC. Being bred for human consumption, these animals have a smaller genetic variability and are harvested at similar age ranges. This likely results in less inter-individual and contralateral variations compared to human donor tissue, especially in groups of animals sacrificed together. Sheep and goat eyes are more readily available than human eyes and its acquisition can be planned better. In addition, both sheep and goat are important as animal models for studying different eye diseases. Sheep has been used to study glaucoma (Gerometta et al., 2010; Kim, Johnston, Gupta, Moore, & Yücel, 2011) and cataracts (Morton et al., 2013). Goat has also been used to study cataracts, in particular as a training model for cataract surgeries (Dada & Sindhu, 2000; Sudan, Titiyal, Rai, & Chandra, 2002). However, it is possible that our findings on collagen architecture and crimp in these animal models may not translate directly to human eyes. We have begun

extending the methodology presented in this dissertation into donor eyes. In the first of these studies, we found that the regional patterns of crimp around the globe are similar between sheep and human eyes (Gogola et al., 2018). More studies using human eyes are needed to confirm if the rest of the collagen microstructural patterns we report for sheep and goat are similar to human.

Several of our experiments were done using PLM from cryosections of fixed tissues. It is possible that chemical fixation and sectioning introduced artifacts like shrinking or warping of the tissue which would affect the measurements of collagen fiber orientation and crimp. We have previously shown that formalin fixation does not change the collagen crimp (Jan et al., 2015) and that it has minimal effects on the overall tissue size and shape (Tran et al., 2017). However, studies using fresh, intact eyes would allow in-situ observations and analyses of the collagen architecture with changes in IOP.

Our PLM methods quantified the collagen fiber orientation and crimp of the eye in 2D, yet collagen bundles most often have out-of-plane components. We have been careful about adhering to anatomical planes when sectioning and to focus our analyses on in-plane collagen bundles, but it is possible that our crimp measurements were affected. For example, it is plausible that our measurements underestimated the crimp period, which would appear to be smaller if the collagen bundle is tilted relative to the plane of sectioning. Future studies should use advanced PLM methods that allow for full 3D analyses of collagen fiber orientation. A recent study describes mapping ocular collagen fiber orientation in 3D (B. Yang et al., 2018).

Collagen crimp is but one determinant of the nonlinear biomechanics of the eye. Strain-dependent fiber rotations and realignment, fiber slip, and matrix components like elastin and proteoglycan can also contribute to the macro-scale nonlinear biomechanics of the tissue (Birch et al., 2013; C Ross Ethier et al., 2004; Fazio et al., 2014; Fratzl, 2008; Holzapfel, 2001). For

example, it has been shown that in tissues such as bladder and heart valves that changes in meso-scale anisotropy from fiber rotations and realignment can occur with strain (Gilbert et al., 2008; Keyes, Borowicz, et al., 2011; Pant et al., 2018). However, these seem to be very small in ocular tissues, perhaps because of the relatively small strains to which they are subjected. For example, from our images of the ONH fixed at different IOPs, we did not see any large differences in meso-scale anisotropy. Also, inflation tests suggest low single digit sclera strains at physiologic pressures, an order of magnitude or more smaller than heat valves (Coudrillier et al., 2012a; Myers, Coudrillier, Boyce, & Nguyen, 2010). Future studies should investigate the role of these other factors in determining the macroscale nonlinear biomechanics of eye tissue.

8.3 FUTURE WORK

Our long-term goal was to identify biomechanical markers of individual-specific sensitivity to IOP. Future work can expand upon the groundwork laid out by this dissertation to accomplish this goal.

In this dissertation, we have shown the first experimental quantifications of collagen crimp for many parts of the eye. The crimp measurements provide valuable information about ocular biomechanics, specifically the microstructural mechanism underlying the nonlinear mechanical behavior of the eye. This information can be used to develop improved constitutive model formulations of ocular tissues. Because we found that there are significant regional differences in the crimp around the eye, including variable crimp properties between LC trabeculae beams, future models should incorporate region-specific crimp properties around the eye. Previously, models have not been able to be this detailed because such crimp quantifications did not exist. The

improved constitutive formulations, in turn, will help understand the effects of IOP, including what makes an eye sensitive to IOP.

In addition to providing crimp quantifications that can drive fiber-based constitutive models of the eye, we have also quantified many aspects of the crimp, including the collagen crimp period, tortuosity, waviness, and amplitude. Through the work of this dissertation, we found that different collagen fibers can have different combinations of each of these parameters. Biomechanical models have focused generally on one aspect of the crimp, the amount of slack in the fiber, because this determines how much a fiber can stretch before triggering the stiffening effect during recruitment. However, two fibers can have the same amount of slack but different shapes. For example, these two fibers could have different crimp periods, despite having the same amount of slack. Very little is reported about why and how these different combinations form in the eye and how these affect the overall biomechanics of the eye. Our measurements show that the crimp characteristics, while variable, are remarkably consistent across individuals. This suggests the existence of mechanisms that regulate these properties. Future studies should investigate the relationship between the shape of crimped fibers, the structural organization of the tissue, and ocular biomechanics. In addition, future studies could target the mechanisms that regulate these properties, opening the door for their control. These could, for example, allow the development of treatments through the modulation of sensitivity to IOP.

8.4 CONCLUSION

We have established that PLM is an appropriate and robust method of quantifying ocular collagen fiber orientation and used PLM to identify complex aspects of the ocular collagen architecture,

including previously unreported fibers that are oriented radially around the ONH. We have also applied PLM to provide the first experimental characterization of collagen crimp and recruitment in several regions of the eye. This dissertation provided a greater understanding of the relationship between crimp and ocular biomechanics than previously reported and laid out techniques and experimental groundwork for the development of more sophisticated fiber-based constitutive models of the eye. These studies have shed light on the collagen patterns that may be of importance to individual-specific sensitivity to IOP and susceptibility to glaucoma.

APPENDIX A

COMPARISON OF COLLAGEN FIBER ARCHITECTURE USING POLARIZED LIGHT MICROSCOPY AND POLARIZATION-SENSITIVE SECOND HARMONIC IMAGING

This content of this section was adapted from a presentation at the Annual Meeting for the Association for Research in Vision and Ophthalmology (Li JJ, et al IOVS 2015; 59; ARVO E-Abstract 6157).

A.1 EXPERIMENTAL SETUP

Thin coronal sections (20 micron) of the lamina cribrosa from sheep eyes were imaged in 3D using custom PLM and polarization-sensitive second harmonic optical microscopy (SHOM). microscopes. SHOM was done with an ultrafast Ti:Sapphire laser in conjunction with a pair of spatial light modulators to obtain linear, circular and radial incident polarizations (Figure 65) (Li, Valente, Castillo, & Vohnsen, 2014). The 40x SHOM objective with NA = 0.95 provided a transverse resolution of 0.30μm/pixel and 1μm/pixel axial resolution. PLM was done using polarization and retardation filters into a commercial optical microscope. The 10x PLM objective

with NA = 0.30 provided a pixel resolution of 0.73μm/pixel. The images were analyzed using custom code to determine pixel-level collagen fiber orientation. SHOM and PLM images of the same sections were overlaid and compared. Selected regions were scanned at high-resolution with SHOM to probe collagen fibril 3D structural details.

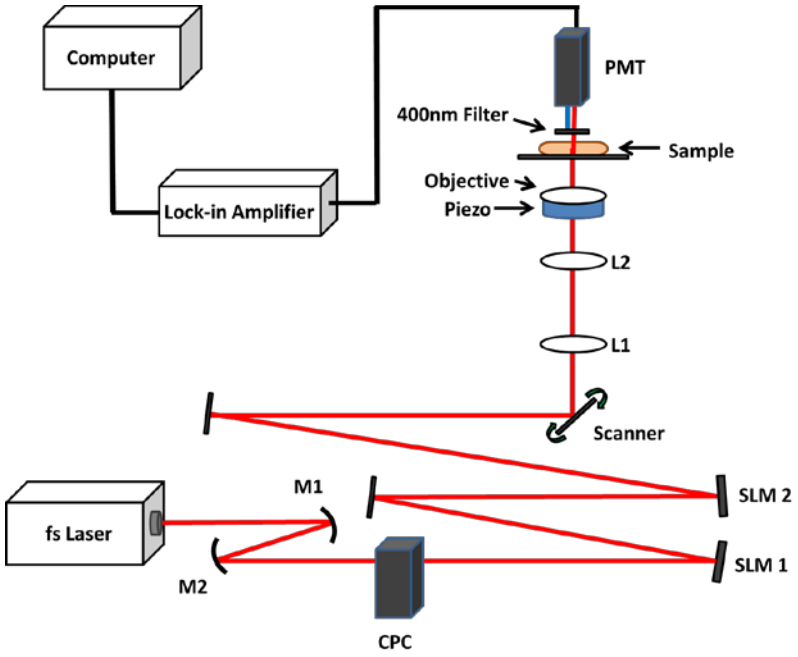

Figure 65. The microscope setup of the polarization-sensitive second harmonic optical microscope.

A.2 COMPARING PLM WITH SHOM

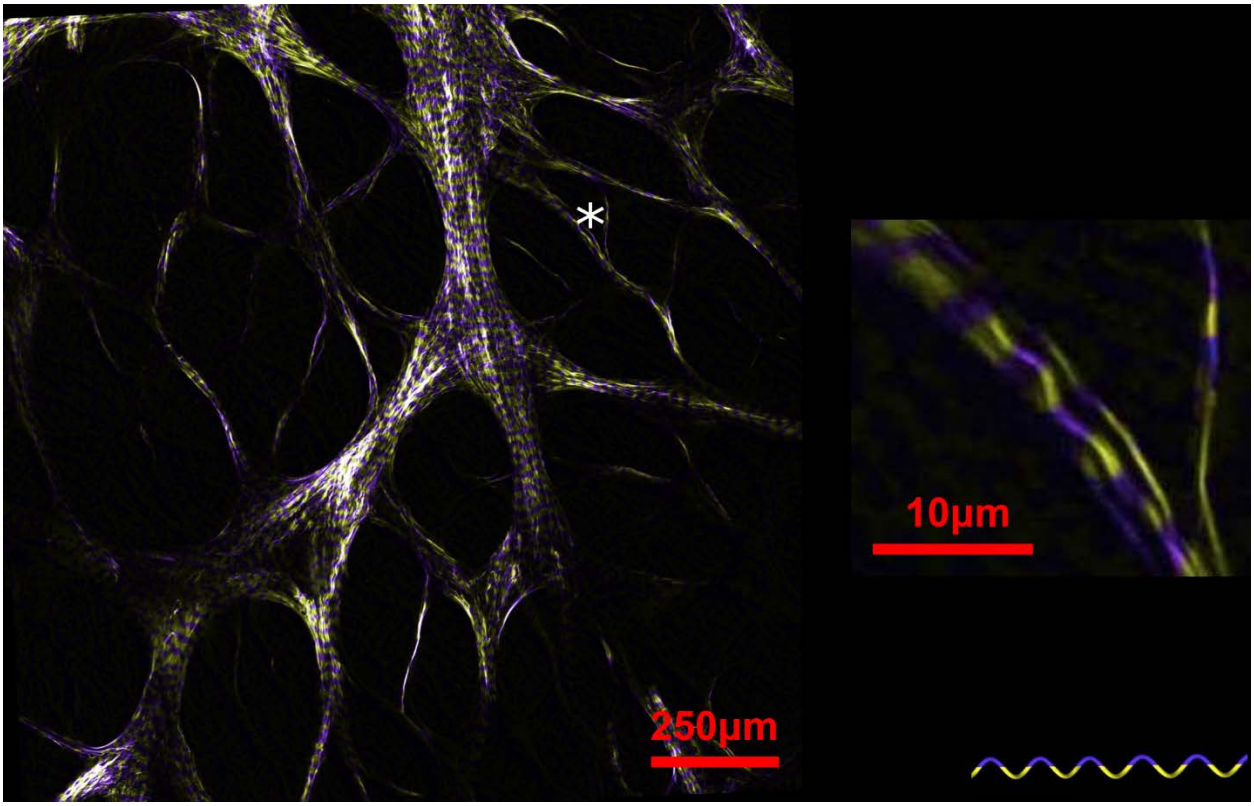

Figure 66. Overlaid combinations of PLM and SHOM images.

The pixels of the PLM images were colored yellow and purple according to the orientation of a pixel relative to its neighborhood. This helps visualize the collagen fiber crimp. The PLM images were then made translucent and overlaid with SHOM images. Note that each yellow or purple band in the PLM images corresponded with half the crimp period seen in SHOM images

The overlaid combination of the extended PLM and SHOM images revealed excellent correspondence between the two complementary approaches (Figure 66). The results revealed clear visualization of fibril crimp. SHOM allowed optical sectioning, providing high detail of the 3D structure, including intricately interwoven fibrils of the laminar beams. PLM was faster with

wider field-of-view, enabling visualization of dense peripapillary sclera architecture. The various polarization states of the SHOM illumination revealed differences in orthogonal directions highlighting the orientation of the collagen fibrils both in- and out-of-the plane.

A.3 CONCLUSIONS

The SHOM images highlight additional structural detail which is not apparent with PLM alone. PLM produced quick wide field-of-view images. The combination of the two techniques holds promise for improved mechanical understanding of the lamina cribrosa and the underlying biomechanical changes related to glaucoma which we are currently targeting in our research.

APPENDIX B

THE ROBUSTNESS OF THE RECRUITMENT CURVE TO CHANGES IN THE WAVINESS THRESHOLD IN THE PPS

The waviness threshold we chose for this study was the 90th percentile (6.7° for the PPS) of the waviness of collagen bundles at 50 mmHg IOP. Here we show the recruitment curves using 9 different waviness thresholds, varying from the 10th percentile through the 90th percentile of the waviness at 50 mmHg IOP (Figure 67). A higher threshold allows for wavier fibers to be considered recruited. Conversely, a lower threshold is more restrictive, expecting fibers to be closer to straight to be considered recruited. Consequently, a higher threshold resulted in higher fraction of fibers to be deemed recruited, and the opposite for a lower threshold. Interestingly, the overall shape of the recruitment curves changes little with variations in the threshold. The main change is on the convexity vs. concavity of effects at 10 mmHg. This demonstrates that the recruitment curve we present is robust to changes in waviness threshold.

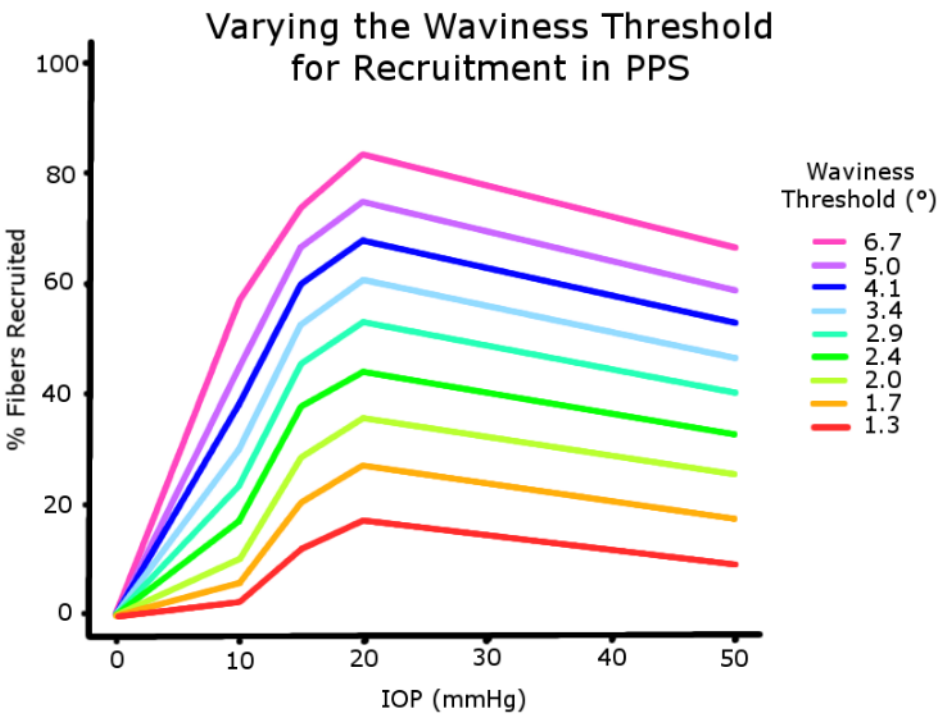

Figure 67. Recruitment curves constructed from different waviness thresholds.

BIBLIOGRAPHY

A Bouhenni, R., Dunmire, J., Sewell, A., & Edward, D. P. (2012). Animal models of glaucoma. *BioMed Research International, 2012*.

Abahussin, M., Hayes, S., Knox Cartwright, N. E., Kamma-Lorger, C. S., Khan, Y., Marshall, J., & Meek, K. M. (2009). 3D Collagen Orientation Study of the Human Cornea Using X-ray Diffraction and Femtosecond Laser Technology. *Investigative Ophthalmology & Visual Science, 50*(11), 5159-5164. doi:10.1167/iovs.09-3669

Aghamohammadzadeh, H., Newton, R. H., & Meek, K. M. (2004). X-ray scattering used to map the preferred collagen orientation in the human cornea and limbus. *Structure, 12*(2), 249-256.

Al-Redah, S. A. A. (2016). Ultrasonographic anatomy of the goat eye. *Journal of Veterinary Medical Science, 15*(1), 160-164.

Albon, J., Farrant, S., Akhtar, S., Young, R., Boulton, M. E., Smith, G., . . . Morgan, J. E. (2007). Connective tissue structure of the tree shrew optic nerve and associated ageing changes. *Investigative Ophthalmology & Visual Science, 48*(5), 2134-2144. doi:10.1167/iovs.06-0084

Albon, J., Karwatowski, W. S., Avery, N., Easty, D. L., & Duance, V. C. (1995). Changes in the collagenous matrix of the aging human lamina cribrosa. *British journal of ophthalmology, 79*(4), 368-375.

Andreo, R., & Farrell, R. (1982). Corneal small-angle light-scattering theory: wavy fibril models. *Journal of the Optical Society of America, 72*(11), 1479-1492.

Bader, A. N., Pena, A.-M., van Voskuilen, C. J., Palero, J. A., Leroy, F., Colonna, A., & Gerritsen, H. C. (2011). Fast nonlinear spectral microscopy of in vivo human skin. *Biomedical optics express, 2*(2), 365-373.

Bailey, A. J. (1987). Structure, function and ageing of the collagens of the eye: Nature Publishing Group.

Baumann, B., Rauscher, S., Glösmann, M., Götzinger, E., Pircher, M., Fialová, S., . . . Hitzenberger, C. K. (2014). Peripapillary Rat Sclera Investigated In Vivo With

Polarization-Sensitive Optical Coherence Tomography. *Investigative Ophthalmology & Visual Science, 55*(11), 7686-7696.

Becher, H., & Osterhage, K. (1933). Über die morphologischen und funktionellen Bezichungen zwischen kollagenen und elastischen Fasern in der Sklera des Rinderauges. *Anatomy and Embryology, 101*(2), 294-306.

Bell, J., Hayes, S., Whitford, C., Sanchez-Weatherby, J., Shebanova, O., Vergari, C., . . . Elsheikh, A. (2018). The hierarchical response of human corneal collagen to load. *Acta Biomaterialia, 65*, 216-225.

Bellezza, A. J., Hart, R. T., & Burgoyne, C. F. (2000). The optic nerve head as a biomechanical structure: initial finite element modeling. *Investigative Ophthalmology & Visual Science, 41*(10), 2991-3000.

Bengtsson, B., & Heijl, A. (2005). A long-term prospective study of risk factors for glaucomatous visual field loss in patients with ocular hypertension. *Journal of glaucoma, 14*(2), 135-138.

Birch, H. L., Thorpe, C. T., & Rumian, A. P. (2013). Specialisation of extracellular matrix for function in tendons and ligaments. *Muscles, Ligaments and Tendons Journal, 3*(1), 12-22. doi:10.11138/mltj/2013.3.1.012

Boorman, R. S., Norman, T., Matsen, F. A., & Clark, J. M. (2006). Using a freeze substitution fixation technique and histological crimp analysis for characterizing regions of strain in ligaments loaded In Situ. *jJournal of Orthopaedic Research, 24*(4), 793-799. doi:10.1002/jor.20081

Boote, C., Hayes, S., Newton, R. H., Puri, H., & Meek, K. M. A. (2003). Collagen fibrils appear more closely packed in the prepupilliary cornea: optical and biomechanical implications. *Investigative ophthalmology & visual science, 44*(7), 2941-2948.

Bromage, T. G., Goldman, H. M., McFarlin, S. C., Warshaw, J., Boyde, A., & Riggs, C. M. (2003). Circularly polarized light standards for investigations of collagen fiber orientation in bone. *The Anatomical Record, 274*(1), 157-168.

Brooks, D. E., Arellano, E., Kubilis, P. S., & Komaromy, A. M. (1998). Histomorphometry of the porcine scleral lamina cribrosa surface. *Veterinary Ophthalmology, 1*(2-3), 129-135.

Brown, D. J., Morishige, N., Neekhra, A., Minckler, D. S., & Jester, J. V. (2007). Application of second harmonic imaging microscopy to assess structural changes in optic nerve head structure ex vivo. *Journal of biomedical optics, 12*(2), 024029.

Burgoyne, C. F. (2011). A biomechanical paradigm for axonal insult within the optic nerve head in aging and glaucoma. *Experimental Eye Research, 93*(2), 120-132. doi:10.1016/j.exer.2010.09.005

Burgoyne, C. F., Crawford Downs, J., Bellezza, A. J., Francis Suh, J. K., & Hart, R. T. (2005). The optic nerve head as a biomechanical structure: a new paradigm for understanding the

role of IOP-related stress and strain in the pathophysiology of glaucomatous optic nerve head damage. *Progress in Retinal and Eye Research, 24*(1), 39-73. doi:http://dx.doi.org/10.1016/j.preteyeres.2004.06.001

Campbell, I. C., Coudrillier, B., & Ethier, C. R. (2014). Biomechanics of the posterior eye: a critical role in health and disease. *Journal of biomechanical engineering, 136*(2), 021005.

Candia, O. A., Gerometta, R. M., & Danias, J. (2014). Tissue plasminogen activator reduces the elevated intraocular pressure induced by prednisolone in sheep. *Experimental eye research, 128*, 114-116. doi:10.1016/j.exer.2014.10.004

Casson, R. J., Chidlow, G., Wood, J. P., Crowston, J. G., & Goldberg, I. (2012). Definition of glaucoma: clinical and experimental concepts. *Clinical & experimental ophthalmology, 40*(4), 341-349.

Chen, Y., Wu, W., Zhang, X., Fan, W., & Shen, L. (2011). Feasibility study on retinal vascular bypass surgery in isolated arterially perfused caprine eye model. *Eye, 25*(11), 1499.

Coudrillier, B., Abel, R. L., Albon, J., Campbell, I. C., & Ethier, C. R. (2014). Micro-computed Tomography (μCT) for the Structural Analysis of the Lamina Cribrosa (LC). *Investigative ophthalmology & visual science, 55*(13), 4253-4253.

Coudrillier, B., Boote, C., Quigley, H. A., & Nguyen, T. D. (2013). Scleral anisotropy and its effects on the mechanical response of the optic nerve head. *Biomechanics and modeling in mechanobiology, 12*(5), 941-963. doi:10.1007/s10237-012-0455-y

Coudrillier, B., Geraldes, D. M., Vo, N. T., Atwood, R., Reinhard, C., Campbell, I. C., . . . Ethier, C. R. (2016). Phase-contrast micro-computed tomography measurements of the intraocular pressure-induced deformation of the porcine lamina cribrosa. *IEEE Transactions on Medical Imaging, 35*(4), 988-999.

Coudrillier, B., Pijanka, J., Jefferys, J., Sorensen, T., Quigley, H. A., Boote, C., & Nguyen, T. D. (2015). Collagen structure and mechanical properties of the human sclera: analysis for the effects of age. *Journal of biomechanical engineering, 137*(4), 041006.

Coudrillier, B., Tian, J., Alexander, S., Myers, K. M., Quigley, H. A., & Nguyen, T. D. (2012a). Biomechanics of the Human Posterior Sclera: Age- and Glaucoma-Related Changes Measured Using Inflation Testing. *Investigative Ophthalmology & Visual Science, 53*(4), 1714-1728. doi:10.1167/iovs.11-8009

Curtin, B. J. (1969). Physiopathologic aspects of scleral stress-strain. *Transactions of the American Ophthalmological Society, 67*, 417.

Dada, V. K., & Sindhu, N. (2000). Cataract in enucleated goat eyes: training model for phacoemulsification. *Journal of Cataract & Refractive Surgery, 26*(8), 1114-1116.

Diamant, J., Keller, A., Baer, E., Litt, M., & Arridge, R. G. C. (1972). Collagen; ultrastructure and its relation to mechanical properties as a function of ageing. *Proceedings of the Royal Society of London B: Biological Sciences, 180*(1060), 293-315.

Downs, J. C., Yang, H., Girkin, C., Sakata, L., Bellezza, A., Thompson, H., & Burgoyne, C. F. (2007). Three-dimensional histomorphometry of the normal and early glaucomatous monkey optic nerve head: neural canal and subarachnoid space architecture. *Investigative Ophthalmology & Visual Science, 48*(7), 3195-3208.

El-Maghraby, H. M., Nyland, T. G., & Bellhorn, R. W. (1995). Ultrasonographic and biometric evaluation of sheep and cattle eyes. *Veterinary Radiology & Ultrasound, 36*(2), 148-151.

Elkington, A. R., Inman, C. B., Steart, P. V., & Weller, R. O. (1990). The structure of the lamina cribrosa of the human eye: an immunocytochemical and electron microscopical study. *Eye, 4*(1), 42-57.

Ethier, C. R., Johnson, M., & Ruberti, J. (2004). Ocular biomechanics and biotransport. *Annual Review of Biomedical Engineering, 6*, 249-273. doi:10.1146/annurev.bioeng.6.040803.140055

Ethier, C. R., & Simmons, C. A. (2007). *Introductory biomechanics: from cells to organisms*: Cambridge University Press.

Faridi, O. S., Park, S. C., Kabadi, R., Su, D., De Moraes, C. G., Liebmann, J. M., & Ritch, R. (2014). Effect of Focal Lamina Cribrosa Defect on Glaucomatous Visual Field Progression. *Ophthalmology, 121*(8), 1524-1530. doi:http://dx.doi.org/10.1016/j.ophtha.2014.02.017

Fata, B., Carruthers, C. A., Gibson, G., Watkins, S. C., Gottlieb, D., Mayer, J. E., & Sacks, M. S. (2013). Regional Structural and Biomechanical Alterations of the Ovine Main Pulmonary Artery During Postnatal Growth. *Journal of biomechanical engineering, 135*(2), 0210221-02102211. doi:10.1115/1.4023389

Fata, B., Zhang, W., Amini, R., & Sacks, M. S. (2014). Insights Into Regional Adaptations in the Growing Pulmonary Artery Using a Meso-Scale Structural Model: Effects of Ascending Aorta Impingement. *Journal of biomechanical engineering, 136*(2), 0210091-02100913. doi:10.1115/1.4026457

Fazio, M. A., Grytz, R., Morris, J. S., Bruno, L., Gardiner, S. K., Girkin, C. A., & Downs, J. C. (2014). Age-related changes in human peripapillary scleral strain. *Biomechanics and modeling in mechanobiology, 13*(3), 551-563.

Filas, B. A., Shah, N. S., Zhang, Q., Shui, Y. B., Lake, S. P., & Beebe, D. C. (2014). Quantitative imaging of enzymatic vitreolysis-induced fiber remodeling. *Invest Ophthalmol Vis Sci, 55*(12), 8626-8637. doi:10.1167/iovs.14-15225

Fischer, E. (1933). Die konstruktive Anordnung der kollagenen Fasern in der Sklera und den Sehnervenscheiden des Rinderauges. *Zeitschrift für Anatomie und Entwicklungsgeschichte, 101*(2), 168-210.

Franchi, M., Fini, M., Quaranta, M., De Pasquale, V., Raspanti, M., Giavaresi, G., . . . Ruggeri, A. (2007). Crimp morphology in relaxed and stretched rat Achilles tendon. *Journal of Anatomy, 210*(1), 1-7. doi:10.1111/j.1469-7580.2006.00666.x

Franchi, M., Raspanti, M., Dell'Orbo, C., Quaranta, M., De Pasquale, V., Ottani, V., & Ruggeri, A. (2008). Different crimp patterns in collagen fibrils relate to the subfibrillar arrangement. *Connective Tissue Research, 49*(2), 85-91.

Fratzl, P. (2008). *Collagen: structure and mechanics*. New York City, NY: Springer Science & Business Media.

Freed, A. D., & Doehring, T. C. (2005). Elastic Model for Crimped Collagen Fibrils. *Journal of biomechanical engineering, 127*(4), 587-593. doi:10.1115/1.1934145

Gałecki, A., & Burzykowski, T. (2013). Linear mixed-effects model *Linear Mixed-Effects Models Using R* (pp. 245-273): Springer.

Gallagher, B., & Maurice, D. (1977). Striations of light scattering in the corneal stroma. *Journal of ultrastructure research, 61*(1), 100-114.

Gathercole, L. J., & Keller, A. (1991). Crimp morphology in the fibre-forming collagens. *Matrix, 11*(3), 214-234.

Gerometta, R., Spiga, M.-G., Borrás, T., & Candia, O. A. (2010). Treatment of sheep steroid–induced ocular hypertension with a glucocorticoid-inducible MMP1 gene therapy virus. *Investigative Ophthalmology & Visual Science, 51*(6), 3042-3048.

Ghaffari, M. S., Shojaei, M., Sabzevari, A., & Khorami, N. (2011). Reference values for intraocular pressure and Schirmer tear test in clinically normal Sanjabi sheep. *Small Ruminant Research, 97*(1–3), 101-103. doi:http://dx.doi.org/10.1016/j.smallrumres.2010.12.008

Gilbert, T. W., Wognum, S., Joyce, E. M., Freytes, D. O., Sacks, M. S., & Badylak, S. F. (2008). Collagen fiber alignment and biaxial mechanical behavior of porcine urinary bladder derived extracellular matrix. *Biomaterials, 29*(36), 4775-4782. doi:https://doi.org/10.1016/j.biomaterials.2008.08.022

Girard, M. J., Dahlmann-Noor, A., Rayapureddi, S., Bechara, J. A., Bertin, B. M. E., Jones, H., . . . Ethier, C. R. (2011). Quantitative Mapping of Scleral Fiber Orientation in Normal Rat Eyes. *Investigative Ophthalmology & Visual Science, 52*(13), 9684-9693. doi:10.1167/iovs.11-7894

Girard, M. J., Downs, J. C., Bottlang, M., Burgoyne, C. F., & Suh, J.-K. F. (2009). Peripapillary and posterior scleral mechanics—part II: experimental and inverse finite element characterization. *Journal of biomechanical engineering, 131*(5), 051012.

Girard, M. J., Dupps, W. J., Baskaran, M., Scarcelli, G., Yun, S. H., Quigley, H. A., . . . Strouthidis, N. G. (2014). Translating Ocular Biomechanics into Clinical Practice: Current State and Future Prospects. *Current eye research, 40*(1), 1-18. doi:10.3109/02713683.2014.914543

Gogola, A., Jan, N.-J., Brazile, B. L., Lam, P., Lathrop, K. L., Chan, K. C., & Sigal, I. A. (2018). Spatial patterns and age-related changes of the collagen crimp in the human cornea and sclera. *Investigative Ophthalmology & Visual Science, In Press*.

Gordon, M. O., Beiser, J. A., Brandt, J. D., Heuer, D. K., Higginbotham, E. J., Johnson, C. A., . . . Wilson, M. R. (2002). The Ocular Hypertension Treatment Study: baseline factors that predict the onset of primary open-angle glaucoma. *Archives of Ophthalmology, 120*(6), 714-720.

Grytz, R., Fazio, M. A., Libertiaux, V., Bruno, L., Gardiner, S., Girkin, C. A., & Downs, J. C. (2014). Age- and Race-Related Differences in Human Scleral Material Properties. *Investigative Ophthalmology & Visual Science, 55*(12), 8163-8172. doi:10.1167/iovs.14-14029

Grytz, R., & Meschke, G. (2009). Constitutive modeling of crimped collagen fibrils in soft tissues. *Journal of the Mechanical Behavior of Biomedical Materials, 2*(5), 522-533.

Grytz, R., & Meschke, G. (2010). A computational remodeling approach to predict the physiological architecture of the collagen fibril network in corneo-scleral shells. *Biomechanics and modeling in mechanobiology, 9*(2), 225-235.

Grytz, R., Meschke, G., & Jonas, J. B. (2011). The collagen fibril architecture in the lamina cribrosa and peripapillary sclera predicted by a computational remodeling approach. *Biomechanics and modeling in mechanobiology, 10*(3), 371-382.

Guedes, G., C Tsai, J., & A Loewen, N. (2011). Glaucoma and aging. *Current aging science, 4*(2), 110-117.

Hamrah, P., Huq, S. O., Liu, Y., Zhang, Q., & Dana, M. R. (2003). Corneal immunity is mediated by heterogeneous population of antigen-presenting cells. *Journal of Leukocyte Biology, 74*(2), 172-178.

Han, M., Giese, G., & Bille, J. F. (2005). Second harmonic generation imaging of collagen fibrils in cornea and sclera. *Optics express, 13*(15), 5791-5797.

Handsfield, G. G., Slane, L. C., & Screen, H. R. (2016). Nomenclature of the tendon hierarchy: an overview of inconsistent terminology and a proposed size-based naming scheme with terminology for multi-muscle tendons. *Journal of Biomechanics, 49*(13), 3122-3124.

Hansen, K. A., Weiss, J. A., & Barton, J. K. (2001). Recruitment of Tendon Crimp With Applied Tensile Strain. *Journal of biomechanical engineering, 124*(1), 72-77. doi:10.1115/1.1427698

Hayreh, S. S. (1969). Blood supply of the optic nerve head and its role in optic atrophy, glaucoma, and oedema of the optic disc. *The British Journal of Ophthalmology, 53*(11), 721.

Heermann, D. W. (1986). Deterministic Methods *Computer Simulation Methods in Theoretical Physics* (pp. 13-55): Springer.

Helmchen, F., & Denk, W. (2005). Deep tissue two-photon microscopy. *Nature methods, 2*(12), 932-940.

Hernandez, M. R., Andrzejewska, W. M., & Neufeld, A. H. (1990). Changes in the extracellular matrix of the human optic nerve head in primary open-angle glaucoma. *American Journal of Ophthalmology, 109*(2), 180-188.

Hernandez, M. R., Luo, X. X., Andrzejewska, W., & Neufeld, A. H. (1989). Age-related changes in the extracellular matrix of the human optic nerve head. *American Journal of Ophthalmology, 107*(5), 476-484.

Hernandez, M. R., Luo, X. X., Igoe, F., & Neufeld, A. H. (1987). Extracellular matrix of the human lamina cribrosa. *American Journal of Ophthalmology, 104*(6), 567-576.

Hill, M. R., Duan, X., Gibson, G. A., Watkins, S., & Robertson, A. M. (2012). A theoretical and non-destructive experimental approach for direct inclusion of measured collagen orientation and recruitment into mechanical models of the artery wall. *Journal of Biomechanics, 45*(5), 762-771. doi:http://dx.doi.org/10.1016/j.jbiomech.2011.11.016

Ho, L. C., Sigal, I. A., Jan, N.-J., Jin, T., Wu, E. X., Kim, S.-G., . . . Chan, K. C. (2015). *Microstructural organization and macromolecular contents in fibrous tissues of normal and hypertensive eyes with diffusion tensor imaging and magnetization transfer imaging.* Paper presented at the ISMRM 23rd Annual Meeting & Exhibition cum SMRT 24th Annual Meeting Proceedings.

Ho, L. C., Sigal, I. A., Jan, N.-J., Squires, A., Tse, Z., Wu, E. X., . . . Chan, K. C. (2014). Magic Angle–Enhanced MRI of Fibrous Microstructures in Sclera and Cornea With and Without Intraocular Pressure Loading. *Investigative Ophthalmology & Visual Science, 55*(9), 5662-5672.

Ho, L. C., Sigal, I. A., Jan, N.-J., Yang, X., van der Merwe, Y., Yu, Y., . . . Jin, T. (2016). Non-invasive MRI Assessments of Tissue Microstructures and Macromolecules in the Eye upon Biomechanical or Biochemical Modulation. *Scientific Reports, 6*, 32080.

Holzapfel, G. A. (2001). *Handbook of Materials Behavior Models* (Vol. 3). San Diego, CA: Academic Press.

Holzapfel, G. A., & Ogden, R. W. (2006). *Mechanics of biological tissue*: Springer Science & Business Media.

Huang, W., Fan, Q., Wang, W., Zhou, M., Laties, A. M., & Zhang, X. (2013). Collagen: a potential factor involved in the pathogenesis of glaucoma. *Medical science monitor basic research, 19*, 237.

Ischreyt, G. (1898). Zur Mechanik der Sklera. *Graefe's Archive for Clinical and Experimental Ophthalmology, 46*(3), 677-705.

Ivers, K. M., Li, C., Patel, N., Sredar, N., Luo, X., Queener, H., . . . Porter, J. (2011). Reproducibility of measuring lamina cribrosa pore geometry in human and nonhuman primates with in vivo adaptive optics imaging. *Investigative Ophthalmology & Visual Science, 52*(8), 5473-5480. doi:10.1167/iovs.11-7347

Jacques, S. L., Ramella-Roman, J. C., & Lee, K. (2002). Imaging skin pathology with polarized light. *Journal of biomedical optics, 7*(3), 329-341.

Jammalamadaka, S. R., & Sengupta, A. (2001). *Topics in circular statistics* (Vol. 5): World Scientific Publishing Co.

Jan, N.-J., Brazile, B. L., Hu, D., Grube, G., Wallace, J., Gogola, A., & Sigal, I. A. (2018). Crimp around the globe; patterns of collagen crimp across the corneoscleral shell. *Experimental eye research*.

Jan, N.-J., Gomez, C., Moed, S., Voorhees, A. P., Schuman, J. S., Bilonick, R. A., & Sigal, I. A. (2017). Microstructural Crimp of the Lamina Cribrosa and Peripapillary Sclera Collagen Fibers. *Investigative Ophthalmology & Visual Science, 58*(9), 3378-3388.

Jan, N.-J., Grimm, J. L., Tran, H., Lathrop, K. L., Wollstein, G., Bilonick, R. A., . . . Sigal, I. A. (2015). Polarization microscopy for characterizing fiber orientation of ocular tissues. *Biomedical optics express, 6*(12), 4705-4718. doi:10.1364/BOE.6.004705

Jan, N.-J., Iasella, M., Lester, M., Hu, D., Lathrop, K. L., Voorhees, A. P., . . . Sigal, I. A. (2016). Novel method reveals heterogeneous micro-scale response of sclera collagen bundles to homogeneous macro-scale stretch. *Investigative Ophthalmology & Visual Science, 57*(12), 3566-3566.

Jan, N.-J., Lathrop, K., & Sigal, I. A. (2017). Collagen Architecture of the Posterior Pole: High-Resolution Wide Field of View Visualization and Analysis Using Polarized Light Microscopy. *Investigative Ophthalmology & Visual Science, 58*(2), 735-744. doi:10.1167/iovs.16-20772

Jan, N.-J., & Sigal, I. A. (2018). Collagen fiber recruitment: a microstructural basis for the nonlinear response of the posterior pole of the eye to increases in intraocular pressure. *Acta Biomaterialia*.

Jonas, J. B., Königsreuther, K. A., & Naumann, G. O. H. (1992). Optic disc histomorphometry in normal eyes and eyes with secondary angle-closure glaucoma. *Graefe's archive for clinical and experimental ophthalmology, 230*(2), 134-139.

Jones, H. J., Girard, M. J., White, N., Fautsch, M. P., Morgan, J. E., Ethier, C. R., & Albon, J. (2015). Quantitative analysis of three-dimensional fibrillar collagen microstructure within the normal, aged and glaucomatous human optic nerve head. *J R Soc Interface, 12*(106). doi:10.1098/rsif.2015.0066

Joyce, E. M., Liao, J., Schoen, F. J., Mayer Jr, J. E., & Sacks, M. S. (2009). Functional Collagen Fiber Architecture of the Pulmonary Heart Valve Cusp. *Annals of Thoracic Surgery, 87*(4), 1240-1249. doi:http://dx.doi.org/10.1016/j.athoracsur.2008.12.049

Kalwani, N. M., Ong, C. A., Lysaght, A. C., Haward, S. J., McKinley, G. H., & Stankovic, K. M. (2013). Quantitative polarized light microscopy of unstained mammalian cochlear sections. *Journal of biomedical optics, 18*(2), 026021-026021.

Kamma-Lorger, C. S., Boote, C., Hayes, S., Moger, J., Burghammer, M., Knupp, C., . . . White, N. (2010). Collagen and mature elastic fibre organisation as a function of depth in the human cornea and limbus. *Journal of Structural Biology, 169*(3), 424-430.

Keikhosravi, A., Liu, Y., Drifka, C., Woo, K. M., Verma, A., Oldenbourg, R., & Eliceiri, K. W. (2017). Quantification of collagen organization in histopathology samples using liquid crystal based polarization microscopy. *Biomedical optics express, 8*(9), 4243-4256.

Keyes, J. T., Borowicz, S. M., Rader, J. H., Utzinger, U., Azhar, M., & Vande Geest, J. P. (2011). Design and Demonstration of a Microbiaxial Optomechanical Device for Multiscale Characterization of Soft Biological Tissues with Two-Photon Microscopy. *Microscopy and microanalysis : the official journal of Microscopy Society of America, Microbeam Analysis Society, Microscopical Society of Canada, 17*(2), 167-175. doi:10.1017/S1431927610094341

Keyes, J. T., Yan, D., Rader, J. H., Utzinger, U., & Vande Geest, J. P. (2011). A Gimbal-Mounted Pressurization Chamber for Macroscopic and Microscopic Assessment of Ocular Tissues. *Journal of biomechanical engineering, 133*(9), 95001-NaN. doi:10.1115/1.4004921

Kim, M., Johnston, M. G., Gupta, N., Moore, S., & Yücel, Y. H. (2011). A model to measure lymphatic drainage from the eye. *Experimental eye research, 93*(5), 586-591.

Komatsu, K., Mosekilde, L., Viidik, A., & Chiba, M. (2002). Polarized light microscopic analyses of collagen fibers in the rat incisor periodontal ligament in relation to areas, regions, and ages. *Anatomical Record, 268*(4), 381-387. doi:10.1002/ar.10179

Lee, E. J., Kim, T.-W., Kim, M., Girard, M. J., Mari, J. M., & Weinreb, R. N. (2014). Recent Structural Alteration of the Peripheral Lamina Cribrosa Near the Location of Disc Hemorrhage in Glaucoma. *Investigative Ophthalmology & Visual Science, 55*(4), 2805-2815.

Li, J., Valente, D., Castillo, S., & Vohnsen, B. (2014). Polarization Controlled Second-Harmonic Microscopy For Cornea Collagen-I Fibril Imaging. *Investigative Ophthalmology & Visual Science, 55*(13), 2474-2474.

Liu, X., Wang, L., Ji, J., Yao, W., Wei, W., Fan, J., . . . Fan, Y. (2014). A Mechanical Model of the Cornea Considering the Crimping Morphology of Collagen Fibrils. *Investigative Ophthalmology & Visual Science, 55*(4), 2739-2746.

Lowe, D. G. (2004). Distinctive image features from scale-invariant keypoints. *International journal of computer vision, 60*(2), 91-110.

Malik, R., Swanson, W. H., & Garway-Heath, D. F. (2012). 'Structure–function relationship'in glaucoma: past thinking and current concepts. *Clinical & experimental ophthalmology, 40*(4), 369-380.

Martola, E.-L., & Baum, J. L. (1968). Central and peripheral corneal thickness: a clinical study. *Archives of Ophthalmology, 79*(1), 28-30.

Mattheck, C. (1998). *Design in Nature: Learning from Trees* (1 ed.). Berlin Heidelberg: Springer-Verlag Berlin Heidelberg.

Meek, K. M., & Boote, C. (2004). The organization of collagen in the corneal stroma. *Experimental eye research, 78*(3), 503-512.

Meek, K. M., & Boote, C. (2009). The use of X-ray scattering techniques to quantify the orientation and distribution of collagen in the corneal stroma. *Progress in retinal and eye research, 28*(5), 369-392.

Meek, K. M., & Fullwood, N. J. (2001). Corneal and scleral collagens—a microscopist's perspective. *Micron, 32*(3), 261-272.

Mega, Y., Robitaille, M., Zareian, R., McLean, J., Ruberti, J., & DiMarzio, C. (2012). Quantification of lamellar orientation in corneal collagen using second harmonic generation images. *Optics Letters, 37*(16), 3312-3314.

Midgett, D. E., Pease, M. E., Jefferys, J. L., Patel, M., Franck, C., Quigley, H. A., & Nguyen, T. D. (2017). The pressure-induced deformation response of the human lamina cribrosa: Analysis of regional variations. *Acta Biomaterialia, 53*, 123-139. doi:10.1016/j.actbio.2016.12.054

Midgett, D. E., Quigley, H. A., Pease, M. E., Franck, C., Toyjanova, J., & Nguyen, T. D. (2016). Inflation test of the human optic nerve head using digital volume correlation. In S. A. Tekalur, P. Zavattieri, & C. S. Korach (Eds.), *Mechanics of Biological Systems and Materials, Volume 6* (pp. 7-15). Orlanda, FL: Springer.

Misson, G. P. (2007). Circular polarization biomicroscopy: a method for determining human corneal stromal lamellar organization in vivo. *Ophthalmic and Physiological Optics, 27*(3), 256-264.

Morishige, N., Wahlert, A. J., Kenney, M. C., Brown, D. J., Kawamoto, K., Chikama, T.-i., . . . Jester, J. V. (2007). Second-harmonic imaging microscopy of normal human and keratoconus cornea. *Investigative ophthalmology & visual science, 48*(3), 1087.

Morrison, J. C., Jerdan, J. A., Dorman, M. E., & Quigley, H. A. (1989). Structural proteins of the neonatal and adult lamina cribrosa. *Arch Ophthalmol, 107*(8), 1220-1224.

Morrison, J. C., L'Hernault, N. L., Jerdan, J. A., & Quigley, H. A. (1989). Ultrastructural location of extracellular matrix components in the optic nerve head. *Arch Ophthalmol, 107*(1), 123-129.

Morton, J. D., Lee, H. Y., McDermott, J. D., Robertson, L. J., Bickerstaffe, R., Jones, M. A., . . . Abell, A. D. (2013). A macrocyclic calpain inhibitor slows the development of inherited cortical cataracts in a sheep model. *Investigative Ophthalmology & Visual Science, 54*(1), 389-395.

Mountain, K. M., Bjarnason, T. A., Dunn, J. F., & Matyas, J. R. (2011). The functional microstructure of tendon collagen revealed by high-field MRI. *Magnetic Resonance in Medicine, 66*(2), 520-527. doi:10.1002/mrm.23036

Myers, K. M., Coudrillier, B., Boyce, B. L., & Nguyen, T. D. (2010). The inflation response of the posterior bovine sclera. *Acta Biomaterialia, 6*(11), 4327-4335. doi:https://doi.org/10.1016/j.actbio.2010.06.007

Nadler, Z., Wang, B., Schuman, J. S., Ferguson, R. D., Patel, A., Hammer, D. X., . . . Wollstein, G. (2014). In vivo three-dimensional characterization of the healthy human lamina cribrosa with adaptive optics spectral-domain optical coherence tomography. *Invest Ophthalmol Vis Sci, 55*(10), 6459-6466. doi:10.1167/iovs.14-15177

Nadler, Z., Wang, B., Wollstein, G., Nevins, J. E., Ishikawa, H., Kagemann, L., . . . Schuman, J. S. (2013). Automated lamina cribrosa microstructural segmentation in optical coherence tomography scans of healthy and glaucomatous eyes. *Biomedical Optics Express, 4*(11), 2596-2608. doi:10.1364/boe.4.002596

Nemesure B, W. S., Hennis A, Leske M. (2003). Factors related to the 4-year risk of high intraoculat pressure - The Barbados Eye Studies. *Arch Ophthalmol, 121*(6), 856-862.

Neu, C. P., & Genin, G. M. (2014). *Handbook of Imaging in Biological Mechanics*: CRC Press.

Newton, R. H., Brown, J. Y., & Meek, K. (1996). *Polarized light microscopy technique for quantitatively mapping collagen fibril orientation in cornea.* Paper presented at the BiOS Europe'96.

Niklas, K. J. (1992). *Plant biomechanics: an engineering approach to plant form and function*. Chicago and London: University of Chicago Press.

Nordin, M., & Frankel, V. H. (2001). *Basic Biomechanics of the Musculoskeletal System* (H. A. Rybacki & D. Leger Eds.). Baltimore, MD: Lippincott Williams & Wilkins.

Norman, R. E., Flanagan, J. G., Rausch, S. M., Sigal, I. A., Tertinegg, I., Eilaghi, A., . . . Ethier, C. R. (2010). Dimensions of the human sclera: thickness measurement and regional changes with axial length. *Experimental eye research, 90*(2), 277-284.

Norman, R. E., Flanagan, J. G., Sigal, I. A., Rausch, S. M., Tertinegg, I., & Ethier, C. R. (2011). Finite element modeling of the human sclera: influence on optic nerve head biomechanics and connections with glaucoma. *Experimental eye research, 93*(1), 4-12.

Omens, J. H., Miller, T. R., & Covell, J. W. (1997). Relationship between passive tissue strain and collagen uncoiling during healing of infarcted myocardium. *Cardiovascular Research, 33*(2), 351-358. doi:10.1016/S0008-6363(96)00206-4

Ostrin, L. A., & Wildsoet, C. F. (2016). Optic nerve head and intraocular pressure in the guinea pig eye. *Experimental eye research, 146*, 7-16.

Ottani, V., Raspanti, M., & Ruggeri, A. (2001). Collagen structure and functional implications. *Micron, 32*(3), 251-260.

Pant, A. D., Thomas, V. S., Black, A. L., Verba, T., Lesicko, J. G., & Amini, R. (2018). Pressure-induced microstructural changes in porcine tricuspid valve leaflets. *Acta Biomaterialia, 67*, 248-258. doi:https://doi.org/10.1016/j.actbio.2017.11.040

Pierlot, C. M., Lee, J. M., Amini, R., Sacks, M. S., & Wells, S. M. (2014). Pregnancy-induced remodeling of collagen architecture and content in the mitral valve. *Annals of Biomedical Engineering, 42*(10), 2058-2071.

Pijanka, J. K., Abass, A., Sorensen, T., Elsheikh, A., & Boote, C. (2013). A wide-angle X-ray fibre diffraction method for quantifying collagen orientation across large tissue areas: application to the human eyeball coat. *Journal of Applied Crystallography, 46*(5), 1481-1489.

Pijanka, J. K., Coudrillier, B., Ziegler, K., Sorensen, T., Meek, K. M., Nguyen, T. D., . . . Boote, C. (2012). Quantitative mapping of collagen fiber orientation in non-glaucoma and glaucoma posterior human sclerae. *Investigative Ophthalmology & Visual Science, 53*(9), 5258-5270.

Pijanka, J. K., Spang, M. T., Sorensen, T., Liu, J., Nguyen, T. D., Quigley, H. A., & Boote, C. (2015). Depth-Dependent Changes in Collagen Organization in the Human Peripapillary Sclera. *PloS one, 10*(2), e0118648.

Preibisch, S., Saalfeld, S., & Tomancak, P. (2009). Globally optimal stitching of tiled 3D microscopic image acquisitions. *Bioinformatics, 25*(11), 1463-1465.

Pruett, R. C. (1988). Progressive myopia and intraocular pressure: what is the linkage?: A literature review. *Acta Ophthalmologica, 66*(S185), 117-127. doi:10.1111/j.1755-3768.1988.tb02685.x

Püspöki, Z., Storath, M., Sage, D., & Unser, M. (2016b). Transforms and Operators for Directional Bioimage Analysis: A Survey *Focus on Bio-Image Informatics* (Vol. 219, pp. 69-93). Switzerland: Springer International Publishing.

Quantock, A. J., Winkler, M., Parfitt, G. J., Young, R. D., Brown, D. J., Boote, C., & Jester, J. V. (2015). From nano to macro: studying the hierarchical structure of the corneal extracellular matrix. *Experimental eye research, 133*, 81-99.

Quigley, H. A. (2005). Glaucoma: macrocosm to microcosm the Friedenwald lecture. *Investigative Ophthalmology & Visual Science, 46*(8), 2663-2670.

Quigley, H. A. (2011). Glaucoma. *The Lancet, 377*(9774), 1367-1377.

Quigley, H. A., & Addicks, E. M. (1981). Regional differences in the structure of the lamina cribrosa and their relation to glaucomatous optic nerve damage. *Archives of Ophthalmology, 99*(1), 137-143.

Quigley, H. A., Dorman-Pease, M. E., & Brown, A. E. (1991). Quantitative study of collagen and elastin of the optic nerve head and sclera in human and experimental monkey glaucoma. *Current eye research, 10*(9), 877-888. doi:10.3109/02713689109013884

Quigley, H. A., Hohman, R. M., Addicks, E. M., Massof, R. W., & Green, W. R. (1983). Morphologic changes in the lamina cribrosa correlated with neural loss in open-angle glaucoma. *American Journal of Ophthalmology, 95*(5), 673-691.

Rada, J. A. S., Shelton, S., & Norton, T. T. (2006). The sclera and myopia. *Experimental eye research, 82*(2), 185-200.

Read, S. A., Collins, M. J., Carney, L. G., & Franklin, R. J. (2006). The topography of the central and peripheral cornea. *Investigative Ophthalmology & Visual Science, 47*(4), 1404-1415.

Reynaud, J., Lockwood, H., Gardiner, S. K., Williams, G., Yang, H., & Burgoyne, C. F. (2016). Lamina Cribrosa Microarchitecture in Monkey Early Experimental Glaucoma: Global Change. *Investigative Ophthalmology & Visual Science, 57*(7), 3451-3469. doi:10.1167/iovs.16-19474

Rezakhaniha, R., Agianniotis, A., Schrauwen, J. T. C., Griffa, A., Sage, D., Bouten, C., . . . Stergiopulos, N. (2012). Experimental investigation of collagen waviness and orientation in the arterial adventitia using confocal laser scanning microscopy. *Biomechanics and modeling in mechanobiology, 11*(3-4), 461-473.

Ribeiro, A. P., Santos, N. L., Campos, A. F., Teixeira, I. A. M. d. A., & Laus, J. L. (2010). Ultrasonographic and ecobiometric findings in the eyes of adult goats. *Ciência Rural, 40*(3), 568-573.

Roberts, M. D., Grau, V., Grimm, J., Reynaud, J., Bellezza, A. J., Burgoyne, C. F., & Downs, J. C. (2009). Remodeling of the connective tissue microarchitecture of the lamina cribrosa in early experimental glaucoma. *Investigative ophthalmology & visual science, 50*(2), 681.

Romero-Jiménez, M., Santodomingo-Rubido, J., & Wolffsohn, J. S. (2010). Keratoconus: a review. *Contact lens and anterior eye, 33*(4), 157-166.

Ruberti, J. W., & Zieske, J. D. (2008). Prelude to corneal tissue engineering–gaining control of collagen organization. *Progress in retinal and eye research, 27*(5), 549-577.

Schindelin, J., Arganda-Carreras, I., Frise, E., Kaynig, V., Longair, M., Pietzsch, T., . . . Schmid, B. (2012). Fiji: an open-source platform for biological-image analysis. *Nature Methods, 9*(7), 676-682.

Shah, J., Jayson, M., & Hampson, W. (1977). Low tension studies of collagen fibres from ligaments of the human spine. *Annals of the Rheumatic Diseases, 36*(2), 139.

Shribak, M., & Oldenbourg, R. (2003). Techniques for fast and sensitive measurements of two-dimensional birefringence distributions. *Applied Optics, 42*(16), 3009-3017.

Sigal, I., Grimm, J., Jan, N.-J., Bilonick, R., Wollstein, G., Kagemann, L., . . . Lathrop, K. (2013). IOP elevation reduces the waviness of the load bearing collagen fibers in the lamina cribrosa. *Investigative Ophthalmology & Visual Science, 54*(15), 3158-3158.

Sigal, I. A., & Ethier, C. R. (2009). Biomechanics of the optic nerve head. *Experimental eye research, 88*(4), 799-807. doi:http://dx.doi.org/10.1016/j.exer.2009.02.003

Sigal, I. A., Flanagan, J. G., Lathrop, K. L., Tertinegg, I., & Bilonick, R. (2012). Human Lamina Cribrosa Insertion and Age. *Investigative Ophthalmology & Visual Science, 53*(11), 6870-6879.

Sigal, I. A., Flanagan, J. G., Tertinegg, I., & Ethier, C. R. (2004). Finite element modeling of optic nerve head biomechanics. *Investigative Ophthalmology & Visual Science, 45*(12), 4378-4387.

Sigal, I. A., Flanagan, J. G., Tertinegg, I., & Ethier, C. R. (2010). 3D morphometry of the human optic nerve head. *Experimental eye research, 90*(1), 70-80. doi:http://dx.doi.org/10.1016/j.exer.2009.09.013

Sigal, I. A., Grimm, J. L., Jan, N.-J., Bilonick, R. A., Wollstein, G., Kagemann, L., . . . Lathrop, K. L. (2013). IOP elevation reduces the waviness of the load bearing collagen fibers in the lamina cribrosa. *Investigative Ophthalmology & Visual Science, 54*(15), 3158-3158.

Sigal, I. A., Grimm, J. L., Jan, N.-J., Reid, K., Minckler, D. S., & Brown, D. J. (2014). Eye-Specific IOP-Induced Displacements and Deformations of Human Lamina Cribrosa. *Investigative Ophthalmology & Visual Science, 55*(1), 1-15.

Sigal, I. A., Grimm, J. L., Jan, N. J., Reid, K., Minckler, D. S., & Brown, D. J. (2014). Eye-specific IOP-induced displacements and deformations of human lamina cribrosa. *Invest Ophthalmol Vis Sci, 55*(1), 1-15. doi:10.1167/iovs.13-12724

Sigal, I. A., Jan, N.-J., Moed, S., O'Malley, R., Tran, H., Bilonick, R. A., . . . Wollstein, G. (2015). A microstructural basis for nonlinear effects of IOP on the lamina cribrosa and sclera. *Investigative Ophthalmology & Visual Science, 56*(7), 4821-4821.

Standring, S. (2016). *Gray's anatomy: the anatomical basis of clinical practice* (Forty-first ed.). New York: Elsevier Limited.

Stokes, I. A. F., McBride, C., Aronsson, D. D., & Roughley, P. J. (2011). Intervertebral disc changes with angulation, compression and reduced mobility simulating altered mechanical environment in scoliosis. *European Spine Journal, 20*(10), 1735-1744. doi:10.1007/s00586-011-1868-5

Sudan, R., Titiyal, J. S., Rai, H., & Chandra, P. (2002). Formalin-induced cataract in goat eyes as a surgical training model for phacoemulsification. *Journal of Cataract & Refractive Surgery, 28*(11), 1904-1906.

Szczesny, S. E., & Elliott, D. M. (2013). *Evidence for Interfibrillar Shear Load Transfer Between Sliding Fibrils in Tendon.* Paper presented at the ASME 2013 Summer Bioengineering Conference.

Szczesny, S. E., Peloquin, J. M., Cortes, D. H., Kadlowec, J. A., Soslowsky, L. J., & Elliott, D. M. (2012). Biaxial tensile testing and constitutive modeling of human supraspinatus tendon. *Journal of biomechanical engineering, 134*(2), 021004.

Tauer, U. (2002). Advantages and Risks of Multiphoton Microscopy in Physiology. *Experimental Physiology, 87*(6), 709-714. doi:10.1113/eph8702464

Team, R. C. (2013). R foundation for statistical computing. *Vienna, Austria, 3*(0).

Teng, S.-W., Tan, H.-Y., Peng, J.-L., Lin, H.-H., Kim, K. H., Lo, W., . . . Jee, S.-H. (2006). Multiphoton autofluorescence and second-harmonic generation imaging of the ex vivo porcine eye. *Investigative Ophthalmology & Visual Science, 47*(3), 1216-1224.

Thale, A., & Tillmann, B. (1993a). The collagen architecture of the sclera--SEM and immunohistochemical studies. *Annals of Anatomy, 175*(3), 215-220.

Thale, A., Tillmann, B., & Rochels, R. (1996a). Scanning electron-microscopic studies of the collagen architecture of the human sclera--normal and pathological findings. *Ophthalmologica, 210*(3), 137-141.

Tham, Y.-C., Li, X., Wong, T. Y., Quigley, H. A., Aung, T., & Cheng, C.-Y. (2014). Global prevalence of glaucoma and projections of glaucoma burden through 2040: a systematic review and meta-analysis. *Ophthalmology, 121*(11), 2081-2090.

Thornton, G. M., Shrive, N. G., & Frank, C. B. (2002). Ligament creep recruits fibres at low stresses and can lead to modulus-reducing fibre damage at higher creep stresses: a study in rabbit medial collateral ligament model. *Journal of Orthopaedic Research, 20*(5), 967-974. doi:10.1016/S0736-0266(02)00028-1

Tran, H., Jan, N.-J., Hu, D., Voorhees, A., Schuman, J. S., Smith, M. A., . . . Sigal, I. A. (2017). Formalin Fixation and Cryosectioning Cause Only Minimal Changes in Shape or Size of Ocular Tissues. *Scientific Reports, 7*(1), 12065.

van Zuijlen, P. P., de Vries, H. J., Lamme, E. N., Coppens, J. E., van Marle, J., Kreis, R. W., & Middelkoop, E. (2002). Morphometry of dermal collagen orientation by Fourier analysis is superior to multi-observer assessment. *The Journal of pathology, 198*(3), 284-291.

Vogel, R., Crick, R. P., Newson, R. B., Shipley, M., Blackmore, H., & Bulpitt, C. J. (1990). Association between intraocular pressure and loss of visual field in chronic simple glaucoma. *British Journal of Ophthalmology, 74*(1), 3-6. doi:10.1136/bjo.74.1.3

Voorhees, A., Millwater, H., & Bagley, R. (2011). Complex variable methods for shape sensitivity of finite element models. *Finite Elements in Analysis and Design, 47*(10), 1146-1156. doi:http://dx.doi.org/10.1016/j.finel.2011.05.003

Voorhees, A. P., Ho, L. C., Jan, N.-J., Tran, H., van der Merwe, Y., Chan, K., & Sigal, I. A. (2017). Whole-globe biomechanics using high-field MRI. *Experimental eye research, 160*, 85-95.

Voorhees, A. P., Jan, N.-J., Flanagan, J. G., Sivak, J. M., & Sigal, I. A. (2016). A Microstructure Based Model of Lamina Cribrosa Mechanical Insult under IOP. *Investigative Ophthalmology & Visual Science, 57*(12).

Voorhees, A. P., Jan, N. J., & Sigal, I. A. (2017). Effects of collagen microstructure and material properties on the deformation of the neural tissues of the lamina cribrosa. *Acta Biomaterialia*. doi:10.1016/j.actbio.2017.05.042

Wainwright, S. A., Biggs, W., Currey, J., & Gosline, J. (1982). *Mechanical design in organisms*. Princeton, NJ: Princeton University Press.

Wallace, J., Jan, N.-J., Gogola, A., Iasella, M., Lathrop, K. L., Voorhees, A. P., . . . Sigal, I. A. (2017). Stretch-Induced Collagen Bundle Uncrimping and Recruitment are Independent of Depth in Equatorial Sclera. *Investigative Ophthalmology & Visual Science, 58*(8), 3162-3162.

Wang, B., Nevins, J. E., Nadler, Z., Wollstein, G., Ishikawa, H., Bilonick, R. A., . . . Schuman, J. S. (2013). In Vivo Lamina Cribrosa Micro-Architecture in Healthy and Glaucomatous Eyes as Assessed by Optical Coherence TomographyIn Vivo Assessment of 3D LC Micro-Architecture. *Investigative Ophthalmology & Visual Science, 54*(13), 8270-8274. doi:10.1167/iovs.13-13109

Wang, R., Raykin, J., Gleason, R. L., Jr., & Ethier, C. R. (2015). Residual deformations in ocular tissues. *Journal of the Royal Society, Interface, 12*(105). doi:10.1098/rsif.2014.1101

Watson, P. G., & Young, R. D. (2004). Scleral structure, organisation and disease. A review. *Experimental eye research, 78*(3), 609-623.

Weinreb, R. N., Aung, T., & Medeiros, F. A. (2014). The pathophysiology and treatment of glaucoma: A review. *JAMA, 311*(18), 1901-1911. doi:10.1001/jama.2014.3192

Whitford, C., Joda, A., Jones, S., Bao, F., Rama, P., & Elsheikh, A. (2016). Ex vivo testing of intact eye globes under inflation conditions to determine regional variation of mechanical stiffness. *Eye and Vision, 3*(1), 21.

Winkler, M., Chai, D., Kriling, S., Nien, C. J., Brown, D. J., Jester, B., . . . Jester, J. V. (2011). Nonlinear optical macroscopic assessment of 3-D corneal collagen organization and axial biomechanics. *Investigative Ophthalmology & Visual Science, 52*(12), 8818-8827.

Winkler, M., Jester, B., Nien-Shy, C., Massei, S., Minckler, D. S., Jester, J. V., & Brown, D. J. (2010). High resolution three-dimensional reconstruction of the collagenous matrix of the human optic nerve head. *Brain Research Bulletin, 81*(2-3), 339-348.

Winkler, M., Shoa, G., Xie, Y., Petsche, S. J., Pinsky, P. M., Juhasz, T., . . . Jester, J. V. (2013a). Three-Dimensional Distribution of Transverse Collagen Fibers in the Anterior Human Corneal Stroma. *Investigative Ophthalmology & Visual Science, 54*(12), 7293-7301.

Woo, S. L. Y., Kobayashi, A. S., Schlegel, W. A., & Lawrence, C. (1972). Nonlinear material properties of intact cornea and sclera. *Experimental eye research, 14*(1), 29-39. doi:http://dx.doi.org/10.1016/0014-4835(72)90139-X

Wood, M. F. G., Vurgun, N., Wallenburg, M. A., & Vitkin, I. A. (2011). Effects of formalin fixation on tissue optical polarization properties. *Physics in Medicine and Biology, 56*(8), N115.

Yan, D., McPheeters, S., Johnson, G., Utzinger, U., & Vande Geest, J. P. (2011). Microstructural Differences in the Human Posterior Sclera as a Function of Age and Race. *Investigative Ophthalmology & Visual Science, 52*(2), 821-829. doi:10.1167/iovs.09-4651

Yang, B., Jan, N.-J., Lam, P., Lathrop, K. L., & Sigal, I. A. (2017). Collagen architecture in the third dimension: 3D polarized light microscopy (3DPLM) for mapping in-plane (IP) and out-of-plane (OOP) collagen fiber architecture. *Investigative Ophthalmology & Visual Science, 58*(8), 4825-4825.

Yang, B., Jan, N. J., Brazile, B., Voorhees, A., Lathrop, K. L., & Sigal, I. A. (2018). Polarized light microscopy for 3D mapping of collagen fiber architecture in ocular tissues. *Journal of Biophotonics*, e201700356.

Yang, H., Downs, J. C., Bellezza, A., Thompson, H., & Burgoyne, C. F. (2007). 3-D histomorphometry of the normal and early glaucomatous monkey optic nerve head: prelaminar neural tissues and cupping. *Investigative Ophthalmology & Visual Science, 48*(11), 5068-5084.

Yang, H., Williams, G., Downs, J. C., Sigal, I. A., Roberts, M. D., Thompson, H., & Burgoyne, C. F. (2011). Posterior (outward) migration of the lamina cribrosa and early cupping in

monkey experimental glaucoma. *Investigative Ophthalmology & Visual Science*, *52*(10), 7109-7121.

Yang, Y., Li, X., Yan, N., Cai, S., & Liu, X. (2009). Myopia: A collagen disease? *Medical hypotheses*, *73*(4), 485-487.

Zhang, L., Albon, J., Jones, H., Gouget, C. L., Ethier, C. R., Goh, J. C., & Girard, M. J. (2015). Collagen Microstructural Factors Influencing Optic Nerve Head Biomechanics. *Investigative Ophthalmology & Visual Science*, *56*(3), 2031-2042.

Zyablitskaya, M., Takaoka, A., Munteanu, E. L., Nagasaki, T., Trokel, S. L., & Paik, D. C. (2017). Evaluation of Therapeutic Tissue Crosslinking (TXL) for Myopia Using Second Harmonic Generation Signal Microscopy in Rabbit Sclera. *Investigative Ophthalmology & Visual Science*, *58*(1), 21-29. doi:10.1167/iovs.16-20241